ASYMPTOTIC MULTIPLE-SCALES ANALYSIS OF HYDRAULIC TRANSIENTS IN ELASTIC AND VISCOELASTIC PRESSURIZED CONDUITS

by

Yue (Edward) Yao

Submitted in partial fulfillment of the requirements
for the degree of Doctor of Philosophy

at

Dalhousie University
Halifax, Nova Scotia
June 2017

Table of Contents

List of Tables

List of Figures

Abstract

The hydraulic transient phenomenon known as water hammer has a long history [35]. To date, only relatively simple cases have been studied analytically among the numerous publications. In this research, a formal asymptotic wave attenuation form is found for each of three water hammer models, i.e., the classic model, an unsteady friction model, and a generalized Kelvin-Voight model. Explicit dependence of pressure-wave attenuation on lumped parameters is found and a deeper and more direct understanding of the water hammer phenomenon is obtained that is unavailable from numerical methods. Firstly, (Yao et al. [99], Chapter 4), water hammer is treated for variable valve-closure time using a momentum equation extended to partially developed turbulence (Hansen et al. [43] 1995, [42] 2011). A closed-form pressure-wave attenuation, found via multiple-scales asymptotics, is useful over much longer times than previous *ad hoc* results (Tijsseling et al. [52] 2000). Numerical validation of analytical results is obtained using the method of characteristics and convergence verified through a time and space grid reductions. Experimental validation was not considered. The contribution includes: (i) understanding of parametric dependence of pressure-wave attenuation, (ii) capacity to handle time-varying closure cases which is currently unavailable, and (iii) validity in case of flow reversals given uniform fluid movement. Secondly, (Yao et al. [98], Chapter 5), an unsteady friction model introduced by Brunone et al. [16] 1990 to account for turbulence, is considered. An extension of Chapter 4 is used to find the wave attenuation form. Increased attenuation due to unsteady friction is reduced to a single time-dependent exponential factor involving the product of Brunone's unsteady-friction parameters. The numerical solution, found as before, was used to verify analytic results. Model parameters chosen to match experimental results (Bergant et al. [8]) were used here. The analytic form surprisingly predicts that the steady viscous extension (Hansen et al. [42] 2011), accounting for partially developed turbulence, provides an equally viable explanation for the increased pressure-wave attenuation given a weak spatial dependence. Finally, (Yao et al. [100], Chapter 6), the multiple-scales method (Chapters 4 and 5) is further extended to water hammer in viscoelastic pipe modelled using a Kelvin-Voight representation. Pipe plasticity is found to increase the pressure wave attenuation rate via a third time scale driven by weak strain-rate feedback. A Preissmann weighted four-point box-scheme (Weinerowska-Bords [90] 2006) is used to obtain numerical solutions to the mathematical model. The analytic work is validated by matching to a numerical solution matched to experimental data (Mitosec et al. [59]). This contribution includes: (i) resolution of an outstanding paradox (Weinerowska-Bords [90] 2006) involving an order of magnitude mismatch between predicted Kelvin-Voight parameters and those required to match numerical and experimental data, and (ii) introduction of a novel classification method for the prediction of the scale of lumped-parameters without access to experimental data. Both (i) and (ii) predict that this work will be useful in the planning and design phases of experiment and field installations.

List of Abbreviations and Symbols Used

$(C_dA_G)_0$	steady-state condition of C_dA_G
A	pipe cross-sectional area; dimensionless scaling $A'\epsilon$
A'	head scale $\alpha' h^{*\prime}/C_4'$
A_G	area of valve opening
A_t	nozzle area at time t
B	Allievi constant or pipeline constant aV_0/gH_0; dimensionless scaling $B'\epsilon^{-1}$
B'	velocity scale $\alpha' h^{*\prime}/\sqrt{C_4'}$
B_1	Brunone unsteady friction parameter $k/2$
B_2	Brunone unsteady friction parameter $c_p v_\infty/gh_{12}$
B_t	pipeline constant B at time t
C	dimensionless scaling $C'\epsilon^{-4}$
C'	strain scale $h^{*\prime}$
C^*	Vardy's shear decay coefficient
C^+	symbol of characteristic equations with positive slope of characteristic curve
C^-	symbol of characteristic equations with negative slope of characteristic curve
C_1	advection effect v_0^2/gh_{12}
C_2	viscous effect rv_0/h_{12}
C_3	inertial effect sv_0^2/h_{12}

C_4	local velocity $(gh_{12}/c_p v_0)^2$
C_4'	dimensionless parameter $[(\rho g h_{12})/(\rho a v_\infty)]^2$
C_5	elevation head $gL\sin\theta/c_p^2$
C_d	valve discharge coefficient
D	inner radius of pipe
D_c	conduit diameter
E	Young's modulus of pipe material; instantaneous tensile modulus; Kelvin-Voight Young's modulus
E_0	instantaneous tensile modulus; pipe Young's modulus
E_v	water bulk modulus
E_w	water bulk modulus
$F(t+x/a)$	function represents an F wave moving upstream
$F_{nj}(\alpha_n(X-ct))$	oscillatory wave components with dimensionless wave speed $c=1/\sqrt{(1+B_1)c_4}$
$G_{nj}(\beta_n(X-ct))$	oscillatory wave components with dimensionless wave speed $c=1/\sqrt{(1+B_1)c_4}$
H	dimensional head; dimensionless head
$H(X,\tau)$	multiple-scales approximation of head wave
$H(X,q,s,\tau)$	multiple-scales approximation of head wave
H_0	steady-state head

J	friction term in Brunone's unsteady friction model
$J(t)$	creep function
$J_0(z)$	Bessel function of first kind of zero order
$J_1(z)$	Bessel function of first kind of first order
J_n	creep compliances
K	bulk modulus of fluid
K_1	dimensionless steady friction parameter a^2A
K_2	dimensionless head-to-strain coupling parameter $\beta A/h^*$
L	pipe length; linear combination of L_1 and L_2
L_1	symbol of momentum equation in characteristic method
L_2	symbol of continuity equation in characteristic method
M	positive integer
N	number of Kelvin-Voight elements arranged in series; number of equal reaches
O	Bachmann-Landau notation
P	intersection of two characteristic curves C^+ and C^-
$P_j(\tau)$	long time-scale pressure-wave attenuation functions
$P_n(\tau)$	first approximation to the nth mode wave attenuation
$R(\epsilon)$	cost function

Re	Reynolds number
T	rigid-column time scale
T_n	time scales in multiple-scales method
T_r	dimensionless parameter $T_r'\epsilon^2$
T_r'	dimensionless parameter T/T_w
T_w	relaxation time of single Kelvin-Voight element
V	dimensional velocity; instantaneous mean flow velocity; dimensionless velocity
$V(X,\tau)$	multiple-scales approximation of velocity wave
$V(X,q,s,\tau)$	multiple-scales approximation of velocity wave
$V(X,t,\tau)$	multiple-scales approximation of velocity wave
V_0	steady-state velocity
$W(X,q,s,\tau)$	multiple-scales approximation of strain
$W(\tau)$	Zielke's function in dimensionless $\tau = \nu t/D^2$ where $D =$ inner radius of pipe
X	dimensionless spatial scale
ΔH	piezometric head change
ΔP	pressure change
ΔV	velocity change
Δh_{t_1}	dimensionless head change at time t_1
Δt	time change; time step advance

Δt_c	dimensionless parameter $\Delta t'_c/T$
$\Delta t'_c$	valve closure time
Δv_{t_1}	dimensionless velocity change at time t_1
Δx	space step advance
Ψ	coefficient depending on pipe support conditions
$\Re(\alpha_1)$	the real part of α_1
α	dimensionless parameter $\alpha'\epsilon$
α_1	free complex constant
α_n	complex modes with imaginary part $n\mathbf{i}$
β'	dimensionless parameter $c_1(\rho g h_{12})/[2 \cdot E(e/D)]$
β_n	complex modes with imaginary part $n\mathbf{i}$
$\mathbf{i}$	imaginary unit $\sqrt{-1}$
δ	Brunone's piecewise-defined function
ϵ	strain; artificial small parameter in multiple-scales method
ϵ_c	relative roughness of conduit
η	viscosity coefficient
$\hat{F}$	Laplace transform of F
λ	multiplier in characteristic method; friction factor; strain-rate term
$\lvert P_0(s,\tau)\rvert$	pressure wave attenuation function

$\lvert P_1(\tau)\rvert$	first mode pressure wave attenuation function
ν	kinematic viscosity
ϕ	weighting coefficient for distributing terms in time in Preissmann scheme
ρ	fluid density
ρ_f	mass density of fluid
σ	pipe wall stress
τ	dimensionless number $C_dA_G/(C_dA_G)_0$; retardation time of Voight element; dimensionless time scale; long trending time scale
τ_c	valve closure time
τ_r	dimensionless wave transit time t_r/T
τ_t	dimensionless number τ at time t
τ_w	shear stress at pipe wall
θ	elevation angle of pipe; weighting coefficient for distributing terms in space in Preissmann scheme
$\tilde{A}$	free constant
$\tilde{D}$	free constant
$\tilde{H}(X,t)$	rescaled dimensionless head
$\tilde{H}(X,t,\tau)$	multiple-scales approximation of head wave
$\tilde{V}(X,t)$	rescaled dimensionless velocity
$\tilde{W}(X,t)$	rescaled dimensionless strain

$\zeta_1(z)$	modified quotient of Bessel functions of order one
a	wave propagation speed; empirical wavespeed; dimensionless scaling $a'\epsilon^{-2}$
a'	wave speed timescale $\sqrt{C_4'}$
a_0	theoretical wavespeed
c	wave speed
c_1	pipe fastening constant
c_f	velocity of sound in fluid
c_p	wave celerity
e	thickness of pipe wall
f	Darcy-Weisbach friction factor
$f(t - x/a)$	function represents an f wave moving downstream
g	acceleration due to gravity
h	dimensionless head; initial head
$h(x, t')$	dimensional pressure head
h_1	initial head at $x = 0$
h_2	initial head at $x = L$
h_{12}	applied head change $h_1 - h_2$
i	imaginary unit $\sqrt{-1}$; subscript in multiple-scales method; i^{th} section in characteristic method
j	advance level on time–axis in numerical methods

k	Brunone coefficient
k'	constant $\sqrt{C^*}$
k_3	Brunone's coefficient
p	pressure
p_r	peak pressure
p'_r	fraction of full pressure transient
q	dimensionless water hammer fast time scale
r	radial coordinate; viscous constant
s	dimensionless strain time scale; inertial constant
t	temporal coordinate; dimensionless rigid column slower time scale; defined as $j\Delta t$ in characteristic method; short wave time scale
t'	dimensional time
t_1	any particular time
t_C	valve closure time
t_r	wave transient time $2L/c_p$
v	dimensionless velocity
$v(x,t')$	dimensional fluid velocity
v_∞	steady-state velocity
w	conduit wall thickness

x	spatial coordinate along pipe line; asymptotic solution in multiple-scales method; defined as $i\Delta x$ in characteristic method
x_n	solutions in multiple-scales method
z	complex number
h^*	dimensionless parameter $h^{*\prime}\epsilon^{-4}$
$h^{*\prime}$	dimensionless parameter $(\rho g h_2)/[2 \cdot E(e/D)]$; strain scale
EGL	energy grade line
FSI	fluid-structure interaction
HDPE	high-density polyethylene
HGL	hydraulic grade line
KV	Kelvin-Voight
MDPE	medium-density polyethylene
PE	polyethylene
PVC	polyvinyl chloride
R	Reynolds number

Acknowledgements

The research work presented within this dissertation was helped by the close supervision by Dr. Guy Kember, who is an active researcher in the fields of applied mathematics and physics. Dr. Kember's expertise, research ideas and thoughts, math techniques, programming skills, and unique teaching philosophy are the main driving force by which I was led into this research area. Without his tremendous help I don't think I could learn and possess the adequate knowledge and special math tools to complete my PhD study. To him, there are not enough words to express my heartfelt thanks.

My thanks are also given to Dr. David Hansen for his supervision and help in this research work. My knowledge of hydraulics is credited to his teaching and explanation.

I want to express my deep appreciation to Dr. William Phillips for his sincere support during my PhD study in the Department of Engineering Mathematics.

In the last, I would like to sincerely thank my wife, Yaping, for her time accompanied with me in this special period and my other family members for their care and understanding of the expectations placed on me by this work.

Chapter 1

Introduction

Water hammer or unsteady transient flow is a phenomenon that exists in pipeline systems. Water hammer can be induced by sudden valve closure or opening, pump trip-off or sudden start, load rejection of a turbine, seismic excitation, changing elevation of a reservoir, and changes in valve settings (either accidental or planned). During a water hammer event the rapid change of unsteady transient flow, with accompanying rapid fluctuation of pressure wave, propagates a pressure wave through pipelines that leads to the displacement of pipe machinery, pipe leakage, pipe rupture, or even the collapse of pipelines.

Research into water hammer has been mainly focused on obtaining the maximum and minimum values of pressure wave piezometric head and these are useful in the design phase of pipeline systems. To limit water hammer damage in conduits, it is common to use wave suppressors such as surge tanks, air chambers, flexible hoses, pump flywheels, relief valves and rupture disks. The predicted strength of maximum wave pressure from a rapid varying transient flow is useful for engineers to determine whether or not such devices are necessary and, if so, to establish their design characteristics.

The background of water hammer history is presented in Section 1.1 in order to provide a context for the work considered here. In Section 1.2, the mathematical models and methods are reviewed for unsteady transient flow occurred in pipes made by metal or concrete (i.e., steel pipes). For plastic pipes comprised of polyvinyl chloride (PVC), polyethylene (PE), or polypropylene (i.e., plastic pipes), the previous work is summarized in Section 1.3.

1.1 Water Hammer History

Formal research into water hammer began in 1858 when a French engineer L. F. Menabrea [55] published a paper titled "Note on Effects of Water Shock in Conduits".

Later in 1870, Rankine [68] obtained the late-called Joukowsky's formulae in a more general context. In 1878, Michaud [58] examined the use of air chambers and safety valves for controlling water hammer. In the same year, Korteweg [49] took into account both the compressibility of the fluid and the elasticity of the pipe walls and derived his wave speed formula

$$c_f = \sqrt{\frac{\frac{K}{\rho_f}}{1 + \Psi \frac{KD}{Ee}}} \tag{1.1}$$

where K = bulk modulus of fluid, E = Young's modulus of pipe material, D = inner diameter of pipe, e = thickness of pipe wall, and Ψ = coefficient depending on the pipe support conditions.

Weston [93] in 1885, Carpenter [22] in 1893, and Frizell [32] in 1898 attempted to develop expressions relating pressure and velocity changes in a pipe. In Frizell's work, the effects of branch lines, and reflected and successive waves on turbine speed regulation were also discussed.

Joukowsky [46] in 1898 found a well-known equation in transient flow theory. He studied wave reflections from an open branch, the use of air chambers and surge tanks, and spring type safety valves as well. Joukowsky's fundamental equation of water hammer (though Rankine, Korteweg and Frizell also discovered it independently), related pressure changes ΔP to velocity changes ΔV, by the constant factor $\rho_f c_f$, with ρ_f the mass density of the fluid and c_f the velocity of sound in the fluid.

$$\Delta P = \rho_f c_f \Delta V \tag{1.2}$$

Allievi [3] in 1903 developed a general theory of water hammer from first principles where the friction is neglected. His method had been widely used until the late 1920's.

Gibson [38] in 1908 performed water hammer experiments with closure and opening of a downstream valve in a laboratory pipeline apparatus. He indicated that a low-pressure wave initiated gas release.

Allievi's work was extended to include friction with the combined effort of Jaeger [45] in 1933, Wood [95] in 1937, Rich [70, 69] in 1944 and 1951, Parmakian [62] in 1955, Streeter and Lai [78] in 1962, and Streeter and Wylie [77] in 1963, in the

following momentum and continuity equations

$$g\frac{\partial H}{\partial x} + \frac{\partial V}{\partial t} + \tau_w \frac{4}{\rho D} = 0 \tag{1.3}$$

$$\frac{\partial H}{\partial t} + \frac{a^2}{g}\frac{\partial V}{\partial x} = 0 \tag{1.4}$$

where H = head, V = velocity, a = wave propagation speed, τ_w = shear stress at the pipe wall, g = acceleration due to gravity, D = inner diameter of pipe, x = the spatial coordinate along the pipe line, and t = temporal coordinate.

The above equations were re-derived by Chaudhry [23] in 1987, Watters [89] in 1984, Wylie [96] in 1984, and Wylie and Streeter [97] in 1993 as follows:

$$g\frac{\partial H}{\partial x} + V\frac{\partial V}{\partial x} + \frac{\partial V}{\partial t} + \frac{f}{2D}V|V| = 0 \tag{1.5}$$

$$\frac{a^2}{g}\frac{\partial V}{x} + V\frac{\partial H}{\partial x} + \frac{\partial H}{\partial t} + V\sin(\theta) = 0 \tag{1.6}$$

where f = Darcy-Weisbach friction factor and θ = the elevation angle of pipe.

1.2 Steel Pipes: Mathematical Models Relating to Steady and Unsteady Friction

In this Section, mathematical models and related methods are reviewed for steel pipes experiencing a water hammer event as might be caused by a sudden valve closure. Steel pipes are assumed to have linear elastic strain $\epsilon = \sigma/E$ where constant E = Young's modulus of the pipe material and σ = pipe wall stress.

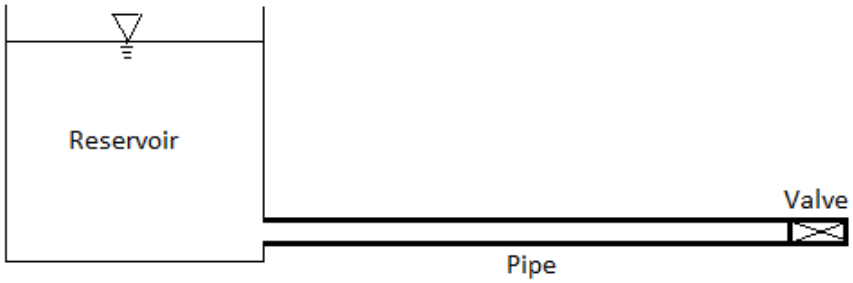

Figure 1.1: System of reservoir, pipe, and valve

The *Arithmetic Method* proposed by (Allievi [4, 3]) was used particularly until 1930's. This method neglects friction and assumes a horizontal pipe which relates piezometric head change ΔH to velocity change ΔV in Eq.(1.7)

$$\Delta H = \frac{a\Delta V}{g}\left(1 + \frac{2V_0}{a}\right) \approx \frac{a\Delta V}{g} \tag{1.7}$$

where a = wave propagation speed, V_0 = steady-state velocity, and g = acceleration due to gravity. After nondimensionalizing with $h = H/H_0$ and $v = V/V_0$, H_0 = steady-state head, gives the equation

$$\Delta h = B\Delta v \tag{1.8}$$

where $B = aV_0/gH_0$. The valve is treated as an orifice and the discharge (flow rate) out of the orifice is (by Daugherty [29])

$$VA = C_d A_G \sqrt{2gH} \tag{1.9}$$

where A = pipe cross-sectional area, A_G = area of valve opening, and C_d = valve discharge coefficient. Before the introduction of any transients, the steady-state discharge at the valve is

$$V_0 A = (C_d A_G)_0 \sqrt{2gH_0} \tag{1.10}$$

where coefficient $(C_d A_G)_0$ is for the steady-state condition. Thus, dividing Eq.(1.9) by Eq.(1.10) gives the non-dimensional valve equation

$$v = \tau\sqrt{h} \tag{1.11}$$

where $\tau = C_d A_G/(C_d A_G)_0$ is usually a function of time t with a scaled value 1 at the steady state and reducing to 0 as the valve closes.

Eq.(1.8) is solved together with the gate equation in the form

$$v - \Delta v_{t_1} = \tau_{t_1}\sqrt{h + \Delta h_{t_1}} \tag{1.12}$$

for any particular time t_1. The gate equation is reasonable since pressure head change

Δh_{t_1} increases while velocity change Δv_{t_1} decreases with a partially adjusted orifice coefficient τ_{t_1} at each time t_1, assuming the valve closure time $t_C \leq 2L/a$, L = the pipe length. For the valve closure time $t_C > 2L/a$, the pressure rise is reduced after reflected waves arrived at the valve and the gate equation is revised as

$$v - \Delta v_{t_1} = \tau_{t_1} \sqrt{1 - \sum \Delta h + \Delta h_{t_1}} \tag{1.13}$$

where $\sum \Delta h$ represents the sum of all direct and reflected waves up to time t_1. The integer 1 represents the scaled steady-state head at the reservoir.

By selecting a different time t_1, the corresponding pressure head h_{t_1} and velocity v_{t_1} are found through a series of tabular calculations using the Eqs.(1.8) and (1.12)–(1.13).

The arithmetic method is simple and convenient but it neglects friction which is an important effect required to further characterize the transient flows.

A *Graphical Method* was proposed by Schnyder [73, 74] and Angus [5] in the absence of friction and for a horizontal pipe. Eliminating the friction term in Eq.(1.3) gives the following general wave equations

$$g\frac{\partial H}{\partial x} + \frac{\partial V}{\partial t} = 0 \tag{1.14}$$

$$\frac{\partial H}{\partial t} + \frac{a^2}{g}\frac{\partial V}{\partial x} = 0 \tag{1.15}$$

Further eliminating V from the Eqs.(1.14) and (1.15) yields

$$\frac{\partial^2 H}{\partial t^2} = a^2 \frac{\partial^2 H}{\partial x^2} \tag{1.16}$$

In a similar manner

$$\frac{\partial^2 V}{\partial t^2} = a^2 \frac{\partial^2 V}{\partial x^2} \tag{1.17}$$

The standard solution to the wave equation Eq.(1.16) is given by

$$H - H_0 = F\left(t + \frac{x}{a}\right) + f\left(t - \frac{x}{a}\right) \tag{1.18}$$

Similarly integrating Eq.(1.17) gives

$$V - V_0 = -\frac{g}{a}\left[F\left(t + \frac{x}{a}\right) - f\left(t - \frac{x}{a}\right)\right] \tag{1.19}$$

where the functions $F(t + x/a)$ and $f(t - x/a)$ are arbitrary and can be selected to satisfy the conditions given at the upstream-end (reservoir) and the downstream-end (valve). The function $F(t+x/a)$ represents an F wave moving upstream (i.e., negative direction of positive x) and the function $f(t - x/a)$ represents an f wave moving downstream (i.e., direction of positive x). It is assumed there is no wave interference if waves meet within the pipe. Combining Eqs.(1.18) and (1.19) to eliminate the f function

$$H(t, x) - H_0 - \frac{a}{g}(V(t, x) - V_0) = 2F\left(t + \frac{x}{a}\right) \tag{1.20}$$

Noting that the F wave travels upstream at a speed of $-a$, at the time $t_1 = t+\Delta t$ the wave front is at location $x_1 = x - a\Delta t$ given $x_1 < x$. Applying Eq.(1.20) at (t, x) and (t_1, x_1) and subtracting the two resultant equations, and noting that $2F(t + x/a) - 2F(t_1 + x_1/a) = 0$, gives

$$H(t_1, x_1) - H(t, x) = \frac{a}{g}(V(t_1, x_1) - V(t, x)) \tag{1.21}$$

with a dimensionless form

$$h(t_1, x_1) - h_{t,x} = \frac{a}{g}(v(t_1, x_1) - v(t, x)) \tag{1.22}$$

or

$$\Delta h = B\Delta v \tag{1.23}$$

where $B = aV_0/gH_0$. The line (by Eq.(1.23)) is plotted with positive slope B passing through the point (t_1, x_1) on the h–v plane, representing the F wave. Following a similar argument

$$\Delta h = -B\Delta v \tag{1.24}$$

which is a line with slope $-B$ passing through the same point (t_1, x_1) on the h–v plane, corresponding to the f wave.

A graphical solution of head h and velocity v can be found on the h–v plane by using the following Steps (it is assumed without loss of generality that the sudden valve closure is at $t = L/a$).

Step 1: Starting from a steady-state point ($v = 1, h = 1$), denoted by B_0 (the subscript refers to the time and the letter to the location), draw an f wave line from the point on the h–v plane. The conditions at $A_{L/a}$ must fall on this line since the direct wave increases pressure head. At the time $t = 2L/a$, the valve closes instantaneously and $v = 0$, so $A_{L/a}$ must also fall on the h-axis when $v = 0$.

Step 2: Draw an F wave line from $A_{L/a}$, the conditions at $B_{2L/a}$ must fall on this line since the reflected wave reduces pressure head. At time $t = 3L/a$, pressure head $h = 1$ and $B_{2L/a}$ must also fall on the line $h = 1$, thus $B_{2L/a}$ is located at the intersection of the two lines.

Step 3: Draw an f wave line from $B_{2L/a}$, the conditions at $A_{3L/a}$ must fall on this line since the reflected wave reduces pressure head. At time $t = 4L/a$, velocity $v = 0$ and $A_{3L/a}$ must also fall on the h–axis.

Step 4: Draw an F wave line from $A_{3L/a}$, the conditions at $B_{4L/a}$ must fall on this line since the reflected wave increases pressure head. At time $t = 5L/a$, pressure head $h = 1$ and $B_{4L/a}$ must also fall on the line $h = 1$, thus $B_{4L/a}$ is at the intersection of the two lines.

Step 5: Repeat this cycle to locate $A_{5L/a}$, $B_{6L/a}$, $A_{7L/a}$, and $B_{8L/a}$, and so on for the succeeding cycles.

For a gradual valve closure (without loss of generality, assuming the closure time $t_C = 4L/a$) the gate equation Eq.(1.11) is used and these are plotted as parabolas at a series of τ values $\tau_{L/a}$, $\tau_{2L/a}$, $\tau_{3L/a}$, and $\tau_{4L/a}$. Now, the pressure head h and velocity v can be solved graphically on the h–v plane using the following Steps.

Step I: Draw parabolas by Eq.(1.11) on the h–v plane with the values $\tau = \tau_{L/a}$, $\tau_{2L/a}$, $\tau_{3L/a}$, and $\tau_{4L/a}$, respectively. Note that each parabola corresponds to a time ($t = L/a$, $2L/a$, $3L/a$, and $4L/a$, respectively).

Step II: Starting from a steady-state point ($v = 1, h = 1$), denoted by B_0 (the subscript refers to the time and the letter to the location), draw an f wave line from the point on the h–v plane. The conditions at $A_{L/a}$ must fall on this line since the direct wave increases pressure head. However, $A_{L/a}$ must also fall on the $t = L/a$

parabola. Thus $A_{L/a}$ is located at the intersection of the f wave line and the $t = L/a$ parabola.

Step III: Draw an F wave line from $A_{L/a}$, the conditions at $B_{2L/a}$ must fall on this line since the reflected wave reduces pressure head. At time $t = 2L/a$, pressure head $h = 1$ and $B_{2L/a}$ must also fall on the line $h = 1$, thus $B_{2L/a}$ is located at the intersection of the two lines.

Step IV: Draw an f wave line from $B_{2L/a}$, the conditions at $A_{3L/a}$ must fall on this line since the reflected wave increases pressure head. At time $t = 3L/a$, however, $A_{3L/a}$ must also fall on the $t = 3L/a$ parabola. Thus $A_{3L/a}$ is located at the intersection of the f wave line and the $t = 3L/a$ parabola.

Step V: Draw an F wave line from $A_{3L/a}$, the conditions at $B_{4L/a}$ must fall on this line since the reflected wave reduces pressure head. At time $t = 4L/a$, pressure head $h = 1$ and $B_{4L/a}$ must also fall on the line $h = 1$, thus $B_{4L/a}$ is at the intersection of the two lines.

Step VI: Draw an f wave line from $B_{4L/a}$, the conditions at $A_{5L/a}$ must fall on this line since the reflected wave increases pressure head. At time $t = 5L/a$, however, the valve has been closed. So $A_{5L/a}$ is located on the h-axis when $v = 0$.

Step VII: Starting from the conditions at $A_{5L/a}$, the rest of $B_{6L/a}$, $A_{7L/a}$, $B_{8L/a}$, $A_{9L/a}$, are located by repeating from Step 2 to Step 5 in the sudden valve closure case.

The advantage of the graphical method is that it allows the water hammer process to be visualized within a single diagram. However, it is difficult to maintain accuracy due to the accumulated errors in locating B_0, $A_{L/a}$, $B_{2L/a}$, $A_{3L/a}$, $B_{4L/a}$, etc.

Since the advent of digital computer era in the late 1950's and the early 1960's, the *Method of Characteristics*, introduced by Gray [40], Lister [54], and Streeter [78, 77], has prevailed. Unlike the preceding two methods, the method of characteristics includes the friction term in the momentum equation and allows for sloping pipes. This method converts the two partial differential equations (Eqs.(1.5) and (1.6)) into four total differential equations that are expressed in finite-difference form and solved by digital computer. The method is illustrated by considering the following form for

a somewhat simplified format (details are in Streeter [78, 77])

$$g\frac{\partial H}{\partial x}+\frac{\partial V}{\partial t}+\frac{f}{2D}V|V|=0 \tag{1.25}$$

$$\frac{a^2}{g}\frac{\partial V}{\partial x}+\frac{\partial H}{\partial t}=0 \tag{1.26}$$

We let

$$L_1=g\frac{\partial H}{\partial x}+\frac{\partial V}{\partial t}+\frac{f}{2D}V|V|=0 \tag{1.27}$$

$$L_2=\frac{a^2}{g}\frac{\partial V}{\partial x}+\frac{\partial H}{\partial t}=0 \tag{1.28}$$

and then combine the Eqs.(1.27) and (1.28) with an unknown multiplier λ as

$$L=L_1+\lambda L_2=\lambda\left(\frac{\partial H}{\partial x}\frac{g}{\lambda}+\frac{\partial H}{\partial t}\right)+\left(\frac{\partial V}{\partial x}\lambda\frac{a^2}{g}+\frac{\partial V}{\partial t}\right)+\frac{f}{2D}V|V|=0 \tag{1.29}$$

The unknown multiplier λ is chosen so that Eq.(1.29) becomes an ordinary differential equation. This can be seen by relating the term in the brackets of Eq.(1.29) to the total differential form of the dependent variables $H=H(x,t)$ and $V=V(x,t)$, respectively. That is

$$\frac{dH}{dt}=\frac{\partial H}{\partial x}\frac{dx}{dt}+\frac{\partial H}{\partial t}=\frac{\partial H}{\partial x}\frac{g}{\lambda}+\frac{\partial H}{\partial t} \tag{1.30}$$

$$\frac{dV}{dt}=\frac{\partial V}{\partial x}\frac{dx}{dt}+\frac{\partial V}{\partial t}=\frac{\partial V}{\partial x}\lambda\frac{a^2}{g}+\frac{\partial V}{\partial t} \tag{1.31}$$

For Eqs.(1.30) and (1.31) hold, the following must be true

$$\frac{dx}{dt}=\frac{g}{\lambda}=\frac{\lambda a^2}{g} \tag{1.32}$$

Eq.(1.29) then becomes

$$\lambda\frac{dH}{dt}+\frac{dV}{dt}+\frac{f}{2D}V|V|=0 \tag{1.33}$$

Solving Eq.(1.32) gives

$$\lambda=\pm\frac{g}{a} \tag{1.34}$$

and

$$\frac{dx}{dt} = \pm a \tag{1.35}$$

Substituting λ into Eq.(1.33) and grouping Eqs.(1.33) and (1.35), according to the "+" or "−" sign, gives two pairs of equations which shall be indicated as C^+ and C^-

$$\frac{g}{a}\frac{dH}{dt} + \frac{dV}{dt} + \frac{f}{2D}V|V| = 0 \tag{1.36}$$

$$\frac{dx}{dt} = +a \tag{1.37}$$

and

$$-\frac{g}{a}\frac{dH}{dt} + \frac{dV}{dt} + \frac{f}{2D}V|V| = 0 \tag{1.38}$$

$$\frac{dx}{dt} = -a \tag{1.39}$$

Both Eqs.(1.37) and (1.39) plot as curves in the x–t plane, called "characteristic" curves. The numerical solutions of Eqs.(1.36) and (1.38) along these characteristics are the solutions of Eqs.(1.25) and (1.26). This method is continued in Chapter 2.

The method of characteristics provides more accuracy than that of the preceding two methods in that previously neglected terms in the governing equations (Eqs.(1.5) and (1.6)) are retained. Furthermore, it can be used to derive semi-analytic solutions to better understand transients (Leslie [52]). More complex water hammer phenomena, with the effects of unsteady friction, cavitation (column separation), leakage, blockage, and line packing may also be studied using this method. It also affords greater ease in handling the boundary conditions and relative simplicity in programming complex pipeline systems. In what follows, the focus is upon reviewing water hammer models and methods in lieu of unsteady friction in steel pipes.

The numerical solutions of the governing equations (Eqs.(1.5) and (1.6)) were found by many researchers and these indicated that the steady-state friction term in the momentum equation was unable to describe pressure wave attenuation to a desired degree. Therefore, the effect of unsteady friction was taken into account or an unsteady friction term was added to the momentum equation (Eq.(1.5)) to improve the match between mathematical model and experimental data.

A variety of models have been proposed by a number of researchers to address the unsteady friction term. Hino et al. [44] (referred to hereafter as 'Hino') assumed that this term related to the instantaneous mean flow velocity V. On the other hand, in [26] an unsteady friction term was added to the instantaneous local acceleration $\partial V/\partial t$. Brunone [18] combined both of these approaches and added an instantaneous convective acceleration $\partial V/\partial x$. Vennatr [85] considered Hino's [44] unsteady friction term to be a diffusion term $\partial^2 V/\partial x^2$. A different approach in [101] included a weighted past velocity change $W(\tau)$ into Hino's unsteady term. Finally, in [94], unsteady friction was represented via consideration of the cross-sectional distribution of instantaneous flow velocity. Details are given below for Zielke's and Brunone's unsteady friction models since these have seen widespread usage.

In [101] the momentum equation (Eq.(1.40)), as derived by Schlichting [72], was considered

$$\frac{\partial^2 v}{\partial r^2} + \frac{1}{r}\frac{\partial v}{\partial r} - \frac{1}{\nu}\frac{\partial v}{\partial t} = \frac{1}{\nu\rho}\frac{\partial p}{\partial t} \tag{1.40}$$

where $v = v(r,t)$ instantaneous velocity, r = radial coordinate, ν = kinematic viscosity, ρ = fluid density, and p = pressure. By applying Laplace transform, Eq.(1.40) becomes

$$\frac{d^2\hat{v}}{dr^2} + \frac{1}{r}\frac{d\hat{v}}{dr} - \frac{s}{\nu}\hat{v} = \frac{1}{\nu}\hat{F} \tag{1.41}$$

and $\hat{F}$ is the Laplace transform of $F = \frac{1}{\rho}\frac{\partial p}{\partial t}$. The last, second-order nonlinear differential equation has the solution

$$\hat{v}(r,s) = \frac{\hat{F}}{s}\left[\frac{J_0\left(i\sqrt{\frac{s}{\nu}}r\right)}{J_0\left(i\sqrt{\frac{s}{\nu}}D\right)} - 1\right] \tag{1.42}$$

where D = the inner radius of pipe, $i = \sqrt{-1}$ and J_0 = the Bessel function of first kind of zero order. The equation that relates the Laplace transform of mean flow velocity $V = \int_0^D 2\pi r v dr/\pi D^2$ and the Laplace transform of the wall shear stress τ_0 is given by

$$\hat{\tau_0}(s) = -\frac{\rho D\hat{F}}{\zeta_1\left(\sqrt{\frac{s}{\nu}}D\right)} \tag{1.43}$$

where $\zeta_1(z) = zJ_0(z)/J_1(z)$ is a modified quotient of Bessel functions of order one

and z a complex number. The inverse transform of $\hat{\tau}_0(s)$ yields

$$\tau_0(t) = \frac{4\rho\nu}{D}V(t) + \frac{2\rho\nu}{D}\int_0^t \frac{\partial V}{\partial t}(u)W(t-u)du \tag{1.44}$$

where W is a function in dimensionless $\tau = \nu t/D^2$ and can be calculated for $\tau > 0.02$

$$W(\tau) = e^{-26.3744\tau} + e^{-70.8493\tau} + e^{-135.0198\tau} + e^{-218.9216\tau} + e^{-322.5544\tau} \tag{1.45}$$

and for $\tau < 0.02$

$$\begin{aligned} W(\tau) = 0.282095\tau^{-1/2} - 1.250000 + 1.057855\tau^{1/2} + 0.937500\tau \\ +0.396696\tau^{3/2} - 0.351563\tau^2 \end{aligned} \tag{1.46}$$

For a transient laminar flow, the friction term in Eq.(1.5) is replaced by

$$\frac{32\nu}{D^2}V(t) + \frac{16\nu}{D^2}\int_0^t \frac{\partial V}{\partial t}(u)W(t-u)du$$

where the first term represents the steady-state friction and the second term for the unsteady friction. Finally, Zielke's unsteady friction model may be formed by the following extended momentum equation and the original continuity equation

$$g\frac{\partial H}{\partial x} + V\frac{\partial V}{\partial x} + \frac{\partial V}{\partial t} + \frac{32\nu}{D^2}V(t) + \frac{16\nu}{D^2}\int_0^t \frac{\partial V}{\partial t}(u)W(t-u)du = 0 \tag{1.47}$$

$$\frac{a^2}{g}\frac{\partial V}{x} + V\frac{\partial H}{\partial x} + \frac{\partial H}{\partial t} + V\sin(\theta) = 0 \tag{1.48}$$

In 1991, Brunone [18] proposed an unsteady friction model in which the friction term in the momentum equation (Eq.(1.5)) was written as $J = J_s + J_u$, where $J_s = \frac{f}{2D}V|V|$ is the original steady-state friction part and J_u is an unsteady friction proportional to the instantaneous local acceleration $\partial V/\partial t$

$$J_u = \frac{k}{g}\delta\frac{\partial V}{\partial t} \tag{1.49}$$

and δ is a piecewise-defined function depending on the sign of $y = V\partial V/\partial t$

$$\delta = \begin{cases} 0 & y \leq 0 \\ 1 & y > 0 \end{cases} \tag{1.50}$$

such that k is a proper coefficient. A drawback is that J_u is not continuous due to presence of δ (Eq.(1.50)). Brunone used the result in [19] and further revised J_u to be

$$J_u = \frac{k_3}{g}\left(1 - \frac{a}{\omega_\nu}\right)\frac{\partial V}{\partial t} \tag{1.51}$$

or

$$J_u = \frac{k_3}{g}\left(\frac{\partial V}{\partial t} - a\frac{\partial V}{\partial x}\right) \tag{1.52}$$

where k_3 = coefficient is obtained empirically or analytically, a = wave speed, and $\omega_\nu = (\partial V/\partial t)/(\partial V/\partial x)$ the ratio of local temporal acceleration to local spatial acceleration. Later, Vitkovsky [86] generalized this to

$$J_u = \frac{k_3}{g}\left(\frac{\partial V}{\partial t} + a * sign(V)\frac{\partial V}{\partial x}\right) \tag{1.53}$$

where $sign(V) = +1$ if $V > 0$ or -1 if $V < 0$ to include the case of flow reversals. It is clear in Brunone's unsteady friction term that the unsteady friction effect represents non-uniformity of the velocity profile and includes the effect of local inertia $\partial V/\partial t$ and the unsteady wall shear stress on flow $a * sign(V)\partial V/\partial x$. Theoretically, k_3 may be estimated as

$$k_3 = \frac{\sqrt{C^*}}{2} \tag{1.54}$$

where C^* is Vardy's shear decay coefficient [82] derived for turbulent transient flows. The Vardy's shear decay coefficient is

$$C^* = \frac{7.41}{Re^{log(14.3/Re^{0.05})}} \tag{1.55}$$

where $Re = DV/\nu$ the Reynolds number. Finally, Brunone's unsteady friction model

is

$$g\frac{\partial H}{\partial x} + V\frac{\partial V}{\partial x} + \frac{\partial V}{\partial t} + \frac{f}{2D}V|V| + \frac{k'}{2}\left(\frac{\partial V}{\partial t} + a * sign(V)\frac{\partial V}{\partial x}\right) = 0 \tag{1.56}$$

$$\frac{a^2}{g}\frac{\partial V}{\partial x} + V\frac{\partial H}{\partial x} + \frac{\partial H}{\partial t} + V\sin(\theta) = 0 \tag{1.57}$$

where $k' = \sqrt{C^*}$.

The friction models reviewed above are all 1D models. For 2D friction models with steel pipes, the unsteady friction effect is estimated by considering the radial variation of flow characteristics. Studies by Bratland [14], Vardy [84], Silva-Araya [76], Pezzinga [63], and Abreu [1], demonstrate a number of detailed approaches based on radial velocity profiles $V(r,t)$ for each cross-sectional area of pipe and time.

1.3 Plastic Pipes: Mathematical Models, Methods and Viscoelasticity

In this section, the models and methods for water hammer in plastic pipes are reviewed. Plastic pipes made of materials like polyvinyl chloride (PVC), polyethylene (PE), or polypropylene behave in a viscoelastic manner which is quite different from that seen in elastic pipes made of steel. Aklonis [2] proposed two approaches to describe viscoelasticity: a macroscopic approach and a microscopic approach. The former is a "mechanical analogue" or "lumped-sum parameters" approach in which a group of springs and dashpots are connected in such a way that the complicated interactions among these elements would resemble the viscoelastic response of real systems. The latter is a "molecular analogue" where viscoelasticity is viewed in terms of a group of flexible molecular threads that ceaselessly change their shape while curling and twisting due to changes in local energy and this leads to a viscoelastic behaviour observed at the larger scale.

The "mechanical analogue" follows two main forms: a Maxwell element that consists of a spring and a dashpot connected in series, or a Voight element where these are connected in parallel. If several of Maxwell's elements are connected in parallel this forms the so-called Maxwell-Weichert model. A few Voight elements connected in series is termed a Kelvin-Voight model. The generalized Kelvin-Voight model depicted in Figure 1.2 includes an extra spring that is attached to the Kelvin-Voight model.

There are many studies of water hammer in plastic pipe based on the generalized Kelvin-Voight model.

In what follows, the Kelvin-Voight viscoelastic model used in this work is derived according to Weinerowska-Bords [91]. A Voight element consists of a spring and a

Figure 1.2: Generalized Kelvin-Voight model [91]

dashpot in parallel in which the Hookean element of spring represents the *elastic* behaviour of the structure described by Hooke's Law

$$\sigma = E\epsilon \tag{1.58}$$

where σ = stress, ϵ = strain, and E = Young's modulus. The Newtonian element of the dashpot plays the role of *viscous* behaviour of the structure described by the Newton's Law

$$\sigma = \eta \frac{\partial \epsilon}{\partial t} \tag{1.59}$$

where η = a viscosity coefficient and t = time. Thus, from a structural point of view, the instantaneous tensile modulus E characterizes the elastic behaviour of the spring and η characterize the viscous response of the element. The total stress of a Voight element is the sum of the stresses of the spring and dashpot

$$\sigma(t) = \epsilon(t)E + \eta \frac{\partial \epsilon}{\partial t} \tag{1.60}$$

Assuming a constant load σ_0 on the Voight element with zero strain at $t = 0$ and integrating Eq.(1.60) gives

$$\epsilon(t) = \frac{\sigma}{E}\left(1 - \exp\left(-\frac{t}{\tau}\right)\right) \tag{1.61}$$

where $\tau = \eta/E$ is called the retardation time of the Voight element.

The generalized Kelvin-Voight model consists of a spring and a finite number N of Kelvin-Voight elements arranged in series. The spring represents the elastic properties of the structure responded immediately after the application of a load,

while the group of Kelvin-Voight elements refer to the further retarded part of stress-strain relation. The total strain ϵ of the material described by the model shown in Figure 1.2 can be expressed as a sum of instantaneous and retarded components, ϵ_0 and ϵ_r, respectively

$$\epsilon = \epsilon_0 + \epsilon_r \tag{1.62}$$

where ϵ_0 = strain of the spring and $\epsilon_r = \sum_{i=1}^{N} \epsilon_i$ total retarded strain of N Kelvin-Voight elements, where ϵ_i is given by Eq.(1.61). The total response of the generalized Kelvin-Voight model to a constant stress σ is given by

$$\epsilon(t) = \frac{\sigma}{E_0} + \sum_{i=1}^{N} \frac{\sigma}{E_i} \left(1 - \exp\left(-\frac{t}{\tau_i}\right)\right) \tag{1.63}$$

The last equation is restated as

$$\epsilon(t) = \sigma J(t) \tag{1.64}$$

where

$$J(t) = J_0 + \sum_{i=1}^{N} J_i \left(1 - \exp\left(-\frac{t}{\tau_i}\right)\right) \tag{1.65}$$

where $J_0 = 1/E_0$ and $J_i = 1/E_i$. $J(t)$ is called *creep function* and describes the viscoelastic properties of the material where J_0 and J_i are the creep compliances.

In summary, plastic pipes possess the properties of viscosity and elasticity. During water hammer in plastic pipe there is an elastic response followed by a gradually retarded deformation of a pipe wall after the pipe is subjected to a sudden constant load (i.e., the surge wave). Previous research work and experiments on water hammer in plastic pipes found that, by comparing with those in steel pipes, the peak wave pressure is lower, wave attenuation is more rapid, and the wave velocity is a function of both the wave frequency and conduit length. In what follows, several studies that relate to the work in Chapter 6 about viscoelastic behaviour in water hammer are presented.

In 1979, Gally [33] began the study of transient flows in pipes to account for viscoelastic behaviour in plastic conduits. He included the circumferential strain

changes of the wall in his characteristic model using:

$$\epsilon = \alpha(p(x,t) - p_0)\frac{D_m}{2e}J_0 + \int_0^t \alpha(p(x,t) - p_0)\frac{D_m}{2e}\frac{dJ(\tau)}{d\tau}d\tau \tag{1.66}$$

The numerical solution was validated by comparison with an experiment using a sudden valve closure to induce the water hammer. In 1995, Pezzenga [65] studied damped unsteady flow oscillations in high-density polyethylene (HDPE) inserted at the upstream of a pipeline in a pumping installation. In that work, it was found that the viscoelastic model described the general phenomenon while the elastic model adequately estimated the maximum and minimum amplitude of pressure and velocity oscillations. In 2003, Bergant [10] used experimental data from a HDPE pipeline to calibrate a transient model without unsteady friction. He applied the Levenberg-Marquardt algorithm to carry out the optimisation and found the creep function $J(t)$ in models with a maximum of six Kelvin-Voight elements. In 2005, Covas [25] created a solver (HTS) including both the unsteady friction and viscoelastic terms in the calculation of hydraulic transients within pressurized polyethylene (PE) pipe systems. In this widely-cited work, the numerical model was validated with several experiments and considered the relative contributions of steady, unsteady, viscoelastic, and fluid-structure interaction (FSI) to investigate the roles these play in the water hammer phenomenon. He found that if only unsteady friction was considered, there was a major disagreement between collected data and numerical results. However, a reduction including only the viscoelastic effect yielded good agreement between data and numerical results and validated the effectiveness of lumped-parameter descriptions such as the Kelvin-Voight model.

In 2010, Duan [30] proposed a 2D model for transient flows in a pressurized PE pipeline. He found that the pressure head attenuation attributable to unsteady friction is comparable to the viscoelastic effect during the initial transient stage. However, the viscoelastic effect becomes dominant both in terms of wave damping and wave phase shift at later stages. He also pointed out that the viscoelastic term within the continuity equation should be referred to as an energy transfer between fluid and pipe wall rather than a form of energy dissipation, a point that highlights the complexity of discussions surrounding the water hammer phenomenon. In 2012, Maniconi [56]

put forth a 2D model in concerning transient behavior of cross-sectional area changes in pressurized liquid flow. His model included both unsteady friction and viscoelastic effects. Numerical results in that work agreed with the laboratory data obtained for the interaction of a surge wave with a partial blockage by a valve, a single pipe contraction or expansion, and a series of pipe contraction/expansion occurring in close proximity. In 2013, Keramat [47] introduced a time-dependent Poisson ratio into the classical water hammer model. The inclusion of time-dependent poisson ratio and unsteady friction allows the usage of viscoelastic creep compliances from independent material creep tests without the need for creep function calibration using flow configuration. In 2014, Pezzenga [64] studied a 2D viscoelastic model calibrated using a microgenetic algorithm on the basis of pressure traces. He found that the viscoelastic model generally presents flatter velocity profiles with respect to the elastic model.

A useful study was published by Weinerowska-Bords [91] where the generalized Kelvin-Voight model was derived in a simpler way and, most importantly, the strength and limitation of various water hammer models were very clearly stated. A number of open questions surrounding current water hammer research on MDPE pipelines were also laid out. In 2015, Weinerowska-Bords [92] analysed the general Kelvin-Voight model with Zielke's unsteady friction term [101] included in the momentum equation

$$g\frac{\partial H}{\partial x}+\frac{\partial V}{\partial t}+\frac{32\nu}{D^2}V(t)+\frac{16\nu}{D^2}\int_0^t\frac{\partial V}{\partial t}(u)W(t-u)du=0 \tag{1.67}$$

An alternative convolution expression of the viscoelastic term in the continuity equation was presented [92] as:

$$\frac{\partial H}{\partial t}+\frac{a^2}{g}\frac{\partial V}{\partial x}+\frac{2a^2}{g}\left(\sum_{i=1}^{N}\left[\frac{J_i}{\tau_i^2}\int_0^t F(x,t-\xi)\exp\left(-\frac{\xi}{\tau_i}\right)d\xi\right]\right)=0 \tag{1.68}$$

By comparing to Zielke's term it was found that both approaches indicate similarities in the forms of impulse response functions and the parameter properties. Weinerowska-Bords' and Zielke's ideas are similar in that they both use the ideas of flow memory and unsteady friction history to describe solutions to the continuity and momentum equations, in terms of a convolution integral.

Chapter 2

Related Mathematical Tools

Water hammer models are described by coupled, nonlinear partial differential equations. Analytical studies of such equations require the use of specialized mathematical tools. In particular, for this research the primary math tools used are the *Method of Multiple Scales* [60] and *Numerical Methods* suited to the treatment of sharp wave fronts. The former is used to find approximate solutions to water hammer models in an asymptotic sense. The latter, together with the method of characteristics provides solutions of the full models that are used to validate analytic approximations.

2.1 The Method of Multiple Scales

The method of multiple scales is illustrated via a simple example and details are in Nayfeh [60] 1973. Consider a linear damped oscillator

$$\frac{d^2x}{dt^2} + x = -2\epsilon\frac{dx}{dt} \tag{2.1}$$

where variables x and t are order of 1, parameter $\epsilon \ll 1$. Suppose its asymptotic expansion is

$$x = x_0 + \epsilon x_1 + \epsilon^2 x_2 + \cdots \tag{2.2}$$

where the successive correction terms are smaller than the preceding terms, i.e., $x_0 < \epsilon x_1 < \epsilon^2 x_2 < \cdots$. The asymptotic expansion

$$x = b\cos(t+\phi) - \epsilon bt\cos(t+\phi) + \epsilon^2\frac{b}{2}[t^2\cos(t+\phi) + t\sin(t+\phi)] + O(\epsilon^3) \tag{2.3}$$

can be found through the following steps.

Step 1: substitute the asymptotic expansion into the given differential equation and equate the like powers of ϵ to get a sequence of differential/partial differential equations each corresponding to the like powers ϵ^0, ϵ^1,ϵ^2, $\cdots$, respectively.

Step 2: solve the first equation corresponding to the power of ϵ^0 and obtain, say, the solution x_0 with some arbitrary constant(s).

Step 3: substitute the solution obtained from Step 1 into the right-hand side of the second equation referring to the power of ϵ^1 and obtain, say, the solution x_1 with the same arbitrary constant(s).

Step 4: further substitute the solutions obtained from Steps 2 and 3 into the right-hand side of the third equation referring to the power of ϵ^2 and obtain, say, the solution x_3.

Step 5: then substitute the solutions obtained from the previous steps back into the asymptotic expansion to obtain, say, the asymptotic solution x for the given differential equation.

The solution (Eq.(2.3)) is a poor approximation to $x(t)$ when t is as large as, or the order of, ϵ^{-1} since the second term ϵt is not small but is order one. In another words, the truncated expansion is valid only for when t below the order of ϵ^{-1}. On the other hand, the exact solution to Eq.(2.1) is

$$x = be^{-\epsilon t}\cos[\sqrt{1-\epsilon^2}t + \phi] \tag{2.4}$$

and the expansion of the exponential and the cosine functions are

$$e^{-\epsilon t} = 1 - \epsilon t + \frac{1}{2}\epsilon^2 t^2 + \cdots \tag{2.5}$$

$$\cos(\sqrt{1-\epsilon^2}t + \phi) = \cos(t+\phi) + \frac{1}{2}\epsilon^2 t\sin(t+\phi) + \cdots \tag{2.6}$$

Again the truncated expansion Eq.(2.5) is valid only for t up to order of ϵ^{-1}, i.e., $t = O(\epsilon^{-1})$. A time scale $T_1 = \epsilon t = O(1)$ is introduced for which the truncated expansion Eq.(2.5) is valid for $t = O(\epsilon^{-1})$. Similarly, a time scale $T_2 = \epsilon^2 t = O(1)$ is introduced for which expansion Eq.(2.6) is valid for $t = O(\epsilon^{-2})$. With the time scales t , T_1, and T_2, Eq.(2.6) is rewritten as

$$\cos(\sqrt{1-\epsilon^2}t + \phi) = \cos(t - \frac{1}{2}T_2 + \phi) + \frac{1}{8}\epsilon^4 t\sin(t - \frac{1}{2}T_2 + \phi) + \cdots \tag{2.7}$$

where the second term $\frac{1}{8}\epsilon^4 t\sin(t - \frac{1}{2}T_2 + \phi) = \frac{1}{8}\epsilon^2 T_2\sin(t - \frac{1}{2}T_2 + \phi)$ is $O(\epsilon^2)$ by referring to scale T_2 and is valid for $T_2 = O(\epsilon^{-2})$ or $\epsilon^2 t = O(\epsilon^{-2})$ or $t = O(\epsilon^{-4})$ by

referring to t. That is, introducing a new time scale $T_4 = \epsilon^2 T_2 = \epsilon^4 t = O(1)$, the truncated expansion Eq.(2.7) is valid for $t = O(\epsilon^{-4})$. This discussion suggests that $x(t;\epsilon)$ depends explicitly on the independent variables t, ϵt, $\epsilon^2 t$, $\epsilon^3 t$, $\cdots$, as well as ϵ.

To determine a truncated expansion valid for all t up to $O(\epsilon^{-M})$, where M is a positive integer, it is necessary to determine the dependence of $x(t)$ on the $M+1$ different time scales T_0, T_1, T_2, $\cdots$, T_M, where

$$T_m = \epsilon^m t \tag{2.8}$$

For $0 < m < (m+1) < M$, the time scale T_{m+1} is *slower* than T_m. Thus we assume that

$$\begin{aligned} x(t;\epsilon) &= \tilde{x}(T_0, T_1, T_2, \cdots, T_M; \epsilon) \\ &= \sum_{m=0}^{M-1} \epsilon^m \tilde{x}(T_0, T_1, T_2, \cdots, T_M; \epsilon) + O(\epsilon T_M) \end{aligned} \tag{2.9}$$

and the time derivative becomes

$$\frac{d}{dt} = \frac{\partial}{\partial T_0} + \epsilon \frac{\partial}{\partial T_1} + \epsilon^2 \frac{\partial}{\partial T_2} + \cdots + \epsilon^M \frac{\partial}{\partial T_M} \tag{2.10}$$

Substituting the time derivative Eq.(2.10) and the expansion Eq.(2.9) into the oscillator equation Eq.(2.1) and equating the like powers of ϵ, the equations for x_0, x_1, x_2, $\cdots$, x_M may be found. Solutions of these equations contain arbitrary functions of the time scales T_0, T_1, T_2, $\cdots$, T_M. The general conditions required to determine these function are that the correction term must be small compared to all preceding terms in the expansion.

To illustrate, the steps listed above are followed to get the three equations corresponding to the like powers of ϵ^0, ϵ^1, and ϵ^2, respectively

$$\frac{\partial^2 x_0}{\partial T_0^2} + x_0 = 0 \tag{2.11}$$

$$\frac{\partial^2 x_1}{\partial T_0^2} + x_1 = -2\frac{\partial^2 x_0}{\partial T_0^2} - 2\frac{\partial^2 x_0}{\partial T_0 \partial T_1} \tag{2.12}$$

$$\frac{\partial^2 x_2}{\partial T_0^2} + x_2 = -2\frac{\partial x_1}{\partial T_0} - 2\frac{\partial^2 x_1}{\partial T_0 \partial T_1} - \frac{\partial^2 x_0}{\partial T_1^2} - 2\frac{\partial^2 x_0}{\partial T_0 \partial T_2} - 2\frac{\partial x_0}{\partial T_1} \tag{2.13}$$

with solutions

$$x_0 = B_0(T_1, T_2)e^{iT_0} + \bar{B}_0(T_1, T_2)e^{-iT_0} \tag{2.14}$$

$$x_1 = B_1(T_1, T_2)e^{iT_0} + \bar{B}_1(T_1, T_2)e^{-iT_0} - \left(B_0 + \frac{\partial B_0}{\partial T_1}\right) T_0 e^{iT_0} - \left(\bar{B}_0 + \frac{\partial \bar{B}_0}{\partial T_1}\right) T_0 e^{-iT_0} \tag{2.15}$$

Noting that ϵx_1 must be smaller than x_0, $\epsilon T_0 = \epsilon t$ must be small or the solution x is only valid for $t < \epsilon^{-1}$. In order to obtain an expansion valid for t as large as $O(\epsilon^{-1})$, the *secular* terms $T_0 e^{iT_0}$ and $T_0 e^{-iT_0}$ must vanish and this fixes the unknown function B_0. All other unknown functions arising from integration can be determined sequentially in like manner by knocking off secular terms (see [60]).

The final solution

$$x = be^{-\epsilon t}\cos(t - \frac{1}{2}\epsilon^2 t) + R \tag{2.16}$$

is in a good agreement with the exact solution Eq.(2.4) given $R = O(\epsilon^4 t)$.

To summarize, the given differential equation(s) must first be nondimensionlized. Secondly, small parameter(s) must be defined; in this work (Yao [99], Yao [98], and Yao [100]) it was an artificial parameter ϵ. This was done based upon available experimental data that set the context and thus the size of all dimensionless parameters. The discovery of a multiple-scales approximation follows no set procedure but forms a significant component of the work. However, it is clear that a good understanding of the problem of interest, and experimental data relating to it, are necessary starting points. In addition, it was found that a *rescaling* of the non-dimensional form was required in order to construct an approximation that was regular (not singular), in the limit of the small parameter $\epsilon \to 0$.

The specific water hammer problems considered herein are presented in Chapters 4–6. The first approximation of the model gives the solution of pressure and velocity wave functions as $H = f(\lambda(X - q))$ and $V = f(\lambda(X - q))$, where $q = t/a' = t/\sqrt{C_4'} = t/\epsilon^2$ and $t = t'/T$ and these parameters are properly defined, e.g., in Chapter 4. It will be seen that q is the dimensionless water hammer fast time scale and t is the dimensionless rigid column slower time scale. Since $t = \epsilon^2 q$, two time scales are recognized to exist in the water hammer problem and this is similar to $t = T_2$ and $q = T_0$ of the example demonstrated above. T_2, the rigid column time scale, is much slower than T_0 which is the fast water hammer time scale. For the application

involving water hammer in plastic pipe (Chapter 6), a third time scale $s = T_1$ is found and represents what is defined in said application as a "weak strain-rate feedback" due to the viscoelasticity of the pipe wall. The choice of an asymptotic expansion is a 'guess' based on the solution structure and experimental data. The secular terms, as described above, are found in Eq.(6.34) and the constraints associated with their removal lead to the desired pressure wave attenuation function.

2.2 Numerical Methods

Here we illustrate two widely-used numerical methods in water hammer studies: the finite-deference method for the characteristic equations (Eqs.(1.36)–(1.39)), details are gievn in Streeter and Wylie [79] 1967, and the Preissmann scheme (a four-point difference method [66] 1961) for the water hammer model (Eqs.(1.25) and (1.26)) with steady friction in a horizontal pipeline for lower Mach number ($V \ll a$) transient flow.

2.2.1 Finite-Difference Method for Characteristic Equations

According to Streeter and Wylie [79] 1967, the two characteristic curves C^+ and C^- intersect at the point P are depicted in Figure 2.1. Suppose that the values of piezometric head H_A, H_B and velocity V_A, V_B are known at the points A and B initially. To obtain head and velocity values H_P and V_P at point P at the time t_P, we approximate the time and spatial derivatives along curves C^+ and C^-, one step from A to P and from B to P as

$$\frac{\partial H}{\partial t} \approx \frac{H_P - H_A}{t_P - t_A} \tag{2.17}$$

$$\frac{\partial H}{\partial t} \approx \frac{H_P - H_B}{t_P - t_B} \tag{2.18}$$

$$\frac{\partial V}{\partial t} \approx \frac{V_P - V_A}{t_P - t_A} \tag{2.19}$$

$$\frac{\partial V}{\partial t} \approx \frac{V_P - V_B}{t_P - t_B} \tag{2.20}$$

then Eqs.(1.36), (1.37), (1.38), and (1.39 become the following equations

$$V_P - V_A + \frac{g}{a}(H_P - H_A) + \frac{f}{2D}V_A|V_A|(t_P - t_A) \tag{2.21}$$

$$x_P - x_A = a(t_P - t_A) \tag{2.22}$$

$$V_P - V_A - \frac{g}{a}(H_P - H_B) + \frac{f}{2D}V_B|V_B|(t_P - t_B) \tag{2.23}$$

$$x_P - x_B = a(t_P - t_B) \tag{2.24}$$

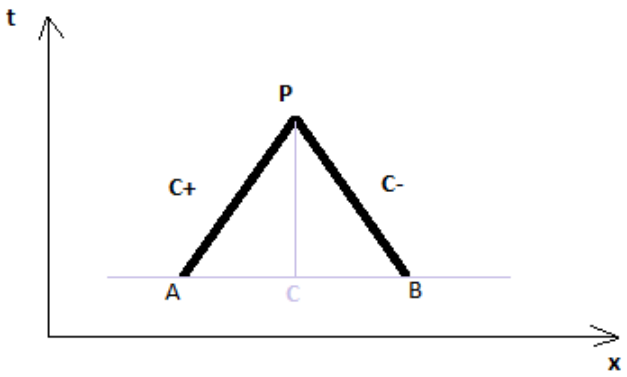

Figure 2.1: Characteristic curves in the x–t plane

In this way, a grid of characteristics is established in which the horizontal pipe of length L is made of N equal reaches $\Delta x = L/N$. The time step advance is determined by $\Delta t = \Delta x/a = t_P - t_A = t_P - t_B$ and the characteristic curves from the sections that intersect at other locations, i.e., the characteristic curves from A and B intersect at P and this is cross-section C, as described in Figure 2.1. Combining Eqs.(2.21) and (2.23) at any interior section i and eliminating H_{P_i} gives the V_{P_i} expressions

$$V_{P_i}^{(j+1)} = \frac{1}{2}\left[V_{i-1}^{(j)} + V_{i+1}^{(j)} + \frac{g}{a}(H_{i-1}^{(j)} - H_{i+1}^{(j)}) - \frac{f\Delta t}{2D}(V_{i-1}^{(j)}|V_{i-1}^{(j)}| + V_{i+1}^{(j)}|V_{i+1}^{(j)}|)\right] \tag{2.25}$$

In a similar manner H_{P_i} is obtained

$$H_{P_i}^{(j+1)} = \frac{1}{2}\left[H_{i-1}^{(j)} + H_{i+1}^{(j)} + \frac{g}{a}(V_{i-1}^{(j)} - V_{i+1}^{(j)}) - \frac{a}{g}\frac{f\Delta t}{2D}(V_{i-1}^{(j)}|V_{i-1}^{(j)}| + V_{i+1}^{(j)}|V_{i+1}^{(j)}|)\right] \quad (2.26)$$

where subscripts (i, j) representing the location of a calculation at $x = i\Delta x$ and $t = j\Delta t$. These last two equations permit the calculation of $V_{P_i}^{(j+1)}$ and $H_{P_i}^{(j+1)}$ at the advance level j on the time–axis based on the known values from either initial condition or from a previous stage of the calculation $V_{P_i}^{(j)}$ and $H_{P_i}^{(j)}$.

When the calculations after the first time step reach the boundaries, the boundary conditions of the water hammer problem start to influence the interior points and must be provided. Suppose that a reservoir is maintained at fixed level at the upstream (left or $i = 0$) end, then $H_{P_0} = H_{0R}$, H_{0R} = constant piezometric head at the reservoir, then (treating Section B at section 1 and Section P at section 0 in Figure 2.1), V_{P_0} is obtained

$$V_{P_0} = V_1 + \frac{g}{a}(H_{P_0} - H_{P_1}) - \frac{f\Delta t}{2D}V_1|V_1| \quad (2.27)$$

Suppose also that a gradually-closed valve is at the downstream (right or $i = N$) of pipe. The discharge out of the valve (treated as a orifice) is give by Daugherty [29]

$$V_{P_N} = -\frac{C_4}{2} + \sqrt{(\frac{C_4}{2}^2 + C_3C_4)} \quad (2.28)$$

and H_{P_N} is obtained through

$$H_{P_N} = \frac{C_2 - V_{P_N}}{C_2} \quad (2.29)$$

where C_2, C_3, and C_4 are known functions related to pipe cross-sectional area, valve-discharge coefficient, and area of valve opening. Thus, adding in proper initial and boundary conditions a numerical approximation to the solution of the water hammer problem may be found at any desired time.

2.2.2 Preissmann Scheme

The Preissmann scheme (Shamaa [75]) is a "weighted four-point" approach that leads to a widely applied implicit finite-difference method that has a simple structure for

both the velocity V and pressure head H at each grid point. The computational grid

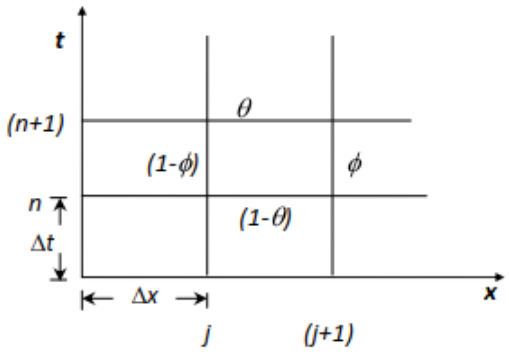

Figure 2.2: Computational grid for the Preissmann scheme [75]

used to formulate the implicit finite-difference scheme is depicted in Figure 2.2. Its advantage lies in the usage of unequal distance steps that are particularly important for rapid transients. The method also supports unequal time steps and this is particularly useful in the case of water hammer that have sharp wave fronts in space and time. In this scheme, the four grid points from the j^{th} and $(j+1)^{\text{th}}$ time lines are used to approximate the terms in the differential equations

$$\frac{\partial f}{\partial t} = \phi \frac{f_{j+1}^{n+1} - f_{j+1}^{n}}{\Delta t} + (1-\phi)\frac{f_{j}^{n+1} - f_{j}^{n}}{\Delta t} \tag{2.30}$$

$$\frac{\partial f}{\partial x} = \theta \frac{f_{j+1}^{n+1} - f_{j}^{n+1}}{\Delta x} + (1-\theta)\frac{f_{j+1}^{n} - f_{j}^{n}}{\Delta x} \tag{2.31}$$

$$f(x,t) = \theta\left[\phi f_{j+1}^{n+1} + (1-\phi) f_{j}^{n+1}\right] + (1-\theta)\left[\phi f_{j+1}^{n} + (1-\phi) f_{j}^{n}\right] \tag{2.32}$$

where $f_j^n = f(j\Delta x, n\Delta t)$, Δx = incremental reach length, Δt = increaemental time, ϕ = a weighting coefficient for distributing terms in time, $0 \leq \phi \leq 1$ and θ a weighting coefficient for distributing terms in space, $0 \leq \theta \leq 1$. The variables with subscripts n in the above expressions are known and the variables with subscripts $n+1$ are the unknowns. Applying these numerical approximations to the governing water hammer equations yields in general

$$CH_j^{n+1} + DV_j^{n+1} + EH_{j+1}^{n+1} + FV_{j+1}^{n+1} + G = 0 \tag{2.33}$$

$$C'H_j^{n+1} + D'V_j^{n+1} + E'H_{j+1}^{n+1} + F'V_{j+1}^{n+1} + G' = 0 \tag{2.34}$$

The last two algebraic equations are nonlinear and an iterative solution technique is required. As there are $N-1$ grids in a time line, a total of $2(N-1)$ equations are formed for one time line between the upstream and downstream boundary. Two boundary conditions provide the necessary $2N$ additional equations to close the system.

Lots of researchers prefer using a ϕ value of 0.5 and approximate the time derivative at the center of grid between j^{th} and $(j+1)^{\text{th}}$ on the time lines. The weighted Preissmann scheme is unconditionally stable for any time step if the value of θ is selected between 0.5 and 1.0, different values of θ are used depending on the particular application. Furthermore, analysis also reveals that the unconditional stability and good accuracy is maintained if θ value runs between 0.55 and 0.6. Finally, the Newton-Raphson iterative technique is most commonly used for the solution of the $2N$ equations in $2N$ variables for an implicit numerical solution of the nonlinear governing equations.

The finite-difference method for the characteristic equations discussed above is an implicit method in which a large number of small time steps are required in order to satisfy the Courant stability condition for the maximum allowable time step. The requirement to satisfy Courant condition usually makes the method of characteristics with explicit techniques very inefficient due to increased computational time. On the other hand, the Preissmann scheme is an *implicit* method allows the use of variable time and spatial steps and this makes it more convenient and efficient than the method of characteristics.

Chapter 3

Research Overview

In this Chapter, the research motivations are provided; water hammer models are derived; the multiple scales method is detailed; and general thoughts on how the multiple scales was set up are given. Related literature reviews can be found in Chapter 1 and the summary of the results and conclusions are in Chapter 7. This Chapter is served to link Chapters 1–2 and Chapters 4–6 that contain the three papers that have appeared in peer-reviewed journals.

3.1 Paper 1 (appears in Chapter 4): Role of Rate of Valve Closure

The research in Chapter 4 was motivated in four ways. Firstly, classic water hammer governing equations (Eqs.(1.5) and (1.6)) and their variants proposed by others in numerous applications are coupled non-linear partial differential equations. Approximate analytic solutions to these models are rarely considered save for *ad hoc* methods applied to a few, simple cases and numerical schemes are only sufficient to provide a qualitative insight. Secondly, formal (as opposed to *ad hoc*) analytic approximations can give quantitative insight to water hammer behaviour and its dependence on the model parameters which is not easily available from numerical solutions. Thirdly, in Han et al. [42], a generic analytical solution for the water hammer wave attenuation function initiated by valve opening was obtained but valve closure that leads to flow reversals was not considered. Finally, an *ad hoc* analytic approximation [52] to a simplified form of the water hammer equations in (Eqs.(1.25) and (1.26)) is found under the assumption of steady friction

$$\Delta P(x) = \pm \rho c (\Delta V)_0 \frac{e^{-\frac{fV_0}{2Dc}x}}{1 + \frac{(\Delta V)_0}{2V_0}[1 - e^{-\frac{fV_0}{2Dc}x}]} \tag{3.1}$$

where c is a wave speed equivalent to c_p used in this thesis, f is the Darcy-Weisbach friction factor, and V_0 is the steady-state velocity. Eqs.(1.25) and (1.26) were converted to compatible characteristic equations, valid along the characteristic curves satisfying $dx/dt = \pm c$. Their results were compared with those found using the method of multiple scales as derived in Chapter 4 and the limitations of such *ad hoc* approaches were identified.

3.1.1 Model and Assumptions

The water hammer model considered here assumes, among other things, that the fluid has no cavitation, entrained air, and column separation; and is not subject to leakage or blockages. It also assumes that the fluid is contained in a pressurized conduit which has linear elastic properties and is supported without longitudinal motion during water hammer. Pipe wall is assumed made of isotropic material and its thickness and cross-sectional area are to be constant throughout the conduit. The flow conditions include low Mach number, steady friction described by a Darcy-Weisbach friction factor, and no unsteady friction and effects of fluid-structure interaction (FSI).

The model presented in Chapter 4 was created by replacing the friction term in Eq.(1.25) with a more general accounting of friction (details given in Chapter 4), i.e., full pipe length friction loss, $(g/L)\Delta h$, where

$$\Delta h = rV + sV^2 \tag{3.2}$$

This allows fully-developed turbulent flows ($r = 0$), laminar flows ($s = 0$), and partially developed turbulent flows ($r > 0, s > 0$).

3.1.2 Multiple Scales Development

Nondimensionalization was used to distinguish the order (or relative importance) of the terms in Eqs.(4.5). The dimensionless lumped-parameter coefficients C_1, C_2, C_3, C_4, and C_5 were obtained. The experimental parameters ([80], [81]) provided in Table 4.1 allowed the introduction of an artificial parameter $\epsilon = 1/\sqrt{c_p}$. With it, the orders of all dimensionless coefficients were assigned based on the parameter magnitudes given in Table 4.1. The assumption of $O(1)$ to the coefficients C_1, C_2, and C_3 was a

choice, consistent with the designing experimental parameters considered in Chapter 4.

The wave form of pressure head H and velocity V in Eq.(4.12) was of a reduction of Eqs.(4.5). These forms were then extended to more generalized forms, $H = 1/(\epsilon\sqrt{c_4})\ f[X - \tau/(\epsilon\sqrt{c_4})]$ and $V = g[X - \tau/(\epsilon\sqrt{c_4})]$, for equations given in Eqs.(4.5) where all terms were retained. It was from these forms that the multiple scales form was hypothesized. In particular, $t = \tau/\epsilon$ represented the fast wave transit timescale in $O(1)$ while $\tau = \epsilon t$ represented the slow-varying trending timescale in $O(\epsilon)$. With the multiple scales applied to the asymptotic approximation of pressure wave attenuation, the wave form of H and V was chosen to have the dependence on these timescales; therefore $H = H(X, t, \tau)$ and $V = V(X, t, \tau)$.

3.1.3 Pressure Wave Attenuation

The water hammer is a phenomenon constrained by boundary conditions and undergoes flow reversals. It was shown in Chapter 4 that the governing equations are unchanged under flow reversals so long as the fluid velocity has one sign within the conduit at all times. This constraint is violated, for example, in the presence of cavitation. Such a constraint is important since the multiple-scales is used to determine the form of the pressure wave attenuation in the absence of any boundary conditions.

Both the head and velocity are represented in the asymptotic expansion as the sum of a trending, slowly-varying component and a superimposed fast-varying wave with a slowly-decaying amplitude. The pressure wave attenuation $P_1(\tau)$ is the slowly-decaying amplitude of the fast-varying wave and found to satisfy an ordinary differential equation with complex coefficients where its magnitude is

$$|P_1(\tau)| = \frac{e^{-C_2\tau/2}}{1 + C_3/(2C_2)\ (1 - e^{-C_2\tau})}$$

The trending velocity is found to satisfy a similar formula and in the case of C_2 small, which is typical, there is a simple relation between the pressure wave attenuation and the trending velocity where

$$V_0(\tau) \approx \frac{1}{2}|P_1(\tau)| \tag{3.3}$$

Thus, the dependence of the pressure wave attenuation $|P_1(\tau)|$ on the model parameters and its link to the trending velocity provide a very simple and direct insight into the way that the model represents the water hammer phenomenon that was unavailable before.

It is useful to note that the results in Chapter 4 do bear a superficial resemblance to a widely-used result [52] found via an *ad hoc* approximation (this point was addressed during reviews of the paper before it was published). However, a point not noted in Chapter 4 is that the results in [52] are valid for very small τ and should not be extended to order one values of the time τ. This becomes clear when the results in [52] are compared with those found in Chapter 4. Note that there was a typo in the published paper (re Chapter 4) where it stated $V_0(\tau) = \frac{1}{2}|P_1(\tau)|$. Actually it is Eq.(3.3) valid for $C_2 \ll 1$.

3.1.4 Strengths and Limitations

The strength of the $|P_1(\tau)|$ formula is that it is simple, its derivation is clearly linked into the global differential equations and it ultimately corrects the results in Eq.(3.1) by [52]. The results presented in Chapter 4 are valid in the presence of flow reversals where the fluid has a single direction at any one time $V \geq 0$ or $V \leq 0$. The trending velocity $V_0(\tau)$ in Eq.(3.3) was first identified here and follows a similar result as that found for the wave attenuation. The results were also shown to be extendable to valve closure times exceeding the wave transit time scale which was not available before.

The limitations of this study conducted in Chapter 4 is that it may only be used for water hammer where the flow is uni-directional. Hence, it cannot handle cavitation since that involves multi-directional flows within the conduit at any one time. Also $V_0(\tau)$ was based on averaging that was not proven and which required a weak x dependence. Hence, for example, the method is not appropriate to represent linepacking since that introduces a strong x dependence.

3.2 Paper 2 (appears in Chapter 5): Steady vs. Unsteady Friction

The research in Chapter 5 was motivated by Brunone's unsteady friction model [17] and [20] in which he related the unsteady fiction to the local inertia $\partial V/\partial t$ and local convection $a\delta\partial V/\partial x$ whereas $\delta = -1$ when kinetic energy increased; $\delta = 0$ when

kinetic energy decreased. Brunone's unsteady friction was empirical result that was qualitatively verified by the experiments carried out in 1990 by [16], [39], and [41]. This model was clearly appropriate for analysis using the techniques developed in Chapter 4 because the parametric analysis of Brunone's model (Chapter 5) could provide insight to the wave attenuation with unsteady friction. The second observation emerged from this work was that the extended steady friction model for partially developed turbulence [98] provided an alternative explanation for the increased damping of pressure wave without the need for an unsteady friction term.

3.2.1 Water Hammer Model and Assumptions

The similar assumptions in Section 3.1.1 were made except that the fluid flow experienced unsteady friction. The water hammer model consisted of the momentum equation [Eq.(5.1)] in which the Brunone's unsteady friction term gJ_u was added whereas J_u in Eq.(1.52) was further generalized by [87]. The continuity equation [Eq.(5.2)] remained the same as Eq.(4.4). Note that there were typos in the published paper (re Chapter 5) where they stated "head is $h(x,t)$" and "fluid velocity is $v(x,t)$". Actually they are "head is $h(x,t')$" and "fluid velocity is $v(x,t')$".

3.2.2 Multiple Scales Development

The nondimensionlization was carried out for the model equations [Eqs.(5.1) and (5.2)] following Chapter 4. The obtained dimensionless equations are in Eq.(5.4). The first approximation

$$H_X + (1 + B_1)V_\tau = 0 \tag{3.4}$$

$$V_X + c_4\epsilon^2 H_\tau = 0 \tag{3.5}$$

gave the pressure head $H(X,\tau)$ and velocity $V(X,\tau)$

$$H = \frac{1}{\epsilon}\sqrt{\frac{1+B_1}{c_4}} f\left(X - ct\right)) \tag{3.6}$$

$$V = g\left(X - ct\right)) \tag{3.7}$$

where $\epsilon^2 = O(1/c_p)$, $c = 1/\sqrt{(1+B_1)c_4}$. From this observation, two timescales were identified that a fast wave transit timescale $t = \tau/\epsilon$; a slow trending timescale $\tau = \epsilon t$. Thus, wave attenuation H and V depended on these timescales t and τ were extended to $H = H(X,t,\tau)$ and $V = V(X,t,\tau)$, respectively. The asymptotic expansion included the forms $P_j(\tau)F_{nj}(\alpha_n(X-ct))$ for H and the forms $P_j(\tau)G_{nj}(\beta_n(X-ct))$ for V, where $\alpha_n = a_n + in$ and $\beta_n = b_n + in$. This led to the inclusion of Brunone's unsteady friction dimensionless coefficients B_1 and B_2 in the final wave attenuation function $|P_1(\tau)|$. Note that there were also typos in the published paper (re Chapter 5) where they stated "$P_j(\tau)G_{nj}(\alpha_n(X-ct))$" and "$P_j(\tau)F_{nj}(\beta_n(X-ct))$". Actually they are "$P_j(\tau)G_{nj}(\beta_n(X-ct))$" and "$P_j(\tau)F_{nj}(\alpha_n(X-ct))$".

3.2.3 Pressure Wave Attenuation

The wave attenuation function $|P_1(\tau)|$ was obtained in Eq.(5.20) from which it was clearly seen that the Brunone's unsteady friction contributed to the classic steady friction model via the factor $\exp(\Re(a_1)B_1B_2)$. The unknown $a_1 = -1$ was chosen as a constant under the assumption that the wave attenuation was of weak spatial dependence and dependent on time τ. Numerical solutions using the experimental parameters from [8] were found to the following three cases: (i) set $C_2 = B_1 = B_2 = 0$, which considered only the Darcy-Weisbach steady friction; (ii) set $C_2 = 0$, $B_1 = 0.0123$, and $B_2 = 207$, which considered only the Brunone's unsteady friction; (iii) set $C_2 = B_1B_2$ and eliminate Brunone's unsteady friction terms from Eq.(5.1), which had the same effect as in case (ii). The results showed two things that: (a) $|P_1(\tau)|$ approximated cases (i) and (ii) very well, and (b) the extended steady friction model with the viscous coefficient C_2 taken as the product of Brunone's coefficients B_1 and B_2 gave the *same* approximation to the wave attenuation excepting a negligible difference in the phase shift $\tau = 0.0004$.

3.2.4 Strengths and Limitations

The strength of the approach is that Brunone's model of unsteady friction simply introduces an additional term in the pressure wave attenuation $|P_1(\tau)|$ given in Eq.(3.3), i.e., $\exp(-B_1B_2)$. The periodic averaging of velocity for flow reversals as in Chapter 4 was considered and was found to apply for the range of parameters considered

here. The intriguing possibility of using the extended steady friction model to replace Brunone's unsteady friction model was evident from the pressure wave attenuation function and validated via the numerics. This point raises the point that, to date, it is not clear whether an extended steady friction model or an extended unsteady friction model are more appropriate. This observation of an approximate equivalence between the two concepts would not be possible without access to the pressure wave attenuation found here for the Brunone's unsteady friction.

A weakness of this work is that $a_1 = -1$ is only qualitatively justified and this work is only valid for uni-directional flows and thus, cavitation and other similar applications are not described by this work. Although it may be possible to extend this work to time-varying valve closures, this case was not considered here.

3.3 Paper 3 (appears in Chapter 6): Role of Strain-Rate Feedback

Polymer pipes have a high resistance to the effects of chemicals, ruptures, and erosion and given their longer-term lower cost they have been widely adopted in water supply systems. Many researchers have studied water hammer in polymer pipes experimentally and numerically since 1979 (Gally [33]). In this early work it was found that the viscoelatic nature of polymer pipe materials provided greater wave attenuation than that seen in elastic (i.e., steel) pipe. Hence, a generalized Kelvin-Voight (KV) model with several Kelvin-Voight elements connected in series to a spring was created and the model was able to successfully describe experimental data. Due to the lumped-parameter nature of this "mechanical analogue", prediction of parameters in the KV model was not possible. In fact, KV parameters exceed those predicted from creep tests by an order of magnitude and, to date, there is no mechanism to explaining this observation.

The motivations for the research conducted in Chapter 6 were to answer two main questions: (i) identify the pressure wave attenutation dependence on the KV model parameters and (ii) use the results of (i) to explain why the KV parameter values are an order of magnitude larger than those predicted from creep tests. The results obtained in Chapter 6 answered these two questions for water hammer dynamics in polymer pipes as observed by Mitosek [59] and in many other studies. Specifically, it was found that the water hammer dynamics in these experimental studies may

be described as belonging to a class of problems where this is a "weak strain-rate feedback". A result that emerged from the study was the concept of model categorization as a way of predicting the magnitudes of lumped-parameters expected within an experiment based only on historical experimental results.

3.3.1 Water Hammer Model and Assumptions

The model assumptions were similar to those stated in Section 3.1.1. The experiment parameters used for comparison (see Table 6.1) was given by Mitosek [59].

The model was given in Eqs.(6.1), (6.2), and (6.4) in which the momentum equation only contained quasi-steady friction term without extended friction or unsteady friction. Viscoelasticity is modelled by the inclusion of a viscous strain-rate term added to the continuity equation along with a third strain equation. All convective accelerations in the governing equations were assumed to be relatively small compared with the retained terms in the equations.

3.3.2 Nondimensionlization and Rescaling

A standard nondimensionlization was carried out following Chapters 4–5. Unlike these previous studies, the artificial small parameter ϵ was not apparent and required a full *rescaling* for its discovery.

The purpose of rescaling was to identify the timescale q corresponding to the pressure wave transit time. To this end, it was necessary to set $\tilde{H} = A'\bar{H}$, $\tilde{V} = B'\bar{V}$, $\tilde{W} = C'\bar{W}$, and $t = a'q$. These scales were found using a "balancing" technique based on the assumption that the dependent variables were $O(1)$ in magnitude with respect to a reference timescale q and the wave transit timescale q was assumed to be unity. In this sense, the wave transit importance, with respect to the timescale q, was found in the rescaled equations and the fast-varying wave was apparent.

A further examination of the parameters in Tables 6.3 and 6.4 suggested the choice of an artificial parameter $\epsilon = 0.1$. At this stage it was also apparent that this choice implied that the dimensionless parameter for the velocity rescaling is $B' = O(\epsilon)$. With ϵ available, all parameters in Table 6.5 may be reduced to their ϵ dependence and this sets the context in which the approximation to the pressure wave attenuation will be made.

3.3.3 Multiple Scales

Given a wave transit timescale $q = t/a' = t/\sqrt{C_4'} = t/O(\epsilon^2)$, the trending timescale was $t = \epsilon^2 q$. Note in Chapter 6, the trending timescale was denoted by $\tau = \epsilon^2 q$ to avoid confusion. Substitution of multiple scales τ and q led to the requirement for an intermediate timescale $s = \epsilon q$ that is slower than q and but faster than τ in order to incorporate the strain-rate in the continuity equation into the expansion as suggested from the experimental parameters. This timescale captured the viscoelasticity effect which retarded the response to the sudden pressure load of pressure caused by the instantaneous valve closure. This was represented in the order of $O(\epsilon)$ strain-rate term $\epsilon \partial W/\partial q$ in the continuity equation that weakly fed back the strain rate to influence the pressure head H and velocity V. Thus, the water hammer was seen to evolve over three timescales and therefore $H = H(X, q, s, \tau)$, $V = V(X, q, s, \tau)$, and $W = W(X, q, s, \tau)$. The wave attenuation now operated over two timescales s and τ (see Figure 6.1) and the fast wave transit form depended on X and q.

3.3.4 Pressure Wave Attenuation

A closed-form analytic approximation of wave attenuation to the first mode $|P_0(s, \tau)|$ was obtained and verified both by comparison with experimental data and a numerical solution found using the Preissmann scheme. $|P_0(s, \tau)|$ was seen to depend only on two dimensionless groups: B and K_2. The former represented the dimensionless velocity rescaling and brought in the steady friction contribution. The latter represented the coupling interaction between the fluid and the pipe wall due to the viscoelasticity. $|P_0(s, \tau)|$ also showed that the steady friction affected the scale of the pressure wave attenuation but not its dynamics.

3.3.5 Parameter Estimation and Cost Function

The $O(1)$ dimensionless parameters A, B, K_1, and K_2 from the final rescaled dimensionless equations provided a means to form a cost function $R(\epsilon)$ (Eq.(6.42)). A minimum value of $R(\epsilon)$ was attained at $\epsilon \approx 0.1$ over the full range of parametric choices seen in the water hammer literature and this independently verified the choice of ϵ made earlier from a single set of experimental data.

3.3.6 Strengths and Limitations

The strengths lie in that: (i) a simple, closed-form wave attenuation form was obtained that clearly demonstrated how the viscoelasticity was predicted by the generalized KV model to influence the water hammer dynamics; (ii) the majority of studies published in the literature were found to adhere to a "weak strain-rate feedback" classification; (iii) it was shown that the KV Young's modulus must exceed the Young's modulus found from creep testing if the model is expected to represent weak strain-rate feedback during water hammer; (iv) any experimental apparatus that fits into a weak strain-rate classification has parameter magnitudes that are known *a priori*.

The limitations of this work include results that could not be extended to the situation where cavitation and linepacking are present. Also these results only applied to experimental situations where there was "weak strain-rate feedback". In addition, it was not possible to find a better estimate for the theoretical wavespeed. The choice made here was to follow the literature where the empirical wavespeed is predicted by typically increasing the theoretical wavespeed by approximately 25%.

Chapter 4

Analysis of Water Hammer Attenuation in Applications with Varying Valve Closure Times

E. Yao; G. Kember; and D. Hansen

Published in: Journal of Engineering Mechanics, 2015, 141(1): 04014107
URL: http://ascelibrary.org/doi/abs/10.1061/%28ASCE%29EM.1943-7889.0000825

4.1 Abstract

A multiple scales asymptotic analysis is developed to describe the attenuation of a water hammer pressure wave initiated by a time-varying valve closure. The analytical results expose a simple rule-of-thumb relationship between water hammer pressure wave attenuation and the periodic average of the absolute flow velocity that is predicted by a quasi-steady friction model. The effect of flow reversals on the pressure wave attenuation is examined through comparison with a similar method applied to the water hammer generated during flow establishment, wherein flow reversals do not occur and there is a nonzero net flow. Although the analytical description is based on the assumption that the water hammer is generated by a sudden valve closure, its practical usefulness is extended by using the numerical solution as a guide to demonstrate its validity for a range of valve closure durations. A qualitative upper limit on closure times to which the analytic results may be applied is also found. All results are numerically verified using the method of characteristics. DOI: 10.1061/(ASCE)EM.1943-7889.0000825. *© 2014 American Society of Civil Engineers.*

Author keywords: Water hammer; Nonlinear; Pressure wave attenuation; Varying valve closure time; Multiple scales analysis.

4.2 Introduction

Water hammer in pipes is typically initiated either by changes in flow caused by valve closure/opening, the flow establishment problem (Lam and Leutheusser [50] 2002), or the flow stoppage problem (Ghidaoui et al. [36] 2005). These changes cause velocity and pressure wave transients that travel along the pipe at the wave celerity. The wave morphology is strongly dependent upon the rapidity of the valve closure.

Analytical studies of water hammer equations confined to sudden valve opening/closings have been mainly designed to meet a particular need and fit roughly into two groups. The first are analytic solutions suited to verify numerical methods or to functions as part of an analytic numerical method. An example is analytic solutions of linearized models, such as that for fluid-structure interactions (Li et al. [53] 2003) that are designed as an alternative to the method of characteristics. The second are parametric analyses that give insight into water hammer phenomenology. These include stability analyses (Ghidaoui and Kolyshkin [34] 2001) and studies of time scale parametric dependence (Tijsseling and Vardy [80] 2004, [81] 2008).

Many studies have focused on the advancement of numerical methods designed, for example, to capture second-order effects in multiphase flows (Leon et al. [51] 2008), wavelet-Galerkin approaches suited to complex geometries (Sattar et al. [71] 2009), or characteristics methods to approximate effects, such as cavitation and column separation, which are outlined in Bergant et al. ([11] 2008a, [12] 2008b). A wide-ranging review covering theoretical and practical aspects of water hammer can be found in Ghidaoui et al. ([36] 2005).

Numerical methods are generally established as a tool for complex applications, whereas analytic methods can provide insight into the basic physics of a phenomenon that may be less available from the outcomes of numerical studies. It is from this point of view that the authors present a multiple scales aysmptotic approximation that has seen much application in the study of physical systems with more than one time scale. The study here is on the classical water hammer equations that have been mildly generalized to include partially developed turbulence. The authors include the common assumptions to a linearly elastic and constant thickness pipe wall, adequate longitudinal restraint to suppress inertial effects and consequent fluid-structure interaction, and frequent axial expansion joints. In addition, the fluid does

not cavitate (no column separation), and there are no leakage or blockages.

The multiple scales asymptotic method (Bender and Orzsag [6] 1978) developed here for water hammer with flow reversals is suited to the analysis of multiple time scale nonlinear models. For the case of water hammer initiated by valve closure, the multiple scales approach is herein adapted to complications, such as flow reversals. As a result, it exposes a simple relationship between the periodically averaged flow velocity and pressure wave attenuation. The dependence of these effects on fluid advection, viscosity, and inertia also becomes evident. The analytical description is constructed under the assumption of sudden valve closure, but a greater range of validity and limitation for slow valve-closure is established using the numerical solution as a guide.

4.3 Water Hammer Equations

The standard momentum equation (Han et al. [42] 2011), including the quadratic head loss (Hansen et al. [43] 1995), may be written as

$$gh_x + vv_x + v_{t'} + \frac{g}{L}(rv + sv|v|) = 0 \tag{4.1}$$

where g = acceleration caused by gravity; $h(x,t)$ = head; $v(x,t)$ = fluid velocity; L = pipe length; and r and s = constant quasi-steady parameters that are subsequently described. The partial derivatives are conveniently written as subscripts.

The steady friction term in Eq. (4.1) has been generalized from the standard Darcy-Weisbach friction factor proportional to $|v|v$ to include a linear term proportional to v where the latter conveniently allows for the analysis of partially developed turbulent and laminar flow regimes. This form of steady friction, based on the Moody diagram, has been presented in Han et al. ([42] 2011) and is briefly restated here.

Steady flow through a conduit is described by the Moody diagram. A single Moody curve may be described by

$$f = \frac{M_1}{\mathrm{R}} + M_2 \tag{4.2}$$

where M_1 and M_2 depend on the relative roughness ϵ_c/D_c where ϵ_c is the conduit roughness and D_c is the conduit diameter. The absolute roughness ϵ_c is determined by the pipe material. Substituting the Darcy-Weisbach friction factor $f = 2gD_c\Delta h/(Lv_0^2)$ and the Reynolds number $\mathrm{R} = v_0 D_c/\nu$ allows the external head to be expressed as

$$\Delta h = M_1 \frac{\nu}{g}\frac{L}{D_c^2} v + M_2 \frac{L}{gD_c} v^2 \tag{4.3}$$

where parameter definitions are provided in Table 4.1. $M_2 = 0$ for laminar flow (not considered herein), whereas $M_1 = 0$ for fully developed turbulent flow. Setting $r = M_1 \nu L/(gD_c^2)$ and $s = M_2 L/(gD_c)$ obtains the momentum Eq. (4.1). In practice, the values of r and s (Hansen et al. [43] 1995) may be found through regression analysis of a given Moody curve determined by pipe properties as previously stated.

The continuity equation is (Han et al. [42] 2011)

$$\frac{c_p^2}{g} v_x + v h_x + h_{t'} + v\sin(\theta) = 0 \tag{4.4}$$

where the wave celerity $c_p = \sqrt{K/\rho}$, $K = E_w/[1 + D_c E_w/(wE)]$, with water bulk modulus E_w, pipe material modulus E, pipe wall thickness w, and pipe slope θ.

The water hammer attenuation was analyzed for the physical setup shown in Figures 4.1 and 4.2. Initially, a linearly declining initial head $h = h_2 + (1 - x/L)(h_1 - h_2)$ drives the fluid at the steady-state velocity $v = v_0$ (Figure 4.1). The water hammer is assumed to be caused by a sudden change in the boundary conditions after $t = 0$ when the velocity at the downstream end ($x = L$) is suddenly zeroed (Figure 4.2), that is, $v(x = L, t > 0) = 0$, whereas the head $h(x = 0, t > 0) = h_1$ makes the upstream boundary condition at $x = 0$ continuous before and after the hammer is initiated.

4.4 Dimensional Analysis

The dimensional steady head and steady velocity in the momentum [Eq. (4.1)] and continuity [Eq. (4.4)] equations are rescaled to vary between zero and unity via $H = (h - h_2)/h_{12}$ and $V = v/v_0$ where $h_{12} = h_1 - h_2$ is the applied head and v_0 is the steady velocity applied before the hammer is initiated. Similarly, the spatial scale

Parameters	Values
Conduit diameter D_c	0.3 m
Conduit length L	$1,000$ m
Conduit roughness ϵ_c	0.0003 m
Conduit wall thickness w	0.005 m
Applied head change (Figure 4.1) at $t = 0$ is $(h_2 - h_1)$	462 m
Young's modulus of iron E	2.0×10^{11} Pa
Water bulk modulus E_w	2.27×10^9 Pa
Kinematic viscosity $\nu = \mu/\rho$	10^{-6} m^2/s
Steady velocity v_0	11.7 m/s (4.17)
Reynolds number R_∞	3.49×10^6
Celerity c_p	1.2×10^3 m/s
Viscous constant r	0.55 s
Inertial constant s	3.34 s^2/m
C_1	0.030
C_2	0.014
C_3 [momentum Eq. (4.8)]	1.0
$C_1 c_4$	3.3
C_4	110
c_5	-1.9
ϵ^2 [continuity Eq. (4.9)]	10^{-3}

Table 4.1: Set of Parameters Used for Numerical Example. Note: Basic dimensional parameters are separated for clarity from computed dimensional parameters and dimensionless parameters.

$X = x/L$ runs between zero and unity where L is the pipe length. The inertial time scale v_0/g is divided by the hydraulic gradient h_{12}/L giving the rigid-column time scale $T = Lv_0/(gh_{12})$. This choice balances the h_x and $v_{t'}$ terms in the momentum equation [Eq. (4.1)]. The rescaled time is then $\tau = t'/T$, and the rescaled momentum and continuity equations are

$$\begin{aligned} H_X + C_1 V V_X + V_\tau + C_2 V + C_3 V|V| = 0 \\ V_X + C_1 C_4 V H_X + C_4 H_\tau + C_5 V = 0 \end{aligned} \tag{4.5}$$

with conditions

$$\begin{aligned} H(X, \tau = 0) = 1 - X, V(X, \tau = 0) = 1 \\ H(X = 0, \tau > 0) = 1,\ V(X = 1, \tau > 0) = 0 \end{aligned} \tag{4.6}$$

and dimensionless parameters

$$C_1 = \frac{v_0^2}{gh_{12}},\ C_2 = \frac{rv_0}{h_{12}}, C_3 = \frac{sv_0^2}{h_{12}}, C_4 = \left(\frac{gh_{12}}{c_p v_0}\right)^2,\ C_5 = \frac{gL\sin\theta}{c_p^2} \tag{4.7}$$

where C_1 = advection effect that includes density ρ. C_1 as $(\rho v_0^2)/(\rho g h_{12})$ is the ratio of a velocity head to a hydraulic head. C_2 is the viscous effect. Because r has units of seconds, C_2 is the kinematic viscous head relative to the applied hydraulic head h_{12} difference. C_3 is the inertial effect. This is an inertial head relative to the applied hydraulic head difference and is increasingly relevant as the level of turbulence increases. C_1C_4 is the advective head. The product C_1C_4 in the continuity equation may be written as $\rho g h_{12}/(\rho c_p^2)$, which is the ratio of the hydraulic head difference (expressed as a pressure) to the pressure from the propagating wave. C_4 is the local velocity. Introducing density, $C_4 = [(\rho g h_{12})/(\rho c_p v_0)]^2$ gives $\sqrt{C_4}$ as the applied hydraulic head difference relative to the local pressure head. C_5 is the elevation head, which is the ratio of the elevation head to the celerity head from the propagating wave.

The momentum dimensionless parameters, C_1, C_2, and C_3, are assumed to be $O(1)$ [O(1)]. For the applications considered herein, the wave speed celerity is such that $O(1/c_p) \ll 1$. The continuity parameters C_4 and C_5 may then be presumed to be small. It is convenient to define $\epsilon^2 = O(1/c_p)$ so that $C_1C_4 = C_1c_4\epsilon^2$, $C_4 = c_4\epsilon^2$, and $C_5 = c_5\epsilon^2$. Terms C_1, c_4, and c_5 are assumed to be of the order one. These definitions give the final form

$$H_X + C_1 V V_X + V_\tau + C_2 V + C_3 V|V| = 0 \tag{4.8}$$

$$V_X + C_1 c_4 \epsilon^2 V H_X + c_4 \epsilon^2 H_\tau + c_5 \epsilon^2 V = 0 \tag{4.9}$$

The boundary and initial conditions are unaffected because they do not contain any dimensionless parameters.

4.5 Invariance under Flow Reversals

The appearance of $|V|$ in the momentum equation Eq. (4.8) ensures that the steady friction $C_2V + C_3V|V|$ opposes the direction of flow. The asymptotic analysis is simplified by noting that after $\tau = 0$, both the momentum and continuity equations

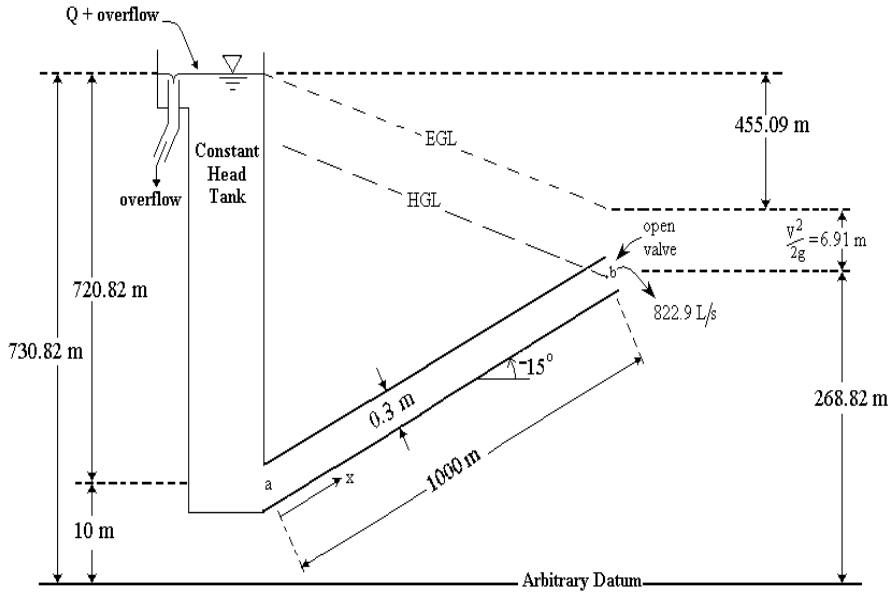

Figure 4.1: Schematic of physical setup just before $t = 0$; entrance losses at Point a are neglected; HGL = hydraulic grade line; EGL = energy grade line

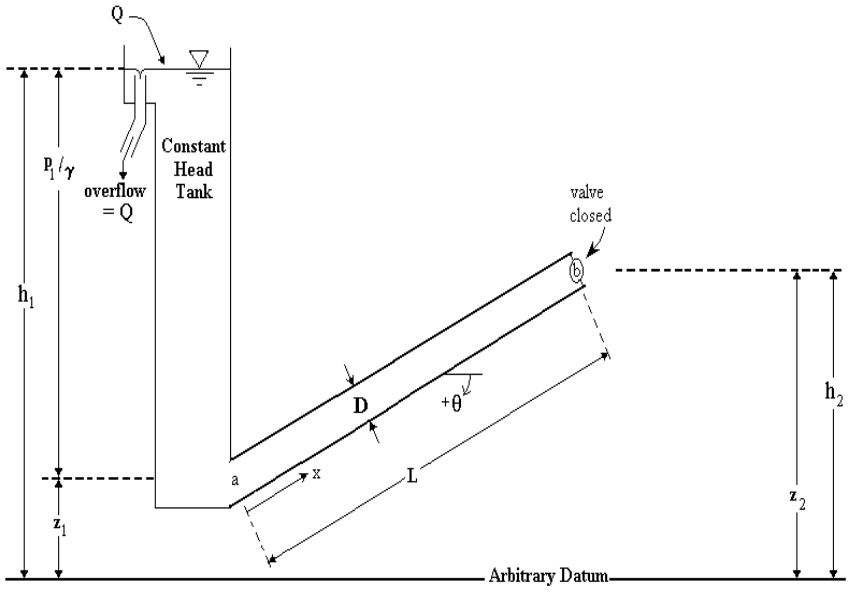

Figure 4.2: Schematic of physical setup just after $t = 0$; water hammer is initiated from the downstream end by applying velocity $v = 0$ at $x = L$, whereas the head at the pipe entrance $x = 0$ remains at $h = h_1$

[Eqs. (4.8) and (4.9)] and the boundary conditions are invariant with respect to flow

reversals. When $V > 0$ throughout the pipe, the quasi-steady friction in Eqs. (4.8) and (4.9) is $C_2V + C_3V^2$. For $V < 0$ throughout the pipe, $Y = 1 - X$ and $W = -V$ is set in Eqs. (4.8) and (4.9)

$$H_Y + C_1WW_Y + W_\tau + C_2W + C_3W^2 = 0 \tag{4.10}$$

$$W_Y + C_1c_4\epsilon^2WH_Y + c_4\epsilon^2H_\tau + c_5\epsilon^2W = 0 \tag{4.11}$$

with boundary conditions $H(Y = 1, \tau > 0) = 1$ and $W(Y = 0, \tau > 0) = 0$. The elevation head term $c_5\epsilon^2$ exceeds zero in the continuity equation because c_5 is proportional to $-\sin(\theta)$ under the change of coordinates $Y = 1 - X$.

4.6 Time Scales

Classical water hammer behaviour is characterized by two time scales: a fast wave superimposed on a slowly varying trend. A qualitative justification of the multiple scales method is presented here as a preamble. This approach where a qualitative approximation is used to motivate a more general asymptotic expansion follows that presented for a range of applications (Bender and Orzsag [6] 1978).

4.6.1 Attenuating Wave

The first approximation to the fast water hammer wave, justified at the end of this section, involves a balance between the dominant terms H_X and V_τ in the momentum equation and the terms V_X and $\epsilon^2c_4H_\tau$ in the continuity equation [Eq. (4.9)]. This leads to the first approximation

$$\begin{aligned} H_X + V_\tau &= 0 \\ V_X + c_4\epsilon^2H_\tau &= 0 \end{aligned} \tag{4.12}$$

The balance of terms in this reduced form is now established for the wave $H = af(X - b\tau)$ and $V = cf(X - b\tau)$. The magnitude scales a and c are independent of the wave direction, and the functional dependence of H and V on $X - b\tau$ is the same because they share the wave speed and period. Substituting the assumed form

of head and velocity into the reduced set yields

$$\begin{aligned} a - bc &= 0 \\ c - c_4 ab\epsilon^2 &= 0 \end{aligned} \tag{4.13}$$

Eliminating $a = bc$ gives $c(1-c_4 b^2\epsilon^2) = 0$, which fixes $b = 1/(\epsilon\sqrt{c_4})$ and $a = c/(\epsilon\sqrt{c_4})$. The undetermined velocity scale parameter c is unity because velocity $V = 1$ just before the water hammer initiation leads to a traveling wave with unit amplitude; therefore, $a = 1/(\epsilon\sqrt{c_4})$.

Generally for the full equations, the head and velocity are then $H = 1/(\epsilon\sqrt{c_4}) \cdot f[X-\tau/(\epsilon\sqrt{c_4})]$ and $V = g[X-\tau/(\epsilon\sqrt{c_4})]$. The short-wave evolution time scale is $t = \tau/\epsilon$ where $\tau = O(\epsilon\sqrt{c_4})$. Therefore, the wave is defined as $H = 1/(\epsilon\sqrt{c_4})f(X-t/\sqrt{c_4})$ and $V = g(X - t/\sqrt{c_4})$ where t is $O(1)$ and this corresponds to $\tau = O(\epsilon)$.

The mathematical basis for neglecting both friction and convection in the first approximation given by Eq. (4.12) is justified because (1) H_X and V_τ are $O(1/\epsilon)$ in the momentum equation [Eq. (4.8)], whereas other terms are $O(1)$ and below, and (2) V_X and $\epsilon^2 H_\tau$ in the continuity equation [Eq. (4.9)] are $O(1)$, whereas the remaining terms are $O(\epsilon)$ or smaller.

It is evident that the head and velocity wave operate at a time scale t. This time scale is short or fast compared to the long or slow trending time scale $\tau = \epsilon t$ over which the wave amplitude attenuates. The trending time scale $\tau = O(1)$ corresponds to the short time scale $t = O(1/\epsilon) \gg 1$. Taken together, the two time scales describing the head and velocity along with the amplitude scales imply that $H = 1/(\epsilon\sqrt{c_4})H(X,t,\tau)$ and $V = V(X,t,\tau)$.

4.6.2 Slow Trend

The trending component depends on the spatial scale X and the slow time scale τ. The slowly varying trend (rigid column motion) and faster evolving (water hammer) wave components are independent to the orders considered here. Because of the previously described invariance to flow reversals, the trending component may be analyzed as if the flow never reverses. This assumption will be shown to require consideration of the absolute value of the flow velocity averaged between flow reversals.

A regular perturbation is assumed for the head and velocity in powers of the small parameter ϵ. Defining the slow trend component as $H(X,\tau) = H_0(X,\tau)+\epsilon H_1(X,\tau)+\ldots$ and $V(X,\tau) = V_0(X,\tau) + \epsilon V_1(X,\tau) + \ldots$ and substituting these into Eqs. (4.8) and (4.9) finds that the zeroth approximation satisfies

$$\begin{aligned} H_{0X} + C_1 V_0 V_{0X} + V_{0\tau} + C_2 V_0 + C_3 V_0^2 &= 0 \\ V_{0X} &= 0 \end{aligned} \tag{4.14}$$

The second equation in Eq. (4.14) requires that $V_0 = V_0(\tau)$, whereas the zeroth steady-state approximation

$$H_0(X) = 1 \tag{4.15}$$

is independent of τ and captures the steady-state head. Substitution of $H_0(X) = 1$ and $V_0 = V_0(\tau)$ to the first equation in Eq. (4.14) gives the first-order separable equation

$$V_{0\tau} = -C_2 V_0 - C_3 V_0^2 \tag{4.16}$$

with solution

$$V_0(\tau) = \frac{\tilde{D} e^{-C_2 \tau}}{1 - \tilde{D} C_3 / C_2 e^{-C_2 \tau}} \tag{4.17}$$

where $\tilde{D}$ = free constant, subsequently chosen under the constraint that $V_0(\tau)$ approximates the averaged absolute flow velocity between flow reversals. The trending results for $H_0(X)$ and $V_0(\tau)$ are valid for the order of one τ and $O(\epsilon)$, and they contain the head and velocity steady state. However, neither result is valid at short times $[\tau = O(\epsilon)]$ wherein the shorter time scale t is $O(1)$.

4.7 Multiple Scales

A multiple scales expansion based on the previous observations may now be built for the head and velocity.

4.7.1 Multiple Scales Form

The head in equations Eqs. (4.8) and (4.9) and as previously discussed is proportional to $1/\epsilon$, and any expansion is singular as ϵ tends to zero. This corresponds with the

wave celerity approaching infinity. A regular expansion is found by setting $\tilde{H} = \epsilon H$. Given the multiple scales $t = \tau/\epsilon$ and τ found in the previous sections, the momentum and continuity equations [Eqs. (4.8) and (4.9)] for $\tilde{H}(X,t,\tau)$ and $V(X,t,\tau)$ take the form

$$\tilde{H}_X + \epsilon C_1 V V_X + \epsilon V_\tau + V_t + \epsilon C_2 V + \epsilon C_3 V^2 = 0 \tag{4.18}$$

$$V_X + C_1 c_4 \epsilon V \tilde{H}_X + c_4 \epsilon \tilde{H}_\tau + \tilde{H}_t + c_5 \epsilon^2 V = 0 \tag{4.19}$$

with conditions

$$\begin{aligned} &\tilde{H}(X, \tau = 0) = \epsilon(1 - X), V(X, \tau = 0) = 1 \\ &\tilde{H}(X = 0, \tau > 0) = \epsilon,\ V(X = 1, \tau > 0) = 0 \end{aligned} \tag{4.20}$$

4.7.2 Multiple Scales Expansion

Based on previous observations, it is concluded that

$$\begin{aligned} \tilde{H}(X,t,\tau) = {} & \frac{1}{\sqrt{c_4}} P_1(\tau)[1 + \epsilon Q_{11}(\tau) + \ldots]\left[e^{i(X - t/\sqrt{c_4})} + \epsilon F_{11}(X - t/\sqrt{c_4}) + \ldots\right] + \\ & \frac{1}{\sqrt{c_4}} P_2(\tau)[1 + \epsilon Q_{21}(\tau) + \ldots]\left[e^{2i(X - t/\sqrt{c_4})} + \epsilon F_{21}(X - t/\sqrt{c_4}) + \ldots\right] \\ & + \ldots \text{(attenuated wave modal expansion)} \\ & + \epsilon H_0(X) + \epsilon^2 H_1(X,\tau) + \ldots \text{(trending component expansion)} \end{aligned} \tag{4.21}$$

$$\begin{aligned} V(X,t,\tau) = {} & P_1(\tau)\left[1 + \epsilon \tilde{Q}_{11}(\tau) + \ldots\right]\left[e^{i(X - t/\sqrt{c_4})} + \epsilon G_{11}(X - t/\sqrt{c_4}) + \ldots\right] + \\ & P_2(\tau)\left[1 + \epsilon \tilde{Q}_{21}(\tau) + \ldots\right]\left[e^{2i(X - t/\sqrt{c_4})} + \epsilon G_{21}(X - t/\sqrt{c_4}) + \ldots\right] \\ & + \ldots \text{(attenuated wave modal expansion)} \\ & + V_0(\tau) + \epsilon V_1(X,\tau) + \ldots \text{(trending component expansion)} \end{aligned} \tag{4.22}$$

where the leading terms of the trending component expansions, $H_0(X)$ and $V_0(\tau)$, are previously given. Background for the multiple scales method and averaging method, which have inspired this form, may be found in Nayfeh ([61] 2000) and Bender and Orzsag ([6] 1978).

The wave component is an attenuated complex modal expansion. Its complex

component depends on the short time scale t with $O(\epsilon)$ corrections F_{nj} and G_{nj} generically stated and possibly complex. The complex wave component is attenuated for both the head and velocity through a multiplicative attenuation function $P_n(\tau)[1+\epsilon Q_{nj}(\tau)+\ldots]$ that depends on the slow variable τ. The subscript nj is associated with the nth mode and power ϵ^j. The attenuation multiplier is also defined; therefore, $P_n(\tau)$ conveniently represents the first approximation to the nth mode wave attenuation.

The main assumptions in the head and velocity expressions are that the attenuated wave and trending components are additive, the attenuated wave has a separated dependence on the two time scales t and τ, and the wave attenuation is independent of flow reversals.

4.7.3 Attenuation Function

Substitution of the full form to the dimensionless momentum equation [Eq. (4.8)] yields the complex first-order equation for the first mode of the wave attenuation function $P_1(\tau)$ as

$$\sqrt{c_4}\frac{dP_1(\tau)}{d\tau}+\sqrt{c_4}\left[C_2+2C_3V_0(\tau)+C_1V_0(\tau)i\right]P_1(\tau)+iP_1(\tau)\Delta Q_{11}(\tau)=0 \quad (4.23)$$

where $\Delta Q_{11}(\tau)=Q_{11}(\tau)-\tilde{Q}_{11}(\tau)$. The continuity equation [Eq. (4.9)] similarly yields

$$c_4\frac{dP_1(\tau)}{d\tau}+C_1c_4V_0(\tau)P_1(\tau)i-\sqrt{c_4}iP_1(\tau)\Delta Q_{11}(\tau)=0 \quad (4.24)$$

Eliminating $\Delta Q_{11}(\tau)$

$$2\frac{dP_1(\tau)}{d\tau}+\{C_2+2C_3V_0(\tau)+i[C_1V_0(\tau)+C_1]\}P_1(\tau)=0 \quad (4.25)$$

Therefore, the attenuation function satisfies the first-order ordinary differential equation

$$\frac{dP_1(\tau)}{d\tau}+\lambda(\tau)P_1(\tau)=0 \quad (4.26)$$

where $\lambda(\tau) = \lambda_R(\tau) + i\lambda_I(\tau)$ is the complex term with

$$\lambda_R(\tau) = \frac{C_2 + 2C_3V_0(\tau)}{2}$$
$$\lambda_I(\tau) = \frac{C_1V_0(\tau) + C_1}{2} \tag{4.27}$$

with solution

$$P_1(\tau) = \tilde{A}e^{-\int_0^\tau \lambda(z)dz} \tag{4.28}$$

where $\tilde{A}$ = free constant.

4.7.4 Attenuation Free Constants

The magnitude of the attenuation is $|P(\tau)| = |\tilde{A}| \exp[\int_0^\tau \lambda_R(z)dz]$. Two free constants, $\tilde{A}$ in Eq. (4.28) and $\tilde{D}$ in Eq. (4.17), remain unspecified.

The constant $\tilde{A}$ is found by noting that the magnitude of the oscillatory component of the dimensionless head $\tilde{H}(x,t,\tau)$ may not exceed unity, that is, $\tilde{A} = 1/P(0)$.

The periodic average of the absolute value of the velocity is

$$\bar{V}(X,t) = \frac{\int_t^{t+T} |V(X,z)|dz}{T} \tag{4.29}$$

where T = hammer period. In the presence of flow reversals, it is expected that the velocity trending component expansion defined in Eq. (4.22) will approximate the periodic average of the absolute velocity. In addition, the first approximation to the velocity trending component V_0 is independent of X; therefore, the periodic average $\bar{V}(X,t)$ is weakly dependent on X. Hence, $\tilde{D}$ is chosen; therefore, the first approximation to the velocity trending component expansion is equal to the average of the initial dimensionless velocity at $\tau = 0$ and the zero velocity suddenly imposed at $X = 1$ after $\tau = 0$, that is, $V_0(0) = 1/2$. Eq. (4.17) then yields

$$\tilde{D} = \frac{1}{2[1 + C_3/(2C_2)]} \tag{4.30}$$

Substituting the trending component $V_0(\tau)$ of Eq. (4.17) with $\tilde{D}$ from Eq. (4.30) and

integrating yields the first mode attenuation function

$$|P_1(\tau)| = \frac{e^{-C_2\tau/2}}{1 + C_3/(2C_2)\,(1 - e^{-C_2\tau})} \tag{4.31}$$

where the trending component $V_0(\tau)$, equal to the periodic average of the absolute velocity [Eq. (4.29)], is one-half the attenuation, that is, $V_0(\tau) = 1/2|P_1(\tau)|$. For the standard Darcy-Weisbach quasi-steady friction given by $C_3V|V|$ for $C_2 = 0$, the attenuation is the inverse polynomial $|P_1(\tau)| = 1/(1 + C_3\tau/2)$. The analysis was performed with respect to wavefronts that are allowed to reflect at the boundaries. The analysis used is also valid for wavefronts that travel without reflection and for problems with and without flow reversals [e.g., reflecting wavefronts generated through flow establishment (Han et al. [42] 2011)]. An approach (Leslie and Tijsseling [52] 2000) that uses the dimensional form and works locally by following a characteristic yields results quite similar in form to those that are found here; therefore, the results of Leslie and Tijsseling ([52] 2000) may have a broader scope than the authors realized.

Numerical verification of these results is considered for a range of valve closure rates. The Daugherty and Franzini ([28] 1977) formulation for wave transit times based on frequent axial expansion joints [$\eta = 1$ (Wylie and Streeter [97] 1993; Han et al. [42] 2011] where the full pressure transient is realized for rapid closure times below the transit time $\tau_r = t_r/T$, and $t_r = 2L/c_p$ is the wave transit time divided by the previously described rigid column time scale $T = Lv_0/(gh_{12})$. For slow closure times, $\tau_c > \tau_r$, a fraction τ_c/τ_r of the full head transient is realized. In the discussion that follows, the sudden closure and time-varying valve closures for one-half τ_r, equal to τ_r, 50% longer than τ_r and double τ_r, are described. Parameters used in all examples are provided in Table 4.1, and these parameters follow those used in Han et al. ([42] 2011).

4.7.5 Sudden Valve Closure

The head in the case of sudden valve closure is provided in Figure 4.3. Numerical verification of the pressure wave attenuation is seen in Figures 4.4 and 4.5. The parameters used in the example were for a 1-km pipe inclined upward at an angle

of $\theta = -15^o$ (Table 4.1). Figure 4.4 shows that the analytic attenuation function $|P(\tau)|$ closely approximates the attenuation extracted from the numerical solution, as detailed in the Figure 4.4 legend. The periodic averaging provided by $V_0(\tau)$ is qualitatively clear in Figure 4.5. The maximum value of the head $\sqrt{c_4}\tilde{H}$ at the valve, seen in Figure 4.3, is unity, and this value corresponds to a maximum dimensionless head H, equal to $1/\sqrt{C_4} = c_p v_0/gh_{12}$ as in Daugherty and Franzini ([28] 1977).

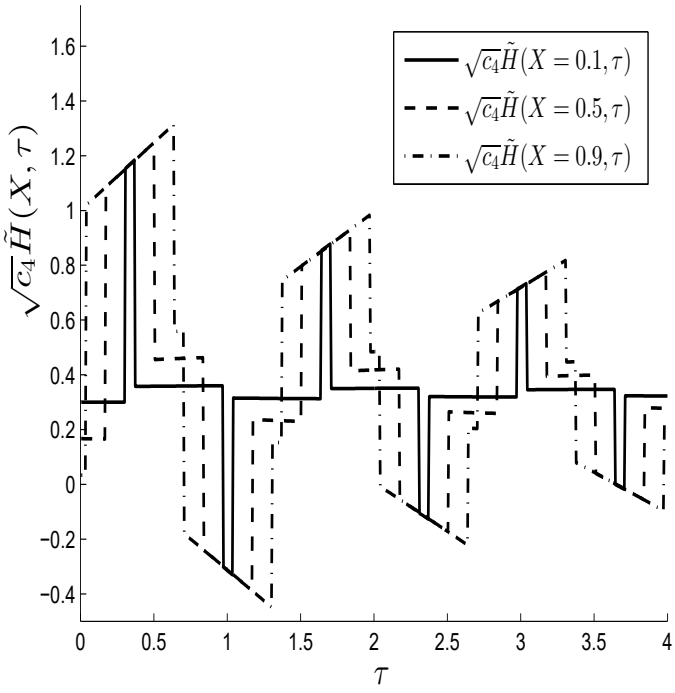

Figure 4.3: Solid, dashed, and dash-dot lines show the method of characteristics numerical approximation (Wylie and Streeter [97] 1993) to the head $\sqrt{c_4}\tilde{H}(X,\tau)$ at dimensionless positions $X = 0.1$, $X = 0.5$, and $X = 0.9$ depicted as a function of dimensionless time τ and based on a numerical grid with $\Delta_x = 0.01$

In this asymptotic analysis, the value of C_1 was assumed to be of the order of one. This means that no approximation was made with respect to this parameter in the asymptotic expansion and it may be possible to use the expansion for values of C_1 that are not of the order of one. This point is borne out in the physical example, $C_1 \ll 1$; therefore, the approximation remains valid. This parametric behaviour is occurring because the solution possesses a regular dependence on C_1 as it vanishes. This point can be further examined by noting that it was assumed in Eq. (4.9)

that $C_4 = c_4\epsilon^2 \ll 1$ and $C_5 = c_5\epsilon^2 \ll 1$ with $\epsilon = 1/c_p \ll 1$, that is, the celerity $c_p \gg 1$, and the remaining parameters in the dimensionless momentum [Eq. (4.8)] are treated without approximation as of the order of one. The multiple scales asymptotic expansion is constructed under two independent assumptions: (1) ϵ is small compared with one and (2) the terms in the differential equation are of the order of one. Because of these two things, an expansion may be expected to be useful for larger values of ϵ if the terms in the differential equation are also small compared with one. This occurrence is difficult to predict and is most easily found by comparison with the numerical solution (Han et al. [42] 2011).

The parametric dependence given in Eq. (4.31) is of practical interest. In particular, it indicates that the exponential decay of the pressure wave damping is predicted by this model to be entirely caused by viscous effects for all order of one values of C_2. This parametric situation is entirely reversed only after viscous effects become small and the Darcy-Weisbach nonlinear friction parameter C_3 becomes dominant. In this latter case, inertial effects give an inverse polynomial time decay of the pressure wave amplitude. Such is the case for the example presented in Figure 4.3. When the viscous effects C_2 are of the order of one and the inertial effects are dominant (such that $C_3 \gg C_2$), an exponential decay is still observed in the pressure wave determined by the viscous effect C_2. This case points out why the order of one viscous effects (C_2) cannot be neglected in favour of inertial effects (C_3), even when the latter appear to be dominant (via $C_3 \gg C_2$).

The classical water hammer equations were considered here for a generalized form that includes quasi-steady friction effects at lower levels of turbulence; this model has been considered for water hammer initiated by flow establishment (Han et al. [42] 2011). It is useful to compare the results for flow establishment with those from a sudden valve closing to highlight differences in the analysis and water hammer physics. The comparison is simplified because the nondimensionalization is similar and the physical setup referenced in Han et al. ([42] 2011) is repeated.

Flow establishment water hammer was studied in Han et al. ([42] 2011) for a suddenly imposed constant head driving a trending flow. A steady state is approached without flow reversals and is characterized by a nonzero net flow with a steady velocity and a constant head gradient everywhere after the water hammer has dampened

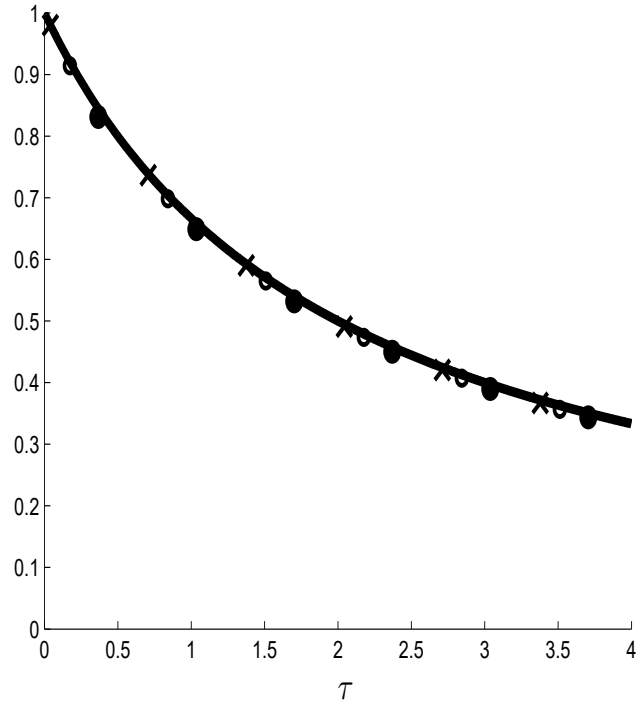

Figure 4.4: Dots, crosses, and circles show the absolute difference $\sqrt{c_4}\cdot\,|\tilde{H}(X,\tau) - \tilde{H}(X,\infty)|$ (steady head has been removed) of the numerical solution in Figure 4.3 evaluated at $X = 0.1$, $X = 0.5$, and $X = 0.9$ at the midpoint of the sloped head; analytic pressure wave attenuation is expected to approximate the local maxima of the absolute head after removal of the steady head; heavier solid line is the wave attenuation function $|P_1(\tau)|$ [Eq. (4.31)] found here, and it closely approximates the dots, crosses, and circles taken from the numerical solution

out. Three points of comparison are noted: (1) the flow establishment dimensionless velocity is an order of magnitude smaller than the dimensionless head, whereas herein $V(X,t,\tau)$ and $\tilde{H}(X,t,\tau)$ are both of the order of one, resulting in multimodal effects that are absent in the flow establishment case; (2) the trending velocity approximates the flow velocity in flow establishment cases because there are no flow reversals; and (3) the trending velocity and pressure wave attenuation function in flow establishment satisfy a more complex hyperbolic relationship, that is, $[V_0(\tau)+b]^2/a^2 - [b^2/a^2 - 1]P^2(\tau) = 1$, $b = C_2/(2C_3)$ and $b > a = \sqrt{b^2 + 1/C_3}$ where $|P(\tau)| = \operatorname{sech}(aC_3\tau + \tilde{D})/\sqrt{1-b^2/a^2}$ and $\tilde{D} = \operatorname{arctanh}(b/a)$.

The simple relationship observed here between the pressure wave attenuation and

the periodic average of the absolute flow velocity is caused by a zero net flow represented by the trending velocity $V_0(\tau)$. The same cannot be said for the flow establishment case because there the trending flow represents a nonzero net flow. This adds to the complexity of the relationship between $|P(\tau)|$ and $V_0(\tau)$.

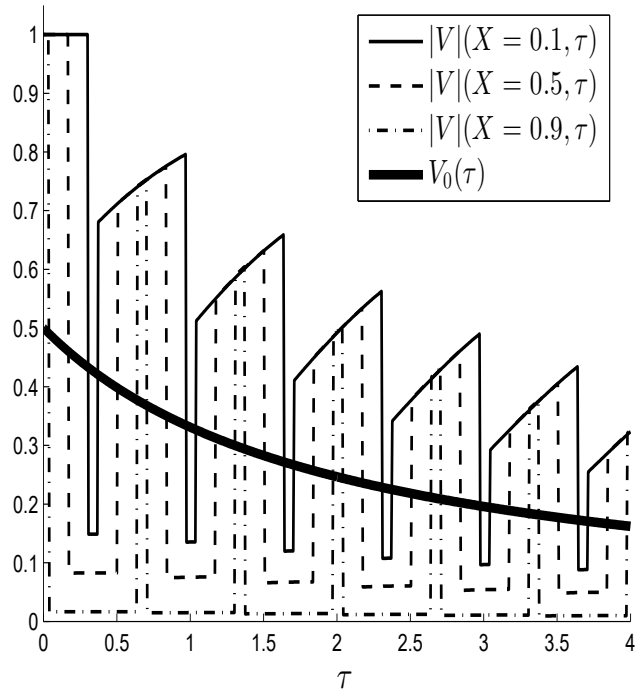

Figure 4.5: Lighter solid, dashed, and dash-dotted lines show the numerical approximation to the velocity $|V|(X,\tau)$ at dimensionless positions $X = 0.1$, $X = 0.5$, and $X = 0.9$, respectively, depicted as a function of dimensionless time τ, dimensionless spatial grid spacing of $\Delta X = 0.01$ is used over $0 \leq X \leq 1$; heavier solid line is the trend $V_0(\tau)$, which closely approximates the periodic average of $|V|$ [Eq. 4.29]

4.7.6 Time-Varying Valve Closure

To extend results for sudden valve closure to longer closure times, the authors turn to Daugherty and Franzini ([28] 1977) as a way to choose the free constant $\tilde{A} = 1/P(0)$. For rapid closure, which includes sudden closure in the previous subsection, $\tau_c < \tau_r$ (τ_r is previously defined), and $P(0) = 1$ and $V_0(0) = 1/2$ remain the same as those for sudden closure. The pressure wave attenuation results for closure times, one-half the wave transit time and equal to the wave transit time, are shown in Figures 4.6 and

4.7. Because the water hammer shows the least dissipation near the downstream end $X = 1$ where it is initiated, it is expected that the analytic pressure wave attenuation forms the closest approximation near $X = 1$ and to a lesser extent away from $X = 1$ where the dissipation becomes significant. This is seen in Figures 4.6 and 4.7. Furthermore, near the pipe entrance $X = 0$ where the water hammer is significantly dissipated, the analytic results do not approximate the pressure wave attenuation.

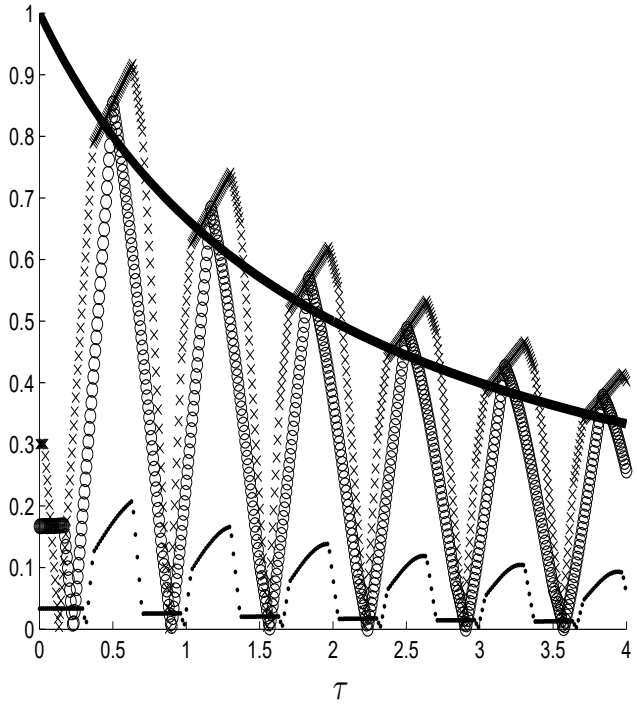

Figure 4.6: Dots, crosses, and circles show the absolute difference $\sqrt{c_4} \cdot |\tilde{H}(X,\tau) - \tilde{H}(X,\infty)|$ evaluated at $X = 0.1$, $X = 0.5$, and $X = 0.9$ for a closure time equal to one-half the wave transit time and whose local maxima are expected to be approximated by the analytic pressure wave attenuation; it is expected that the pressure wave attenuation will approximate the local maxima of the absolute head after removal of the steady head; water hammer dissipates the least near the location where it is initiated; therefore, the analytic pressure wave attenuation forms a reasonable approximation near $X = 1$ and, to a lesser extent, near the midpoint $X = 0.5$; near the pipe entrance $X = 0$, the water hammer is significantly dissipated, and the analytic results do not approximate the pressure wave attenuation

Next, the effect of increasing the closure times 50% beyond the pipe transit time and twice the pipe transit time is considered. These cases are interesting because

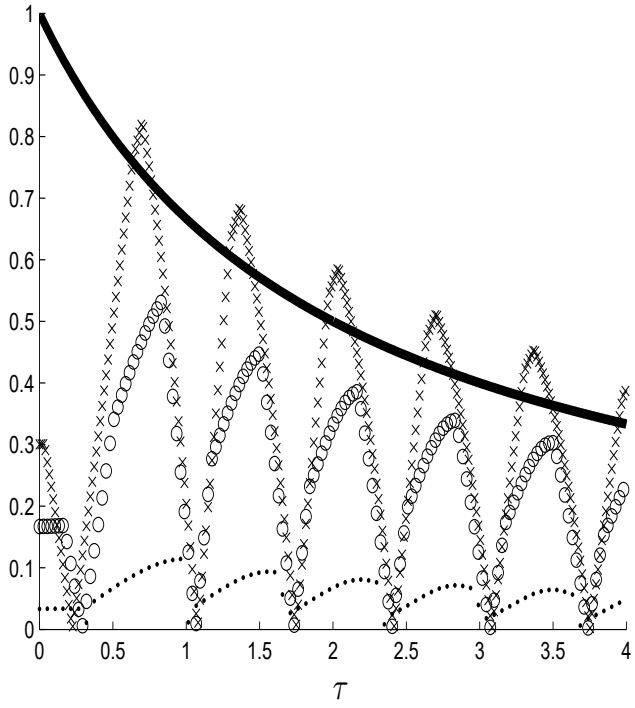

Figure 4.7: Dots, crosses, and circles show the absolute difference $\sqrt{c_4} \cdot |\tilde{H}(X,\tau) - \tilde{H}(X,\infty)|$ evaluated at $X = 0.1$, $X = 0.5$, and $X = 0.9$ for a closure time equal to the wave transit time; water hammer shows the least dissipation near $X = 1$ where it is initiated; therefore, the analytic pressure wave attenuation forms a reasonable approximation near there to the local maxima of the absolute head after removal of the steady head and, to a lesser extent, near the midpoint $X = 0.5$; near the pipe entrance at $X = 0.1$, the water hammer is significantly dissipated and the analytic results do not approximate the pressure wave attenuation

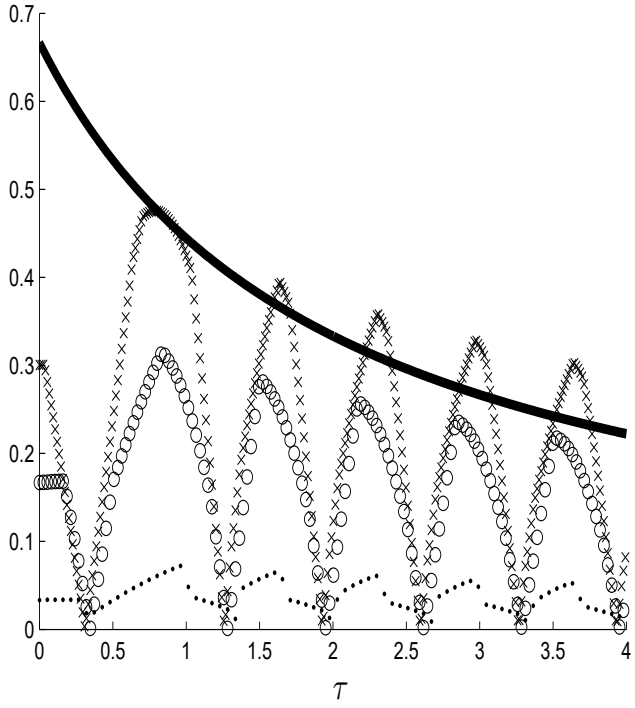

Figure 4.8: Dots, crosses, and circles show the absolute difference $\sqrt{c_4} \cdot |\tilde{H}(X,\tau) - \tilde{H}(X,\infty)|$ evaluated at $X = 0.1$, $X = 0.5$, and $X = 0.9$ for a slow closure time equal to 50 % greater than the wave transit time; water hammer shows some dissipation near $X = 1$ where it is initiated; however, the analytic pressure wave attenuation continues to form a reasonable approximation near there to the local maxima of the absolute head after removal of the steady head; significant dissipation away from $X = 1$ leads to the analytic approximation failing at $X = 0.5$, and near the pipe entrance at $X = 0.1$ the analytic results do not approximate the pressure wave attenuation

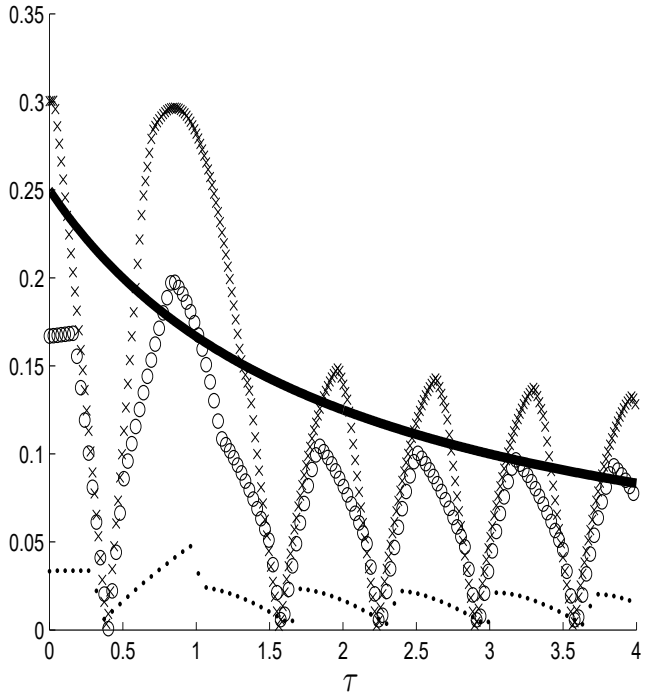

Figure 4.9: Dots, crosses, and circles show the absolute difference $\sqrt{c_4} \cdot |\tilde{H}(X,\tau) - \tilde{H}(X,\infty)|$ evaluated at $X = 0.1$, $X = 0.5$, and $X = 0.9$ for a slow closure time at double the wave transit time; water hammer shows a sharp change after $\tau \approx 1.5$ throughout the pipe, and the analytic pressure wave attenuation ceases to form a reasonable approximation at any location to the local maxima of the absolute head after removal of the steady head

the slow closure regime according to Daugherty and Franzini ([28] 1977) is entered and a fraction of the full pressure transient $p'_r = (2L/c_p)(p_r/t_r)$ is realized. If scaling with respect to the peak pressure p_r, then according to Daugherty and Franzini ([28] 1977), the authors get $P(0) = p'_r/p_r = [(2L/c_p)/t_r]$, whereas the second unknown constant is now $V_0(0) = 1/2P(0)$ [analogous to a previous section where $P(0) = 1$ gave $V_0(0) = 1/2$]. Therefore, for a closure time equal to 50% more than the pipe transit time, the authors set $P(0) = 2/3$ and $V_0(0) = 1/3$; at twice the pipe transit time, the authors set $P(0) = 1/2$ and $V_0(0) = 1/4$. For 50% beyond the pipe transit time, the analytic approximation in Figure 4.8 is a reasonable approximation near the end where the hammer is initiated ($X = 1$). Away from this location, the analytic results cease to be useful. Finally, the analytical results fail for valve closure times more than twice the pipe transit time because the pressure wave attenuation in Figure 4.9 no longer shows the continuous reduction in magnitude that was observed in the previous Figures 4.6–4.8 and is assumed in the analysis. Instead, the pressure wave attenuation in Figure 4.9 undergoes a sharp transition in magnitude after $\tau \approx 1.5$, and this suggests that the pressure wave attenuation has entered a new regime that is outside the scope of the present analysis.

4.8 Conclusions

The method of multiple scales was used to generate an approximation to the water hammer pressure wave attenuation in a generalized form of the classical water hammer equations. The method was developed for water hammer initiated by a sudden valve closing. The results for sudden valve closure found here were also used to highlight respective differences between the water hammer initiated by a sudden flow establishment and a sudden valve closure caused by the presence or absence of a net flow. The method is useful to predict pressure wave attenuation near the location where the water hammer is initiated at valve closure times near the wave transit time. The method cannot be used for valve closure times exceeding double the wave transit time, and in this regime another approximation would need to be found. The approach presented here, although rigorous and generic, is useful to establish rules of thumb and may be generalized to include, for example, the study of a water hammer in the presence of unsteady friction.

Chapter 5

Analysis of Water Hammer Attenuation in the Brunone Model of Unsteady Friction

E. Yao, G. Kember, and D. Hansen

Published in: Quarterly Of Applied Mathematics, June 2014, Vol. LXXII, No. 2, pages 281-290, S 0033-569X(2014)01354-6

URL: http://www.ams.org/journals/qam/2014-72-02/S0033-569X-2014-01354-6/

5.1 Abstract

A multiple-scales asymptotic analysis is used to describe the attenuation of a water hammer pressure wave in the Brunone model of unsteady friction. The method is applied to water hammer caused by sudden valve closure in water reservoir pipelines. The analytical results explain the parametric dependence of the Brunone unsteady friction pressure-wave attenuation. It is also found that viscous head in an extended steady friction model may provide an alternative to the unsteady friction basis for increased attenuation in cases where the attenuation has a weak spatial dependence and is primarily time-dependent. All results are numerically verified using the method of characteristics.

5.2 Introduction

The development of the Brunone model of unsteady friction began from experimental studies ([16], [39], [41]) with the intention of understanding earlier experimental results on oscillatory unsteady pipe flows. These studies were followed by a discussion paper [17] where these results were summarized. The overall thrust of the discussion in [17] was twofold: (i) Quasi-steady friction with the Reynolds number computed as the flow velocity evolves was insufficient to describe pressure-wave attenuation and

other water hammer features. (ii) They empirically resolved this insufficiency by including an unsteady friction proportional to local flow acceleration during the phase of the flow when the kinetic energy is increasing. This unsteady friction model has a natural jump discontinuity between the forward and backward flow phases, and this was later smoothed through a physical argument [20].

The objective of this paper is to develop an analytical pressure-wave attenuation formula for the Brunone model of unsteady friction presented in [20] and studied elsewhere, for example, in [87], [8] and [13]. The results found here explain the physical nature of the increased pressure-wave attenuation according to the Brunone unsteady friction model in comparison with the standard steady friction model.

The water hammer is assumed to be initiated by a sudden valve closure. The steady friction component of the model considered here is an extended steady friction model where the non-linear Darcy-Weisbach friction is generalized to include a linear viscous friction term. A practically useful result predicted by the form of the analytical pressure-wave attenuation and numerically verified is that the extended friction model may be used to describe the pressure-wave attenuation.

5.3 Water Hammer Equations

The unsteady momentum equation [20] based on experiments detailed in [17] and further modified to a form suitable for a wider range of applications [87] (using subscripts for partial derivatives) is

$$gh_x + vv_x + v_{t'} + \frac{g}{L}(rv + sv|v|) + \frac{k}{2}(v_{t'} + c_p \text{sign}(v)|v_x|) = 0 \tag{5.1}$$

The head is $h(x,t)$, fluid velocity is $v(x,t)$, L is pipe length and r and s are constant steady friction parameters proportional to the pipe length L [42]. The extended steady friction term $rv + sv|v|$ in (5.1) includes the linear term rv [42] which extends the steady friction model to partially developed turbulent and laminar flow regimes. The steady friction model $rv + sv|v|$ is hereafter referred to as the 'extended' steady friction model. The unsteady friction model [17] includes the term proportional to $v_{t'} + c_p \text{sign}(v)|v_x|$ where k is the Brunone friction coefficient and c_p is the wave celerity detailed below.

The continuity equation (cf. [42]) is

$$\frac{c_p^2}{g} v_x + v h_x + h_{t'} + v \sin(\theta) = 0 \tag{5.2}$$

with wave celerity $c_p = \sqrt{K/\rho}$, $K = E_v/(1 + D_c E_v/(wE))$, water bulk modulus E_v, pipe material modulus E, pipe wall thickness w, and pipe slope θ.

The water hammer equations are considered here for water hammer initiated by a valve closure and applied to the physical model of valve-closure water hammer described in [8].

5.4 Water Hammer Application

An initial head $h = h_2 + (1 - x/L)(h_1 - h_2)$ initially maintains a steady-state flow velocity $v = v_\infty$. After $t = 0$, the velocity at the pipe downstream boundary $x = L$ is zeroed by suddenly closing a valve, and this initiates a water hammer wave at $x = L$ that travels backward toward the upstream end $x = 0$. The boundary and initial conditions are

$$\begin{aligned} h(x, t = 0) = h_2 + (1 - x/L)(h_1 - h_2),\ v(x, t = 0) &= v_\infty \\ h(x = 0, t > 0) = h_1,\ v(x = L, t > 0) &= 0. \end{aligned} \tag{5.3}$$

At steady-state, the velocity is zero and the head is constant at h_1.

Water hammer initiated by valve closure was studied in [99] in the case of steady friction and is generalized here to include the Brunone model of unsteady friction. A physical application presented in [8] is considered after reduction to dimensionless form in the following section is completed.

5.5 Nondimensionalization

The dimensional head and velocity of equations (5.1) and (5.2) are rescaled to vary between zero and unity via $H = (h - h_2)/h_{12}$ and $V = v/v_\infty$ where $h_{12} = h_1 - h_2$ is applied head. The pipe length L is rescaled to unity with $X = x/L$ and $0 \leq X \leq 1$. An inertial time-scale v_∞/g is scaled by the hydraulic gradient h_{12}/L

yielding the dimensionless time-scale $T = Lv_\infty/(gh_{12})$, and defining $\tau = t'/T$ yields the dimensionless momentum and continuity equations

$$H_X + C_1 V V_X + V_\tau + C_2 V + C_3 V|V| + B_1 V_\tau + B_1 B_2 \text{sign}(V)|V_X| = 0$$
$$V_X + C_1 C_4 V H_X + C_4 H_\tau + C_5 V = 0 \tag{5.4}$$

and dimensionless parameters

$$C_1 = \frac{v_\infty^2}{gh_{12}},\ C_2 = \frac{rv_\infty}{h_{12}}, C_3 = \frac{sv_\infty^2}{h_{12}}, B_1 = \frac{k}{2}, B_2 = \frac{c_p v_\infty}{gh_{12}} \tag{5.5}$$
$$C_4 = \left(\frac{gh_{12}}{c_p v_\infty}\right)^2,\ C_5 = \frac{gL\sin\theta}{c_p^2}. \tag{5.6}$$

The water hammer conditions are

$$H(X, \tau = 0) = 1 - X, V(X, \tau = 0) = 1$$
$$H(X = 0, \tau > 0) = 1,\ V(X = 1, \tau > 0) = 0. \tag{5.7}$$

An explanation of the dimensionless parameters, the C_i, $i = 1, ..., 5$, also appears in [42] and [99], and is briefly restated here for completeness

- C_1*: Advection Effect.* C_1 may be written as $(\rho v_\infty^2)/(\rho g h_{12})$ and then is seen as the ratio of a velocity head to a hydraulic head.

- C_2*: Viscous Effect.* C_2 is the kinematic 'viscous head' relative to the applied hydraulic head h_{12} difference.

- C_3*: Inertial Effect.* This ratio of an inertial head to applied hydraulic head difference is more relevant as turbulence increases.

- C_1C_4*: Advective Head.* The product C_1C_4 may be recast in the form $[\rho g h_{12}/(\rho \cdot c_p^2)]$, whereupon it is the ratio of hydraulic head difference (expressed as a pressure) to the pressure from the propagating wave.

- C_4*: Local Velocity.* $\sqrt{C_4} = (\rho g h_{12})/(\rho c_p v_\infty)$ is the applied hydraulic head difference relative to the 'local' pressure head.

- C_5*: Elevation Head.* This is elevation head relative to propagating wave celerity head.

In the applications considered here, C_1, C_2 and C_3 are $O(1)$ ('O' means 'the order of') while the wave-speed celerity $O(c_p) \gg 1$ so that C_4 and C_5 are small. If $\epsilon = O(1/\sqrt{c_p})$ then $C_1C_4 = C_1c_4\epsilon^2$, $C_4 = c_4\epsilon^2$, and $C_5 = c_5\epsilon^2$ with C_1, c_4 and c_5 treated as order one. Using these definitions,

$$H_X + C_1VV_X + V_\tau + C_2V + C_3V|V| + B_1V_\tau + B_1B_2\text{sign}(V)|V_X| = 0 \tag{5.8}$$

$$V_X + C_1c_4\epsilon^2VH_X + c_4\epsilon^2H_\tau + c_5\epsilon^2V = 0. \tag{5.9}$$

The boundary and initial conditions are unaffected because they do not contain any dimensionless parameters.

5.6 Water Hammer Time Scales

The water hammer is characterized in terms of two time-scales: (i) a slowly evolving trend (rigid-column motion) operating at a time-scale τ and, (ii) a superimposed wave whose amplitude attenuates over the long time-scale τ and has a period of oscillation at the short time-scale $t = \tau/\epsilon$. The reduction in velocity at the downstream end $X = L$, at time $t = 0$ from $V = 1$ to $V = 0$, initiates a backward travelling pressure-wave. The head is proportional to $\sqrt{c_p} = 1/\epsilon$ and, as $\epsilon \to 0$, the wave celerity approaches infinity and the head necessarily becomes singular. The asymptotic expansion of the head is regularized with respect to $\epsilon \to 0$ by setting $\tilde{H} = \epsilon H$.

The multiple-scales analysis is simplified by noting that the water hammer equations are invariant with respect to flow reversals. Specifically, this point can be observed under the substitution $Y = 1 - X$ and $W = -V$ [99], and we find that the invariance remains true in the presence of unsteady friction.

Therefore, working in terms of τ and t, defining a regularized head $\tilde{H}$, and noting

the invariance of the momentum/continuity equations to flow direction, the multiple-scales form of (5.8) and (5.9) is

$$\tilde{H}_X + \epsilon C_1 V V_X + \epsilon V_\tau + V_t + \epsilon C_2 V + \epsilon C_3 V^2 + \epsilon B_1 V_\tau + B_1 V_t - \epsilon B_1 B_2 V V_X = 0 \tag{5.10}$$

$$V_X + C_1 c_4 \epsilon V \tilde{H}_X + c_4 \epsilon \tilde{H}_\tau + c_4 \tilde{H}_t + c_5 \epsilon^2 V = 0 \tag{5.11}$$

with conditions

$$\begin{aligned} \tilde{H}(X, \tau = 0) = \epsilon(1 - X), V(X, \tau = 0) = 1 \\ \tilde{H}(X = 0, \tau > 0) = \epsilon,\ V(X = 1, \tau > 0) = 0. \end{aligned} \tag{5.12}$$

Note that conditions satisfied here by the pressure-wave attenuation will be independent of the flow direction, and thus reference to the invariant form in (5.10) and (5.11) will be sufficient; however, more general conditions may violate this required invariance.

5.7 Multiple-Scales Expansion

Each of the head and velocity are written as the superposition of an attenuating wave and a trend. The wave component [42] is written in a generalized form required for the inclusion of unsteady friction. The attenuating wave component for the head and velocity respectively is a series with terms of the form $P_j(\tau)F_{nj}(\alpha_n(X - ct))$ and $P_j(\tau)G_{nj}(\alpha_n(X - ct))$. The $P_j(\tau)$ are the long time-scale pressure-wave attenuation functions while $F_{nj}(\beta_n(X - ct))$ and $G_{nj}(\beta_n(X - ct))$ are the oscillatory wave components with dimensionless wave speed $c = 1/\sqrt{(1 + B_1)c_4}$. The α_n and β_n are complex modes with imaginary part $n\mathbf{i}$. The subscript j corresponds to the order of expansion ϵ^j. The trending component [99] for the regularized head is $\tilde{H}(X, \tau) = \epsilon H_0(X) + \epsilon^2 H_1(X, \tau) + \ldots$ while the velocity is $V_0(\tau) + \epsilon V_1(X, \tau) + \ldots$.

Altogether these yield the multiple-scales expansion

$$\begin{aligned}
\tilde{H}(X,t,\tau) &= \sqrt{\frac{1+B_1}{c_4}}P_1(\tau)\left(1+\epsilon Q_{11}(\tau)+\ldots\right)\cdot \\
&\quad [F_{10}(\alpha_1(X-ct))+\epsilon F_{11}(\alpha_1(X-ct))+\ldots]+\sqrt{\frac{1+B_1}{c_4}}P_2(\tau)\cdot \\
&\quad (1+\epsilon Q_{21}(\tau)+\ldots)\,[F_{20}(\alpha_2(X-ct))+\epsilon F_{21}(\alpha_2(X-ct))+\ldots] \\
&\quad +\ldots+\epsilon H_0(X)+\epsilon^2 H_1(X,\tau)+\ldots \\
V(X,t,\tau) &= P_1(\tau)\left(1+\epsilon\tilde{Q}_{11}(\tau)+\ldots\right)\cdot \\
&\quad [G_{10}(\beta_1(X-ct))+\epsilon G_{11}(\beta_1(X-ct))+\ldots]+P_2(\tau)\cdot \\
&\quad \left(1+\epsilon\tilde{Q}_{21}(\tau)+\ldots\right)[G_{20}(\beta_2(X-ct))+\epsilon G_{21}(\beta_2(X-ct))+\ldots] \\
&\quad +\ldots+V_0(\tau)+\epsilon V_1(X,\tau)+\ldots. \qquad (5.13)
\end{aligned}$$

The first approximation to the trending head and velocity which depend upon X and τ is found by substituting (5.13) to (5.10) and (5.11), and this yields

$$\begin{aligned}
H_0(X) &= 1 \\
V_0(\tau) &= \frac{\tilde{D}e^{-C_2\tau}}{1-\tilde{D}C_3/C_2e^{-C_2\tau}} \qquad (5.14)
\end{aligned}$$

where the constant $\tilde{D}$ is determined later. In the following section, the wave attenuation function associated with the unsteady friction model is found using (5.13).

5.8 Attenuation Function

The first-mode attenuation function $P_1(\tau)$ is found here, and the numerics will show that this is the dominant mode of the wave attenuation.

Starting with ϵ^0 and substituting (5.13) to each of (5.10) and (5.11) we see that the zeroth approximation to the head and velocity of (5.13) must satisfy $\tilde{H}_X+(1+B_1)V_t=0$ and $V_X+c_4\tilde{H}_t=0$.

Continuing to first order in ϵ with the momentum equation (5.10) and continuity

equation (5.11), we find respectively that

$$P_{1\tau}(\tau) + \left[\frac{\alpha_1 C_1 V_0(\tau) + 2C_3 V_0(\tau) - \alpha_1 B_1 B_2}{1+B_1}\right] P_1(\tau) + \frac{1}{\sqrt{c_4(1+B_1)}} \alpha_1 P_1(\tau) \Delta Q_{11} = 0 \tag{5.15}$$

$$\frac{1}{\sqrt{c_4(1+B_1)}} \alpha_1 P_1(\tau) \Delta Q_{11} = \alpha_1 C_1 V_0(\tau) + P_{1\tau}(\tau) \tag{5.16}$$

where $\Delta Q_{11} = Q_{11} - \tilde{Q}_{11}$ and $V_0(\tau)$ is in (5.14). Substituting (5.16) to (5.16) we eliminate ΔQ_{11}, and the first-mode attenuation satisfies

$$P_{1\tau}(\tau) + \lambda(\tau) P_1(\tau) = 0 \tag{5.17}$$

where the complex rate is

$$\lambda(\tau) = \left[\frac{(\alpha_1 C_1(2+B_1) + 2C_3) V_0(\tau) + C_2 - \alpha_1 B_1 B_2}{2(1+B_1)}\right]. \tag{5.18}$$

The magnitude of the first-mode attenuation $P_1(\tau)$ follows as

$$|P_1(\tau)| = \tilde{A} e^{-\int_0^\tau \Re(\lambda(z)) dz} \tag{5.19}$$

where $\tilde{A} = |P_1(0)|$ is a free constant.

The two free constants $\tilde{A}$ and $\tilde{D}$ are found similarly to the approach used in [99] while the real part of the third constant α_1 is found numerically.

Firstly, the initial condition $P_1(0) = 1$ ensures that the head does not exceed $1/\sqrt{c_4}$ at $\tau = 0$ and this gives $\tilde{A} = 1/P(0)$. Secondly, the constant $\tilde{D}$ would generally require a numerical optimization involving a comparison of the numerical and analytic approximations to the attenuation function to obtain an optimal value of D, e.g. via least squares. However, a nearly optimal choice of $\tilde{D}$ may be found by setting $V(0) = 1/2$. This choice implies the first-order trend $V_0(\tau)$ approximates the periodic average of $V(X, \tau)$.

Given $\tilde{A}$ and $\tilde{D}$ we find, after approximating for $(B_1, C_1) \ll 1$ viz. Table 5.1, a

somewhat simplified form of the pressure-wave attenuation

$$|P_1(\tau)| = e^{\Re(\alpha_1)B_1B_2\tau/2}\frac{e^{-C_2\tau/2}}{1+C_3/(2C_2)\ (1-e^{-C_2\tau})}, \tag{5.20}$$

and if the viscous head linear term in the extended steady friction model $C_2V+C_3V^2$ is zeroed, i.e. $C_2=0$,

$$|P_1(\tau)| = e^{\Re(\alpha_1)B_1B_2\tau/2}\frac{1}{1+C_3\tau/2}. \tag{5.21}$$

Hence, the contribution made by unsteady friction in comparison to the steady friction model appears as the factor $\exp(\Re(\alpha_1)B_1B_2\tau/2)$. The unknown constant $\Re(\alpha_1)$ is determined in the following section.

5.9 Results

The pressure-wave attenuation has a weak spatial dependence since its first approximation only depends upon τ, and therefore it approximates the periodic-average of the pressure-wave during a pseudo-period (the water hammer traverses the pipe four times [97] during a pseudo-period). During a single period, the unsteady friction shuttles between a nearly zero value when the flow kinetic energy is decreasing (travelling upstream in our application), and a maximal value when the flow kinetic energy is increasing (travelling downstream in our application). A nearly optimal choice of $\Re(\alpha_1)=-1$ yields $|P_1(\tau)|$ that approximates the periodic-average of the pressure-wave during a pseudo-period.

All results are presented in Figure 5.1, and their derivation is described within the caption. The wave attenuation is numerically computed as the absolute difference $|\tilde{H}(X,\tau)-\tilde{H}(X-2\Delta X,\tau)|$ of the numerical solution. It is found at three dimensionless positions: $X=0.1$ (near upstream entrance), $X=0.5$ (midway along the pipe) and $X=0.9$ (near the downstream end). The same symbols are used for results at each position to enable a comparison between the steady and unsteady friction models. In all cases, the first-mode attenuation function $|P_1(\tau)|$ is compared to the numerical solution for physical parameters given in Table 5.1 that were taken from a physical study [8] (more details of the apparatus used in [8] are available in [12]).

The Brunone coefficient k in Table 5.1 was estimated [8] from the Vardy-Brown decay shear coefficient [83] and a low Reynolds number turbulent flow.

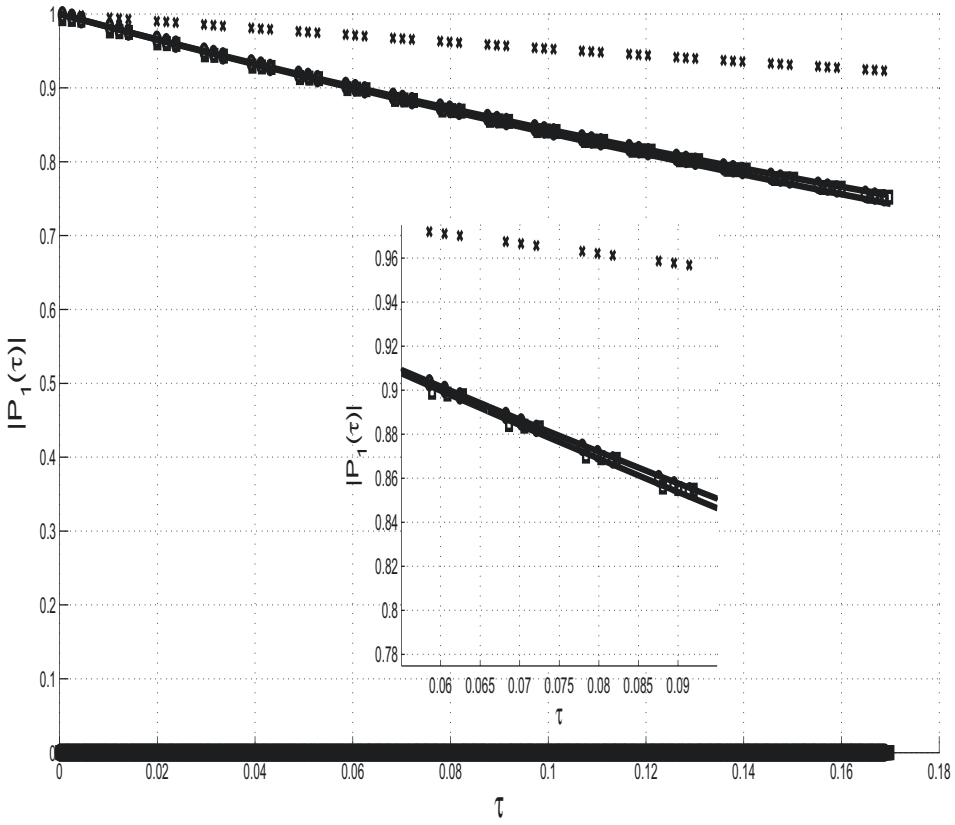

Figure 5.1: The numerically determined pressure-wave attenuation is shown for three cases: (i) the steady friction model (crosses) with zero viscous head ($C_2 = 0$) and zero unsteady friction ($B_1 = 0$, $B_2 = 0$) in (5.4), (ii) the Brunone unsteady friction model (squares) with zero viscous head ($C_2 = 0$) and unsteady parameters $B_1 = 0.0123$, $B_2 = 207$ from [8] (see Table 5.1), and (iii) the extended steady friction model (circles) with non-zero viscous head $C_2 = B_1 B_2$ and zero unsteady friction terms. The wave attenuation is computed as the absolute difference $|\tilde{H}(X, \tau) - \tilde{H}(X - 2\Delta X, \tau)|$ of the numerical solution at dimensionless positions $X = 0.1$ (near upstream entrance), $X = 0.5$ (midway along the pipe) and $X = 0.9$ (near the downstream end). These three locations are not distinguished in the results presented in each of (i), (ii) and (iii) above. Note that absolute differences of head that remain relatively constant in time appear as the heavier line of smaller values along the bottom of the figure while rapid changes in head at each X location are the remaining values that approximate the wave amplitude. The analytical pressure-wave attenuation closely approximates the numerical results in case (ii) as the solid line and in case (iii) as the dashed line.

Firstly, the attenuation found numerically for the unsteady friction model, and the steady friction model with and without the viscous head term C_2V is presented in the figure. The numerical results for the steady friction model attenuation are found without viscous head ($C_2 = 0$) and without unsteady friction ($B_1 = 0$, $B_2 = 0$), and they appear near the top (crosses). The numerical results for attenuation based on unsteady friction parameters $B_1 = 0.0123$, $B_2 = 207$ and zero viscous head ($C_2 = 0$) are shown as squares. In both the steady and unsteady friction models the inertial head coefficient $C_3 = 1$. The increased pressure-wave attenuation predicted by the Brunone model of unsteady friction over the steady friction model is apparent.

Secondly, the analytically computed wave attenuation of equation (5.21) (solid line) for the unsteady friction model with $C_2 = 0$, $B_1 = 0.0123$ and $B_2 = 207$ closely approximates the attenuation found numerically (squares). The analytical wave attenuation in equations (5.20) and (5.21) shows that the increased attenuation due to unsteady friction for weak spatial dependence where the first approximation to the attenuation depends only on τ may be reduced to the factor $\exp(\Re(\alpha_1)B_1B_2\tau/2)$.

An interesting possibility, raised by the analytical form of the wave attenuation in (5.20) and (5.21), is the possibility of a viscous basis for the increased wave attenuation seen in the unsteady friction results (squares). The form of (5.20) and (5.21) indicate that the Brunone unsteady friction results (squares) may be approximated via the steady model if the viscous head C_2V is included as $C_2 = B_1B_2$, followed by zeroing unsteady friction terms. The attenuation $|P_1(\tau)|$ (5.21) with $C_2 = B_1B_2$ is shown in Figure 5.1, with details in the inset, and it closely approximates the unsteady model wave attenuation. The numerical computations show that the dynamics of the unsteady friction model (squares) are also closely matched by the extended steady friction model (circles) to within a phase-shift of $\tau \approx 0.0004$.

The link observed here between the extended steady friction and unsteady friction models is possible when the pressure-wave attenuation has a weak spatial dependence and is only dependent upon τ to a first approximation. For example, in the presence of cavitation ([17] and [20]) or a valve closed at a time-scale approaching the water hammer transit time [13], such a link would not exist due to increased spatial dependence of the pressure-wave attenuation.

Dimensional parameters
Conduit diameter $D_c = 0.0221$ m
Conduit length $L = 37.23$ m
Conduit roughness $\epsilon_c = 0.0003$ m
Conduit wall thickness $w = 0.0016$ m
Applied head change at $t = 0$, $h_{12} = h_1 - h_2 = 0.13\ m$
Young's modulus of iron $E = 2.0 \cdot 10^{11}$ Pa
Water bulk modulus $E_v = 2.27 \cdot 10^9$ Pa
Kinematic viscosity $\nu = \mu/\rho = 10^{-6}\ m^2/s$
Brunone coefficient $k = 0.0245$
Computed dimensional parameters
Steady velocity $v_\infty = 0.2$ m/s
Celerity $c_p = 1319 m/s$
Inertial constant $s = \ 3.25\ s^2/m$
Dimensionless parameters
$C_1 = 0.0318$, $C_2 = 0$, $C_3 = 1$ (Momentum equation (5.8))
$C_1 c_4 = 7.15 \cdot 10^{-4}$, $c_4 = 0.0228$, $c_5 = -7.33 \cdot 10^{-4}$, $\epsilon^2 = 10^{-3}$ (Continuity equation (5.9)), $B_1 = 0.0123$, $B_2 = 207$ (Brunone unsteady friction (5.8))

Table 5.1: The set of parameters used for the valve-closure water hammer. Dimensional, computed dimensional, and dimensionless parameters are separated for clarity. These parameters are taken from the physical model presented in [8] and studied further in [9]. Note: The Brunone coefficient k is estimated in [8] from Vardy-Brown's shear decay coefficient [83], and viscous constant r is described within the figure caption and the results section 5.9.

5.10 Conclusions

A multiple-scales asymptotic analysis was developed for pressure-wave attenuation in the Brunone model of unsteady friction. The analytical form showed that the increased attenuation due to unsteady friction over the standard steady friction model may be reduced to a single time-dependent exponential factor dependent on the product of the Brunone unsteady friction parameters. The method was applied to water hammer caused by sudden valve closure in water reservoir pipelines in [8]. The analytical form of the pressure wave attenuation also predicted that viscous head in an extended steady friction model may account for increased pressure-wave attenuation seen in the unsteady friction model when the attenuation has a weak spatial dependence. The approach used here should be useful to explain the physical basis of pressure-wave attenuation predicted in other water hammer models.

Chapter 6

Water Hammer Analysis and Parameter Estimation in Polymer Pipes with Weak Strain-Rate Feedback

E. Yao; G. Kember; and D. Hansen

Published in: Journal of Engineering Mechanics, August 2016, 142(8): 04016052
URL: http://ascelibrary.org/doi/abs/10.1061/%28ASCE%29EM.1943-7889.0001104

6.1 Abstract

A closed-form, multiple-scales, analytic approximation of a Kelvin-Voight viscoelastic model is developed to describe water hammer pressure wave attenuation in polymer pipe. The analytical results show that the evolution of water hammer for the single-pipe experiment considered in this paper is described by the Kelvin-Voight model as a weak strain-rate feedback occurring over three timescales. The wave transit and frictional timescales are augmented by a third intermediate timescale governed by the weakness of the strain-rate feedback. The scaling analysis also shows that, for weak strain-rate feedback, it is possible to use an optimization approach to estimate the scale of Kelvin-Voight parameters without experimental data. The optimal choice for weakness of the strain-rate feedback also determines the extent to which a weak strain-rate feedback description may be appropriate to describe an experimental design. DOI: 10.1061/(ASCE) EM.1943-7889.0001104. © *2016 American Society of Civil Engineers.*

Author keywords: Water hammer; Multiple scales; Parameter estimation; Polymer; Kelvin-Voight.

6.2 Introduction

Polymer pipes exhibit a viscoelastic behaviour that shows considerably more attenuation under rapidly changing pressure loads than relatively more elastic materials such as steel. The theoretical description of water hammer propagation and attenuation in elastic and viscoelastic pipes and in various configurations continues to be developed and remains the subject of many single-pipe experiments. Substantial flow asymmetry and directional dependence (Das and Arakeri [27] 1998; Brunone et al. [21] 2000; Brunone and Berni [15] 2010) has been observed. A range of models have been found necessary when using two-dimensional models to describe pressure transients, for example, as a function of Reynolds number (Wabha [88] 2009; Ghidaoui and Kolyshkin [34] 2001). The Complexity of the dynamical response of polymer pipes undergoing rapid transients has been shown to depend strongly on the length of pipe (Mitosek and Chorzelski [59] 2003), although anchoring, pipe vibration, gas pockets, and others (Bergant et al. [7] 2013) cannot be ignored. Axial movements have been found to enhance fluid-structure interaction (Keramat et al. ([48] 2012; Wabha [88] 2009) and differentially influence the choice of lumped-parameter viscoelastic model parameters depending on the experimental setting (Keramat et al. [48] 2012). Recent innovative experimental work in two-dimensional viscoelastic models (Pezzinga et al. [64] 2014) and one-dimensional branched polymer pipelines (Evangelista et al. [31] 2015) continues to prove the usefulness of viscoelastic lumped-parameter models while emphasizing dependence of parameters on the experimental setting.

One-dimensional viscoelastic models when compared with two-dimensional models represent a large simplification that has been justified because of a lack of uniqueness in model selection (Brunone et al. [21] 2000) and (Brunone and Berni [15] 2010). In spite of their relative simplicity, these models have been repeatedly shown to give surprisingly good agreement with details of water hammer evolution. In many case studies, the standard steady- and unsteady- friction models are typically extended to include a lumped-parameter viscoelasticity based on a Kelvin-Voight description (Ramos et al. [67] 2004; Covas et al. [24] 2004; Weinerowska-Bords [91] 2006; Bergant et al. [11] 2008a, [12] 2008b). More recently, the further development of one-dimensional unsteady-friction viscoelastic models for the description of plastic-pipe networks with pipes of rapidly varying cross-sectional area that are subject to

partial blockage (Meniconi et al. [56] 2012) has led to the development of innovative calibration techniques based on transient tests carried out on constant diameter plastic pipe. Leak detection in plastic pipes (Meniconi et al. [57] 2013) has also been examined by using one-dimensional model, and it is found that the inclusion of both unsteady friction and viscoelasticity are required for adequate reliability.

The Kelvin-Voight viscoelastic model is a "mechanical analogue." Although the Kelvin-Voight model is widely and successfully used, it is difficult to establish the model parameters from physical measurements because mechanical analogues conceptualize the underlying physics. As a result, optimization of numerical models to match experimental data is normally required to determine model parameters [a full description is in (Weinerowska-Bords [91] 2006)]. Furthermore, a direct understanding of how, for example, the parameters represent the solution dynamics is typically unavailable. Overcoming these two deficiencies motivates this work. A simple closed-form approximation is found to a Kelvin-Voight model of polymer pipe water hammer attenuation for the experiment described in Mitosek and Chorzelski ([59] 2003) and further analyzed in Weinerowska-Bords ([91] 2006). The pressure wave attenuation in this experiment is also found to belong to a class of polymer pipe water hammer with weak strain-rate feedback whose parameter scales can be optimally predicted without access to experimental data. The feedback weakness also provides a measure of the extent to which a weak strain-rate feedback associated with the cost-function minimum is appropriate.

6.3 Viscoelastic Water Hammer Equations

The momentum equation may be written as (Wylie and Streeter [97] 1993)

$$g\frac{\partial h}{\partial x} + \frac{\partial v}{\partial t'} + \frac{\lambda}{2D}v|v| = 0 \tag{6.1}$$

where $h(x,t)$ = head; $v(x,t)$ = fluid velocity; L = pipe length; D = internal pipe diameter; and λ = friction factor. The nonlinear acceleration term $v\partial v/\partial x$ was neglected, as in Weinerowska-Bords ([91] 2006), without loss of generality.

The continuity equation is modified (Ghilardi and Paoletti [37] 1986; Covas et al.

[25] 2005; Weinerowska-Bords [91] 2006)

$$\frac{a^2}{g}\frac{\partial v}{\partial x} + \frac{\partial h}{\partial t'} + \frac{2a^2}{g}\frac{\partial w}{\partial t'} = 0 \tag{6.2}$$

with circumferential strain $w(x,t)$ and empirical wavespeed a, and the nonlinear term $v\partial h/\partial x$ is neglected, as in Weinerowska-Bords ([91] 2006), without loss of generality for the method of analysis presented in this paper.

For clarity and for later reference, the theoretical wavespeed is

$$a_0 = \sqrt{\frac{K/\rho}{1 + c_1 K/[(e/D)E_0]}} \tag{6.3}$$

with liquid density ρ, pipe fastening constant c_1, liquid bulk modulus of elasticity K, pipe wall thickness e, and instantaneous tensile modulus E_0.

The strain $w(x,t)$ is assumed to follow a lumped-parameter Kelvin-Voight viscoelastic solid model, termed the "KV equation" hereafter, with a Hookean spring with Young's modulus E and a liquid-filled dashpot with fluid viscosity η connected in parallel. In this case, the model may be written as

$$\frac{dw}{dt'} = \frac{1}{T_w}\left[\frac{c_1 \rho g h}{2(e/D)E} - w\right] \tag{6.4}$$

where T_w = relaxation time of the single Kelvin-Voight element defined through $\eta = T_w E$. More Kelvin-Voight elements could be considered, but a single element was sufficient here to describe the experimental results presented in Weinerowska-Bords ([91] 2006). Although the analysis derived here may be extended to the more general case, most usage of the Kelvin-Voight model is limited to several elements.

The initial head $h(x, t' = 0) = h_2 + (h_1 - h_2)(1 - x/L)$ drives the fluid at a steady-state velocity $v = v_\infty$. The water hammer begins after a change in the boundary conditions is imposed at the downstream end $x = L$. Specifically, at $t' = 0$ the velocity at $x = L$ is reduced to zero at a constant rate over a time $\Delta t'_c$, so that $v(x = L, t' \geq \Delta t'_c) = 0$. The upstream head at $x = 0$ is maintained at h_1 equal to the value imposed at $t' = 0$, so that $h(x = 0, t' > 0) = h_1$. The head is fed forward to Eq. (6.4), and the initial strain is assumed to be equal to the steady solution of Eq.

Dimensional parameter	Notation	Value
Pipe diameter	D_c	0.3 m
Pipe length	L	36 m
Pipe wall thickness	e	4.6 mm
Friction factor	λ	0.0119
Fastening coefficient	c_1	1
Applied head at $x = 0$	h_1	38.8 m
Applied head change at $t = 0$	$h_1 - h_2$	0.17 m
Water bulk modulus	K	2.2×10^9 Pa
Wave speed (celerity)	a	4.23×10^2 m/s
Kelvin-Voigt Young's modulus	E	1.1×10^{10} Pa
Kelvin-Voigt relaxation time	T_w	0.0541 s
Valve closure time	$\Delta t'_c$	0.024 s
Water density	ρ	$1,000$ kg/m^3
Gravitational acceleration	g	9.81 m/s^2

Table 6.1: Set of Dimensional Parameters Used to Define the Experimental Setup and the Viscoelastic Water Hammer Mathematical Model

(6.4), giving $w(x,0) = c_1 \rho g h(x,0)/[2(e/D)E]$.

The viscoelastic mathematical model with dimensional parameters used to define the experimental setup, and the viscoelastic water hammer mathematical model listed in Table 6.1 was used to predict the progression of water hammer in medium-density polyethylene pipe (MDPE). The experiment and mathematical model are outlined in Weinerowska-Bords ([91] 2006), with full experimental details in Mitosek and Chorzelski ([59] 2003). Briefly, the experiment consisted of a level MDPE pipe with an outside diameter of 50 mm and a length 36 m with the upstream end connected to a large reservoir delivering a constant pressure head of 0.17 m, forcing water to flow at a constant rate of $v_\infty = 0.57$ m/s for $t' \leq 0$. At $t' = 0$, the water hammer was initiated by closing a pipe valve, located at the downstream end $x = 36$ m from the upstream end, over a time period $\Delta t'_c = 0.024$ s. The Kelvin-Voight parameters E and T_w presented in Table 6.1 were found in Weinerowska-Bords ([91] 2006) through least-squares error between experimental and predicted head.

The experimental results (Mitosek and Chorzelski [59] 2003; Weinerowska-Bords [91] 2006) are presented in Figure 6.1 in rescaled form, described in the following sections, and compare well with the mathematical model. Unfortunately, estimating the Kelvin-Voight lumped parameter requires knowledge of the experimental results,

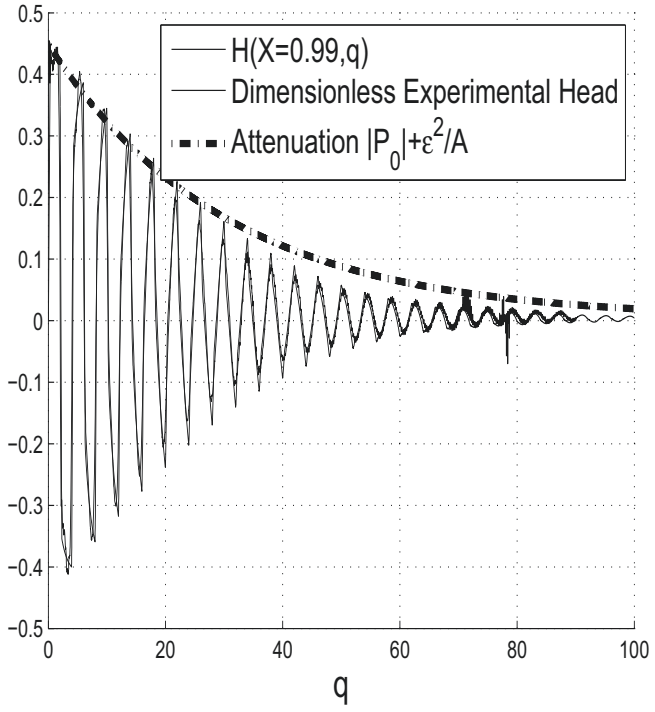

Figure 6.1: Preissmann numerical approximation, with space and time step $\Delta X = \Delta q = 0.01$, to the solution of Eqs. (6.14)–(6.16) is shown at dimensionless position $X = 0.99$ and appears as the solid line; the numerical solution is given in terms of the wave timescale q is nearly superimposed over the dashed line experimental results (Weinerowska-Bords [91] 2006); the pressure wave attenuation approximates the head to $O(\epsilon)$ as expected

and developing ways to circumvent this difficulty forms part of the motivation for this paper. A full discussion of problems and questions encountered in estimating Kelvin-Voight parameters and other model parameters is provided in Weinerowska-Bords ([91] 2006).

In all modelling, it is desirable to gain an understanding of the relationship between model parameters and the dependent variables, and this can be difficult to obtain from numerical solutions. In the case considered here, knowing how the magnitude and attenuation of the water hammer pressure wave depend on the model parameters is practically useful. Therefore, in this work, the method of multiple scales is used to derive a closed-form analytic approximation to pressure wave attenuation. In developing the analytic approximation, it is found that the experiment falls

into a "weak strain-rate" feedback category. The weakness of the strain-rate feedback allows for an optimal estimation of the Kelvin-Voight parameter scales without access to the experimental results.

The mathematical model is first nondimensionalized in the following section, and then the dimensionless equations were rescaled in the subsequent sections to arrive at a form that is regular as a small parameter ϵ vanishes, and this enables the multiple-scales approximation.

6.4 Nondimensionalization

A standard rescaling of the dimensional steady head and steady velocity in the momentum given in Eq. (6.1) and continuity given in Eq. (6.2) is to define $H = (h - h_2)/h_{12}$ and $V = v/v_\infty$, where $h_{12} = h_1 - h_2$ is the applied head. The spatial scale $X = x/L$ is scaled with respect to the pipe length L, and the inertial time-scale v_∞/g is scaled by the hydraulic gradient h_{12}/L, giving the rigid column velocities, and pressure gradients are approximated as quasi-steady (Tijsseling and Vardy [80] 2004)) timescale $T = Lv_\infty/(gh_{12})$. The strain is already dimensionless but is renamed to $\tilde{W}$ for notational consistency and clarity. The rescaled time is then $t = t'/T$, and the rescaled momentum and continuity equations and KV equations are

$$\frac{\partial \tilde{H}}{\partial X} + \frac{\partial \tilde{V}}{\partial t} + \tilde{V}|\tilde{V}| = 0 \tag{6.5}$$

$$C_4' \frac{\partial \tilde{H}}{\partial t} + \frac{\partial \tilde{V}}{\partial X} + \alpha' \frac{\partial \tilde{W}}{\partial t} = 0 \tag{6.6}$$

$$\frac{\partial \tilde{W}}{\partial t} + T_r' \tilde{W} = T_r' \beta' \tilde{H} + T_r' h^{*\prime} \tag{6.7}$$

with initial conditions $\tilde{H}(X, t = 0) = 1 - X$; $\tilde{V}(X, t = 0) = 1$; and $\tilde{W}(X, t = 0) = \beta'(1 - X) + h^{*\prime}$; and boundary conditions $\tilde{H}(X = 0, t > 0) = 1$; $\tilde{V}(X = 1, 0 < t \leq \Delta t_c) = 1 - t/\Delta t_c$; and $\tilde{V}(X = 1, t \geq \Delta t_c) = 0$. The variable t is nondimensional time, whereas the original variable t' was dimensional time.

The parameters that appear in the rescaled continuity given in Eq. (6.6) may be understood by introducing the density ρ to $C_4' = [(\rho g h_{12})/(\rho a v_\infty)]^2$ and $\alpha' = 2\rho g h_{12}/\rho v_\infty^2$. In this case, these parameters are interpreted, respectively, as the ratio of the applied hydraulic head difference relative to the "local" (because of wavespeed

a) and "global" (because of initial steady velocity v_∞) pressure heads before water hammer initiation. Similarly, with the rescaled KV [Eq. (6.7)], $\beta' = c_1(\rho g h_{12})/[2 \cdot E(e/D)]$ and $h^{*\prime} = (\rho g h_2)/[2 \cdot E(e/D)]$ are, respectively, the ratio of applied hydraulic head difference and mean pressure head to a pipe strain e/D scale. The rescaling explicitly shows the relevance, in the continuity and KV equations, of the magnitude of the applied hydraulic head mean and gradient to pressure heads determined from the wavespeed a, initial velocity before water hammer initiation v_∞, and pipe properties E, e, and D. These quantities will ultimately determine the nature of the evolution of the water hammer over a set of three timescales. The constant shift $h^{*\prime}$ has not been subtracted because the analysis of the pressure wave attenuation is not simplified by the removal of this term, and this point is revisited later. The dimensionless groups C_4', α', T_r', β', $h^{*\prime}$, and Δt_c are shown and defined in Table 6.3.

In the following two sections, a multiple-scales approximation is implemented for the attenuation of the water hammer pressure wave. This will require us first to find a scaled form of the dimensionless momentum, continuity, and KV equations that have $O(1)$ (O indicates "the order of") magnitude for all dependent variables and the dimensionless time, so that the relative importance of each term is explicit and not buried in the size of the dependent variable. After this form is discovered, a multiple-scales approximation is constructed in a convenient artificial parameter ($\epsilon \ll 1$) that represents the *relative scale of all dimensionless groups* and for which the equations and conditions *do not exhibit singular behaviour* for ($\epsilon \to 0$). A useful background fully detailing the development of other multiple scales approximations constructed by the authors in water hammer applications may be found, for example, in Yao et al. ([98] 2014, [99] 2015).

6.5 Rescaled Dimensionless Form and Small Parameter

To build the desired multiple-scales expansion, a form is found of the dimensionless momentum, continuity, and KV equations that are regular (not singular) as a small parameter ϵ vanishes (Bender and Orzsag [6] 1978). This requirement is achieved in two parts: (1) by rescaling the dimensionless equations and conditions given in Eqs. (6.5)–(6.7) to a form in which the dependent variables are order 1, subject to an order 1 reference timescale that will be found here to be the wave transit timescale; and (2)

to define an artificial small parameter ϵ in which the final form of the momemtum, continuity, and KV dimensionless equations are regular as the small parameter $\epsilon \to 0$. This objective is achieved in the "Dimensionless Rescaling" and "Regularized Form and Small Parameter" sections.

6.5.1 Dimensionless Rescaling

The appropriate scalings of the dimensionless dependent variables and reference timescale are unknown a priori. Therefore, these are defined, and then knowledge of the parameter sizes in Table 6.3 is used to observe the balancing between terms in Eqs. (6.5)–(6.7).

The unknown dimensionless scalings A', B', and C' are, respectively, for the head $\tilde{H}$, velocity $\tilde{V}$, and strain $\tilde{W}$, whereas a scaling a' is introduced for the dimensionless time t. Introducing these to Eqs. (6.5)–(6.7) gives

$$A'\frac{\partial \bar{H}}{\partial X} + \frac{B'}{a'}\frac{\partial \bar{V}}{\partial q} + B'^2 \bar{V}|\bar{V}| = 0 \tag{6.8}$$

$$\frac{C_4' A'}{a'}\frac{\partial \bar{H}}{\partial q} + B'\frac{\partial \bar{V}}{\partial X} + \frac{\alpha' C'}{a'}\frac{\partial \bar{W}}{\partial q} = 0 \tag{6.9}$$

$$\frac{C'}{a'}\frac{\partial \bar{W}}{\partial q} + T_r' C' \bar{W} = T_r' \beta' A' \bar{H} + T_r' h^{*\prime} \tag{6.10}$$

whereas the initial conditions are $\bar{H}(X, q = 0) = 1/A'\ (1 - X)$; $\bar{V}(X, q = 0) = 1/B'$; and $\bar{W}(X, q = 0) = \beta'/C'\ (1 - X) + h^{*\prime}/C'$; and the boundary conditions become $\bar{H}(X = 0, q > 0) = 1/A'$; $\bar{V}(X = 1, 0 < q \leq \Delta t_c/a') = 1 - qa'/\Delta t_c$; and $\bar{V}(X = 1, q \geq \Delta t_c/a') = 0$.

The discovery of the unknown scalings A', B', C', and a' and assumptions about the nature of the weak strain-rate feedback are outlined in the following. As stated previously, these scalings are found subject to the constraint that the dependent variables are order 1 in magnitude with respect to a reference timescale. This process is outlined as follows:

1. Momentum [Eq. 6.8] and continuity [Eq. 6.9] parameter balance: Two assumptions are first made about the nature of the water hammer problem.

    - Assumption 1: The wave transit timescale is arbitrarily referenced to unity

for convenience and this is achieved by balancing the first two terms that appear in the momentum and continuity equations, giving $A' = B'/a'$ and $C_4'A'/a = B'$. Eliminating B' yields the unit wave transit timescale $a' = \sqrt{C_4'}$, from which $q = t/a'$ is a unit wave transit timescale in the rescaled dimensionless problem.

- Assumption 2: To proceed further, the third term of the continuity equation, representing the viscous damping, is assumed to be balanced with the preceding wave terms in Eq. (6.9), giving $C_4'A' = \alpha' C'$. This last assumption implies that the viscoelastic damping begins from the time of water hammer initiation. However, there will be a delay in the viscoelastic damping affect on head and velocity because of the weakness of the strain-rate feedback in this experiment to a time that is an order of magnitude longer than the $q = O(1)$ wave transit timescale.

The set of scalings A', B', and C' is closed by proceeding to the KV equation to find the strain scaling C', and these will require reference to the parameters in Tables 6.1 and 6.2.

2. KV equation [Eq. (6.10)] parameter balance

   - Step 1: Satisfying Assumption 2: The evolution of the viscous damping at order 1 values of the wave transit timescale q, as stated in Assumption 2, requires the two terms on the left-hand side of the KV equation to balance, which may be accomplished by setting $T_r' = 1/a'$. Given $a' = \sqrt{C_4'}$, it follows that $T_r' = 1/\sqrt{C_4'}$. Hence, the ratio of the relaxation T_w to the rigid column timescale T, i.e., $1/T_r' = \sqrt{C_4'}$, is small, and $T_w \ll T$, viz from Table 6.1, $T_w = 0.0541$ s, and from Table 6.2, $T = 1.2 \cdot 10^1$ s.

   - Step 2: Finding strain scale C': To find the strain scale C', multiply the KV equation by a'/C' and impose $a'T_r' = 1$. The two terms on the left-hand side become unity, whereas the two terms on the right-hand side are $\beta' A'/C'$ and $h^{*\prime}/C'$. In general, the relative sizes of the two terms on the right-hand side are unknown, but it will be seen that $h^{*\prime} \gg \beta' A'$. Under this assumption, the strain scale is $C' = h^{*\prime}$.

- Step 3: Finding head scale A' and velocity scale B': Given the timescale $a' = \sqrt{C_4'}$ and also $C' = h^{*\prime}$, $C_4'A' = \alpha' C'$, and then $A' = \alpha' h^{*\prime}/C_4'$. By substituting A' and a' to $A' = B'/a'$, the velocity scale $B' = \alpha' h^{*\prime}/\sqrt{C_4'}$.

- Comments: With respect to the earlier assumption that $h^{*\prime} \gg \beta' A'$, reference to Tables 6.3 and 6.4 shows that $\beta' A' = 2.16 \cdot 10^{-5}$, which is small compared with $h^{*\prime} = 1.51 \cdot 10^{-4}$ as assumed.

The strain scale could have been found by first subtracting $h^{*\prime}$ from the strain and then using $\beta' A'$ as a strain scale. However, the choice made here is without loss of generality because using the alternative leads to a dependence upon the same number of parameters and the same scale for the artificial parameter ϵ found in the following.

Replacing the relationships between the scalings determined previously into Eqs. (6.8)–(6.10) yields

Dimensional scaling	Notation	Value
Timescale	$T = (Lv_\infty)/(gh_{12})$	1.2×10^1 s
Spatial scale	L	36 m
Head scale	h_{12}	0.17 m
Velocity scale	v_∞	0.57 m/s

Table 6.2: Set of Dimensional Scalings Applied to the Dimensional Problem Based on the Dimensional Parameters in Table 6.1

Dimensionless parameter	Definition	Value	Scale: $\epsilon = 0.1$
Δt_c	$\Delta t_c'/T$	2.0×10^{-3}	$O(\epsilon^3)$
C_4'	$[(\rho g h_{12})/(\rho a v_\infty)]^2$	5.0×10^{-5}	$O(\epsilon^4)$
α'	$2\rho g h_{12}/(\rho v_\infty^2)$	1.05×10^1	$O(\epsilon^{-1})$
T_r'	T/T_w	2.24×10^2	$O(\epsilon^{-2})$
β'	$c_1(\rho g h_{12})/[2 \cdot E(e/D)]$	6.81×10^{-7}	$O(\epsilon^6)$
$h^{*\prime}$	$(\rho g h_2)/[2 \cdot E(e/D)]$	1.51×10^{-4}	$O(\epsilon^4)$

Table 6.3: Set of Dimensionless Parameters and Their Values Determined According to the Dimensional Parameters in Table 6.2

Dimensionless scaling	Definition	Value	Scale $\epsilon = 0.1$
Time: a'	$\sqrt{C_4'}$	7.10×10^{-3}	$O(\epsilon^2)$
Head: A'	$\alpha' h^{*\prime}/C_4'$	3.17×10^{1}	$O(\epsilon^{-1})$
Velocity: B'	$\alpha' h^{*\prime}/\sqrt{C_4'}$	2.24×10^{-1}	$O(\epsilon)$
Strain: C'	$h^{*\prime}$	1.51×10^{-4}	$O(\epsilon^4)$

Table 6.4: Set of Dimensionless Parameters and Their Values Determined According to the Dimensional Parameters in Table 6.2. Note: The scale of each parameter is represented in terms of the artificial parameter $\epsilon = 0.1$.

$$\frac{\partial \bar{H}}{\partial X} + \frac{\partial \bar{V}}{\partial q} + A' a'^2 \bar{V}|\bar{V}| = 0 \tag{6.11}$$

$$\frac{\partial \bar{H}}{\partial q} + \frac{\partial \bar{V}}{\partial X} + \frac{\partial \bar{W}}{\partial q} = 0 \tag{6.12}$$

$$\frac{\partial \bar{W}}{\partial q} + \bar{W} = \frac{\beta' A'}{h^{*\prime}} \bar{H} + 1 \tag{6.13}$$

with initial conditions $\bar{H}(X, q = 0) = 1/A'\ (1 - X)$; $\bar{V}(X, q = 0) = 1/B'$; and $\bar{W}(X, \tau = 0) = \beta'/h^{*\prime}\ (1 - X) + 1$; and boundary conditions $\bar{H}(X = 0, q > 0) = 1/A'$; $\bar{V}(X = 1, 0 < q \leq \Delta t_c/a') = 1 - qa'/\Delta t_c$; and $\bar{V}(X = 1, q \geq \Delta t_c/a') = 0$.

6.5.2 Regularized Form and Small Parameter

A final consideration is the reduction of the rescaled Eqs. (6.11)–(6.13) with conditions to a form that has a small parameter and is regular as the small parameter vanishes.

In light of the parameters in Tables 6.3 and 6.4 derived from the experiment in Figure 6.1, it is proposed that the velocity parameter $B' = \alpha' h^{*\prime}/\sqrt{C_4'}$ be used to set the small parameter scale. This velocity scaling contains three components that represent the viscoelastic coupling:

- Strain scale $h^{*\prime}$;
- Viscous contribution to continuity α'; and
- Wave speed timescale $\sqrt{C_4'}$.

Dimensionless scaling and parameters	ϵ Dependence	Value
a	$a'\epsilon^{-2}$	0.707
A	$A'\epsilon$	3.17
B	$B'\epsilon^{-1}$	2.24
C	$C'\epsilon^{-4}$	1.51
h^*	$h^{*\prime}\epsilon^{-4}$	1.51
$C_4{}'$	$C_4\epsilon^4$	0.501
T_r	$T_r'\epsilon^2$	2.22
α	$\alpha'\epsilon$	1.05
β	$\beta'\epsilon^{-6}$	0.681
K_1	a^2A	1.59
K_2	$\beta A/h^*$	1.43

Table 6.5: Dimensionless Scaling and Parameters Presented with Explicit Dependence on ϵ

Because B' is $O(0.1)$, $\epsilon = 0.1$. This parameter is a nonunique, artificial, and therefore removable parameter that is chosen to make the scales of all dimensionless parameters explicit. Its choice will also be seen to link the mathematical and experimental results and to provide useful physical interpretation because it quantifies the *relative* scales of the model parameters.

The multiple-scales expansion requires regularity in the limit of $\epsilon \to 0$, i.e., Eqs. (6.11)–(6.13) and the conditions cannot be singular as ϵ approaches zero. The initial velocity condition based on the scaling B' is $O(1/\epsilon)$, and this is singular for $\epsilon \to 0$. To remove this singularity, $H = \epsilon\bar{H}$ and $V = \epsilon\bar{V}$, whereas, for convenience, the strain $\bar{W}$ is shifted by a unit constant, and the KV equation is slightly simplified through $W = \bar{W} - 1$. Finally, the ϵ dependence of the dimensionless parameters is made explicit in terms of ϵ, and the parametric dependence on ϵ is in Table 6.5. The explicit ϵ dependence is also placed for cross-reference in Tables 6.3 and 6.4.

The regularized form of Eqs. (6.11)–(6.13) using the scaling parameters with explicit ϵ dependence given in Table 6.5 reduces to

$$\frac{\partial H}{\partial X} + \frac{\partial V}{\partial q} + K_1\epsilon^2 V|V| = 0 \tag{6.14}$$

$$\frac{\partial H}{\partial q} + \frac{\partial V}{\partial X} + \epsilon\frac{\partial W}{\partial q} = 0 \tag{6.15}$$

$$\frac{\partial W}{\partial q} + W = K_2 H \tag{6.16}$$

The final form of the initial conditions is $H(X, q = 0) = \epsilon^2/A\ (1 - X)$; $V(X, q = 0) = 1/B$; and $W(X, q = 0) = K_2/A\epsilon^2\ (1 - X)$; whereas the boundary conditions are $H(X = 0, q > 0) = \epsilon^2/A$ and $V(X = 1, q > 0) = 0$. The four dimensionless parameters K_1, K_2, A, and B are all $O(1)$ as required, and their values are in Table 6.5. Furthermore, the model is regular in the limit of $\epsilon \to 0$.

The time-dependent valve closure at the dimensionless downstream end $X = 1$ is replaced with its final value $V = 0$. The valve closure time is $\Delta t_c = O(\epsilon^3)$ in Table 6.3, giving a rescaled closing duration $q = \Delta t_c/(a\epsilon^2) = O(\epsilon)$. It is assumed that the valve is instantly closed in the approximation, and the water hammer evolution is not resolved during the closure timescale $q \ll 1$. This assumption is consistent with the experimental choice of valve-closure time that was chosen to be short compared with the wave transit time to approximate an instantaneous valve closure.

6.6 Multiple Scales Expansion

The solution of the final form in Eqs. (6.14)–(6.16) is assumed to be composed of steady-state component plus an attenuating wave. The steady-state solution is $H = \epsilon^2/A$; $V = 0$; and $W = K_2\epsilon^2/A$; and the steady-state is dominated by the attenuating wave in Figure 6.1 until $q = O(100) = O(1/\epsilon^2)$. This is quantified by referring to Eq. (6.14), where substituting $\tau = \epsilon^2 q$ into Eq. (6.14) yields a balance between the acceleration $\epsilon^2 \partial V/\partial\tau$ and friction $\epsilon^2 K_1 V|V|$ while $\partial H/\partial X$ is small compared with $O(\epsilon^2)$. In addition, for $\tau = O(1)$, the continuity equation shows that the velocity gradient $\partial V/\partial X = 0$ to first order as expected when approaching the steady-state solution.

Viscous effects are more complex and involve an interaction between the head and rate of change of strain on the short timescale q in the KV equation in Eq. (6.16) that is weakly fed back at $O(\epsilon)$ to the continuity equation in Eq. (6.15) as $\epsilon \partial W/\partial q$. The feedback weakness lengthens the timescale at which the viscous effects influence the head and velocity to a timescale $s = O(1)$, where $s = \epsilon q$ that is intermediate to $\tau = O(1)$ and $q = O(1)$. This is qualitatively evident from Figure 6.1 as coinciding with the timescale $q = O(1/\epsilon)$ when $q = O(10)$.

Hence, the water hammer evolution operates over three timescales, and this evolution can be described by using a multiple-scales expansion (Bender and Orzsag [6]

1978). The solution for small ϵ is written as the steady-state solution with an additive attenuating wave. The attenuating wave is broken up into the product of a slowly damping amplitude operating at the two slower timescales $s = \epsilon q$ and $\tau = \epsilon^2 q$ and a rapidly varying wave dependent on X and the shorter timescale q. The dominant first mode as seen in Figure 6.1 is considered

$$H(X,q,s,\tau) = [P_0(s,\tau) + \epsilon P_1(s,\tau) + \ldots] \cdot F[\lambda(X-q)] + \epsilon^2/A \quad (6.17)$$

$$V(X,q,s,\tau) = [P_0(s,\tau) + \epsilon Q_1(s,\tau) + \ldots] \cdot F[\lambda(X-q)] \quad (6.18)$$

$$W(X,q,s,\tau) = [P_0(s,\tau) + \epsilon R_1(s,\tau) + \ldots] \cdot A_W F[\lambda(X-q)] + K_2\epsilon^2/A \quad (6.19)$$

where $A_W = K_2/(1-\lambda)$ follows from Eq. (6.16); $\lambda = \mathbf{i}$ represents a dimensionless circular frequency unit; and the parameters A_W and λ are kept to fix ideas later. Also, P_0 is used in the head, velocity, and strain expansions, and this simpler format is used for clarity while being indicated from the equations following a brief inspection. The higher modes may be added to each of H, V, and W in Eqs. (6.17)–(6.19) and follow the same format. As was detailed in Yao et al. ([99] 2015), the flow is assumed to be unidirectional within the pipe at all times; therefore, the governing equations are invariant under flow reversals and then $V|V|$ with V^2 in Eq. (6.14).

6.6.1 Attenuation Function

Eqs. (6.14)–(6.16) may be rewritten as partial differential equations in the three timescales q, s, and τ, which gives

$$\frac{\partial H}{\partial X} + \frac{\partial V}{\partial q} + \epsilon\frac{\partial V}{\partial s} + \epsilon^2\frac{\partial V}{\partial \tau} + K_1\epsilon^2 V^2 = 0 \quad (6.20)$$

$$\frac{\partial H}{\partial q} + \epsilon\frac{\partial H}{\partial s} + \epsilon^2\frac{\partial H}{\partial \tau} + \frac{\partial V}{\partial X} + \epsilon\frac{\partial W}{\partial q} = 0 \quad (6.21)$$

$$\frac{\partial W}{\partial q} + \epsilon\frac{\partial W}{\partial s} + \epsilon^2\frac{\partial W}{\partial \tau} + W = K_2 H \quad (6.22)$$

The viscous timescale $s = \epsilon q$ becomes apparent now from this form [Eq. (6.22)], where it is clear that the head H drives the rate of change of the strain at the short timescale q. The strain rate is then weakly fed back to the continuity given in Eq.

(6.21), and the $O(\epsilon)$ terms show that the strain rate at timescale q influences the rate of change of head at the intermediate timescale s.

To find the pressure wave attenuation the expansion in Eqs. (6.17)–(6.19) is substituted into Eq. (6.20). The form $F(\lambda(X-q))$ satisfies the coefficients of ϵ^0 that represent the wave component. Continuing and equating coefficients of ϵ and ϵ^2 yield

$$\epsilon \quad : \quad \lambda(P_1 - Q_1) = -\frac{\partial P_0}{\partial s} \tag{6.23}$$

$$\epsilon^2 \quad : \quad \lambda(P_2 - Q_2) = -\frac{\partial P_0}{\partial \tau} - \frac{\partial Q_1}{\partial s} \tag{6.24}$$

Similarly, a substitution of the expansion into Eq. (6.21) yields

$$\epsilon \quad : \quad \lambda(P_1 - Q_1) = \frac{\partial P_0}{\partial s} - \lambda A_W P_0 \tag{6.25}$$

$$\epsilon^2 \quad : \quad \lambda(P_2 - Q_2) = -\lambda A_W R_1 + A_W \frac{\partial P_0}{\partial s} + \frac{\partial P_0}{\partial \tau} + \frac{\partial P_1}{\partial s} \tag{6.26}$$

Finally, substituting the expansion into Eq. (6.22) yields

$$\epsilon \quad : \quad (1-\lambda) A_W R_1 = K_2 P_1 - A_W \frac{\partial P_0}{\partial s} \tag{6.27}$$

where ϵ^2 has not considered because it does not affect the results of this order.

$\lambda(P_1 - Q_1)$ is eliminated by subtracting Eqs. (6.23) and (6.25), and

$$\frac{\partial P_0}{\partial s} - \frac{\lambda A_W}{2} P_0 = 0 \tag{6.28}$$

Substituting $A_W = K_2/(1-\lambda)$ and $\lambda = \mathbf{i}$ yields

$$\frac{\partial P_0}{\partial s} - \frac{K_2 \mathbf{i}}{2(1-\mathbf{i})} P_0 = 0 \tag{6.29}$$

These last two equations show that $P_0(s,\tau)$ has a separated dependence on s and τ.

To discover how P_0 depends on τ, first eliminate $\lambda(P_2 - Q_2)$ in Eqs. (6.24) and (6.26) to find that

$$-\lambda A_W R_1 + A_W \frac{\partial P_0}{\partial s} + 2\frac{\partial P_0}{\partial \tau} + \frac{\partial P_1}{\partial s} + \frac{\partial Q_1}{\partial s} = 0 \tag{6.30}$$

The desired relation that determines how P_0 depends on the slowest timescale τ may be found by replacing R_1 and $\partial Q_1/\partial s$ in Eq. (6.30) with their dependence on P_0 and P_1 to eliminate all occurrences of $\partial P_0/\partial s$ for convenience.

Therefore, solving for R_1 in Eq. (6.27) and replacing $\partial P_0/\partial s$ from Eq. (6.28) yield

$$R_1 = \frac{K_2 P_1 - \lambda A_W^2/2P_0}{(1-\lambda)A_W} \tag{6.31}$$

To rewrite $\partial Q_1/\partial s$ in terms of P_0 and P_1, note that from Eq. (6.23), $Q_1 = (P_1\lambda + \partial P_0/\partial s)/\lambda$, and replacing $\partial P_0/\partial s$ from Eq. (6.28) this simplifies to

$$Q_1 = P_1 + \frac{1}{2}A_W P_0 \tag{6.32}$$

from which $\partial Q_1/\partial s = \partial P_1/\partial s + \frac{1}{2}A_W \partial P_0/\partial s$, and again replacing $\partial P_0/\partial s$ from Eq. (6.28) yields

$$\frac{\partial Q_1}{\partial s} = \frac{\partial P_1}{\partial s} + \frac{\lambda}{4}A_W^2 P_0 \tag{6.33}$$

Substituting R_1 (6.31) and $\partial Q_1/\partial s$ in Eq. (6.33) to Eq. (6.30) yields the desired relation between P_0 and P_1

$$\frac{\partial P_1}{\partial s} - \frac{\lambda A_W}{2}P_1 = -\left[\frac{\partial P_0}{\partial \tau} + \frac{A_W^2}{8}\frac{\lambda(3-\lambda)}{1-\lambda}P_0\right] \tag{6.34}$$

P_0 has a separated dependence on s and τ, and Eq. (6.34) indicates that the same is true for $P_1(s,\tau)$. Hence, P_0 and $\partial P_0/\partial s$ are proportional to the homogeneous solution of Eq. (6.34) satisfied by P_1. To avoid secular terms proportional to powers of s, the terms involving P_0 on the right-hand side of Eq. (6.34) are set to zero, and further substituting $A_W = K_2/(1-\lambda)$ and $\lambda = \mathbf{i}$ yields

$$\frac{\partial P_0}{\partial \tau} + \frac{K_2^2}{8}\frac{\mathbf{i}(3-\mathbf{i})}{(1-\mathbf{i})^3}P_0 = 0 \tag{6.35}$$

Each of Eqs. (6.29) and (6.35) are constant coefficients differential equations with

complex rate constants. The solution of Eqs. (6.29) and (6.35) yields

$$P_0(s,\tau) \propto \exp\left\{ s\left[\frac{K_2\mathbf{i}}{2(1-\mathbf{i})}\right]\right\} \times \exp\left\{ \tau\left[\frac{K_2^2}{8}\frac{\mathbf{i}(3-\mathbf{i})}{(1-\mathbf{i})^3}\right]\right\} \tag{6.36}$$

The pressure wave attenuation is determined to first order as the magnitude of $P_0(s,\tau)$ that requires only the real parts of the complex rate constants. Furthermore, the initial condition applied is determined to first order by the order 1 initial condition applied to V, i.e., $q = 0$, $V = 1/B$; thus, the head and velocity follow

$$|P_0(s,\tau)| = \frac{1}{B}\exp\left[s\Re\left(\frac{K_2\mathbf{i}}{2(1-\mathbf{i})}\right)\right] \times \exp\left[\tau\Re\left(\frac{K_2^2}{8}\frac{\mathbf{i}(3-\mathbf{i})}{(1-\mathbf{i})^3}\right)\right] \tag{6.37}$$

and the desired head and velocity pressure wave attenuation

$$|P_0(s,\tau)| = \frac{1}{B}\exp\left(-\frac{K_2 s}{4} + \frac{K_2^2\tau}{8}\right) \tag{6.38}$$

whereas the strain attenuation has the additional factor $K_2/|1-\lambda| = K_2/\sqrt{2}$ from Eq. (6.19) multiplying $P_0(s,\tau)$. The pressure wave attenuation in Eq. (6.38) is based on a generic choice of $\lambda = \mathbf{i}$ and a choice of coefficient $1/B$ as suggested from theoretical considerations, and if desired, these can be optimally discovered.

6.7 Discussion

The pressure wave attenuation developed previously is considered, followed by a method to discover the Kelvin-Voight parameter scales without access to experimental data.

6.7.1 Pressure Wave Attenuation

The comparison of the pressure wave attenuation wave in equation Eq. (6.38) with the solution in Figures 6.1–6.3 qualitatively shows that the experimental and numerical solution head, velocity, and strain amplitude, respectively, are being represented to the anticipated order of accuracy $O(\epsilon)$.

From Eq. (6.38), the magnitude of the attenuation is inversely proportional to

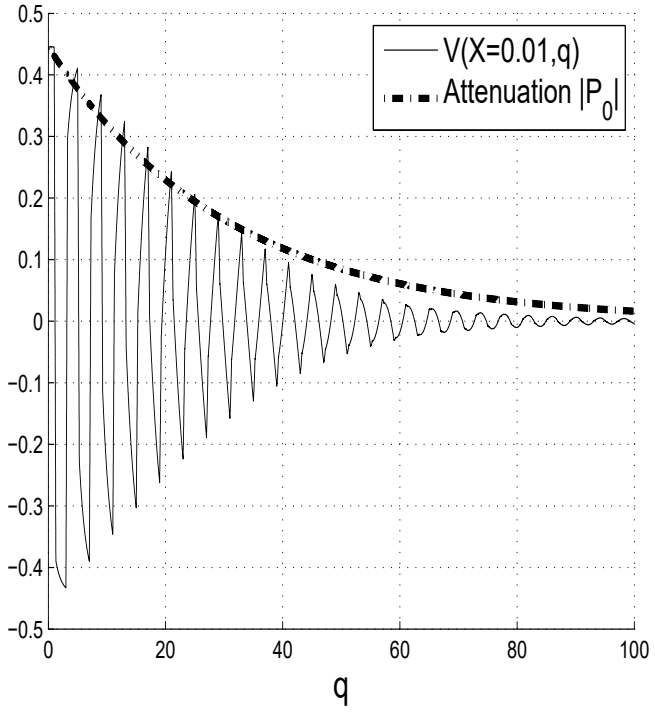

Figure 6.2: Velocity V corresponding to the head H given in Figure 6.1 is shown at the dimensionless position $X = 0.01$; the velocity is shown near $X = 0$, where the scaling $1/B$ applied to the pressure wave attenuation represents the maximal velocity

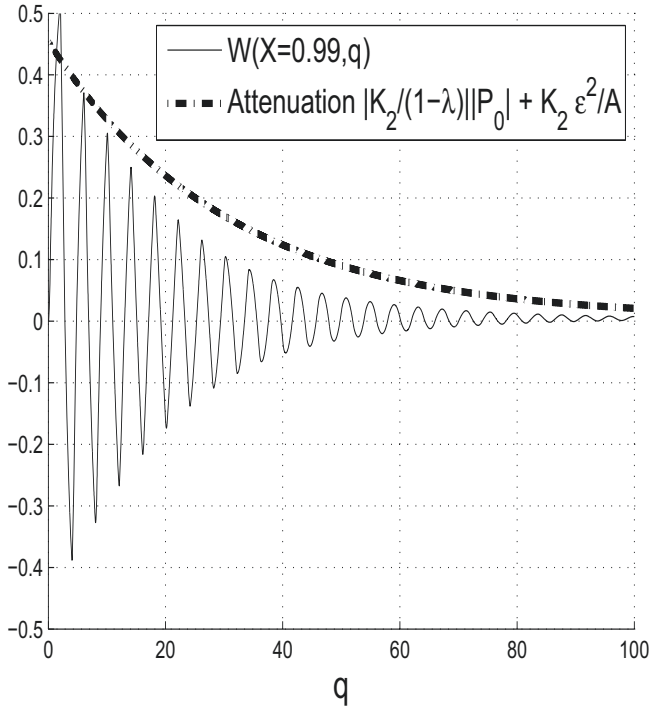

Figure 6.3: Strain W corresponding to the head H given in Figure 6.1 and velocity V in 6.2 is shown at the dimensionless position $X = 0.99$; the pressure wave attenuation, is further scaled by a factor $K_2/(1 - \lambda)$

the scaling B (the strain has an extra factor dependent on λ and A_W because of the first-order strain response process). The scaling B may be rewritten in dimensional terms as

$$B = \frac{\rho g h_2}{(e/D)E} \frac{a}{v_\infty} \tag{6.39}$$

and is equal to the product of (1) the ratio of the static pressure and a pipe strain static pressure scale and (2) the ratio of the elastic wave speed and initial flow velocity. The strain is further scaled by $K_2/|1-\lambda|$, which brings in the feed-forward coupling coefficient K_2 and the strain-rate term λ.

Conversely, the rate of attenuation in Eq. (6.38) is somewhat simpler given it is entirely determined by the coupling strength K_2 between the head and strain. The coupling strength K_2 may be restated in terms of dimensional variables as

$$K_2 = \frac{c_1 \rho a^2}{\epsilon (e/D) E} \tag{6.40}$$

which is proportional to the ratio of a wave speed pressure $1/2\rho a^2$ and inversely proportional to a pipe strain static pressure scale $(e/D)E$. In other words, the relative effects of a wave speed pressure and a pipe strain static pressure scale determine Kelvin-Voight pressure wave attenuation in weak strain-rate problems such as that considered here. This observation jibes with a similar statement in Duan et al. ([30] 2010), in which the viscoelastic attenuation is attributed to a pressure force along with an energy exchange between the fluid and the pipe wall.

The water hammer evolves over three timescales q, $s = \epsilon q$, and $\tau = \epsilon^2 q$. The attenuation occurs over two of these timescales in Eq. (6.38): $s = O(1)$, which corresponds to $q = O(1/\epsilon)$; and a longer timescale $\tau = O(1)$, which is $q = O(1/\epsilon^2)$. The attenuation for the first mode is also determined over *both* timescales solely by the coupling parameter K_2; therefore, the viscoelastic attenuation is active through to the friction timescale τ. Because the analysis has focussed on the first mode, the parameter K_1 representing the friction damping strength does not show up in the pressure wave attenuation to first order. This agrees with Duan et al. ([30] 2010), who found from a two-dimensional model that the pressure wave attenuation in lower modes are mainly driven by viscoelasticity and in higher modes primarily by steady

friction. A similar point is also made in Ramos et al. ([67] 2004), in which viscous attenuation of the pressure wave is termed as an energy dissipation phenomenon. In spite of this observation, the steady friction is still present through the scale $1/B$ [Eq. (6.39)], which depends on the initial velocity v_∞ before the water hammer is initiated.

6.7.2 Parameter Estimation

The dependence of the first mode of the pressure wave attenuation on the parameters in the mathematical model is in Eq. (6.38). The mathematical model rescaling can be used to estimate the scale of the Kelvin-Voight parameters E and T_w, which can be used to find the pressure wave attenuation without experimental data. An approach to do this is presented by way of example and then generalized to the optimization of a cost function.

Weak Strain-Rate Feedback And Parameter Scales

Specifically, the strain-rate feedback term $\epsilon\partial W/\partial q$ is $O(\epsilon)$ and thus a weak feedback. Furthermore, the head and strain response timescale in Eq. (6.16) is completely balanced with the head, given K_2 is order 1. These two features, i.e., the $O(\epsilon)$ weak strain-rate feedback and the balancing of terms in the Kelvin-Voight equation, lead to two constraints that may be used to choose Kelvin-Voight parameters *under the assumption of a weak strain-rate feedback response.*

To begin, note that the choice of relaxation timescale arrived at by optimization in Weinerowska-Bords ([91] 2006) leads to a balance between the strain level and strain rate on the left-hand side of Eq. (6.10); i.e., W is balanced with the $\partial W/\partial\tau$ term, so that $T_r' = 1/a'$, and then $T_w/T = \sqrt{C_4'}$. By applying the experimental design parameters, $T_w = 0.0851$, and this is the same order as $T_w = 0.0541$ chosen in Weinerovska-Bords ([91] 2006). The balance $1/T_r' = a'$ is a criterion that ensures that the relaxation timescale T_r' operates within the wave timescale a' and the viscoelasticity exerts its effect from the time of water hammer initiation. If the balance $T/T_w = 1/\sqrt{C_4'}$ is written in terms of dimensional parameters, the relaxation timescale is $T_w = L/a \ll 1$, and a similar observation made in a more qualitative fashion is in Duan et al. ([30] 2010).

Next, the weak strain-rate feedback also requires that the Kelvin-Voight Young's

modulus E be chosen such that the right-hand-side terms balance with the left-hand-side terms in Eq. (6.10). This balance was found previously to be consistent with $K_2 = O(1)$, and by referring to the dimensional form of K_2 in Eq. (6.40), the second constraint is

$$E = O\left[\frac{c_1 \rho a_0^2}{\epsilon(e/D)}\right] \tag{6.41}$$

where the unknown empirical wavespeed a is replaced with the theoretical wavespeed a_0 from Eq. (6.3).

The theoretical wavespeed in Eq. (6.41) depends on the pipe tensile modulus E_0, and this is to be clearly distinguished from the lumped-parameter Kelvin-Voight Young's modulus E. Assuming a magnitude scale of $E_0 = 1$ GPa for the MDPE pipe, as discussed in Weinerowska-Bords ([91] 2006), and inserting the remaining experimental parameters to Eq. (6.3) lead to a theoretical wave speed of $a_0 = 327$ m/s.

Replacing the theoretical wave speed $a_0 = 327$ m/s and weak strain-rate feedback strength $\epsilon = 0.1$ (chosen earlier), along with the remaining design parameters into Eq. (6.41), yields $E = O(10^{10})$. Thus, the Kelvin-Voight parameter E is predicted to be an order of magnitude *larger* than the pipe Young's modulus $E_0 = 1$ GPa used in the computation of the wave speed from Eq. (6.3). As pointed out in the literature review in Weinerowska-Bords ([91] 2006), this discrepancy between the pipe tensile modulus E_0 and the Kelvin-Voight Young's modulus E reflects the lumped-parameter nature of the Kelvin-Voight model. This observation is taken one step further in the conclusion: "The Kelvin-Voight Young's modulus E is *required* to be an order of magnitude larger than the pipe Young's modulus E_0 if the lumped-parameter model is to capture the $O(\epsilon)$ *weak* strain-rate feedback response."

Cost Function for Parameter Estimation

The previous discussion provides an explanation for the Kelvin-Voight parameter scales but is based on knowledge of the experimental data from Mitosek and Chorzelski ([59] 2003). The Kelvin-Voight parameter estimation is generalized to the optimization of a cost function whose minimum (1) may be used to determine both

the scale of the Kelvin-Voight parameters and strain-rate feedback weakness and (2) provide a measure of the extent to which a weak strain-rate feedback classification is reasonable. These scales are also used to estimate the pressure wave attenuation in the absence of experimental data.

A suitable cost function may be found by noting that the choice of artificial parameter $\epsilon = 0.1$ was based on the requirement that the dimensionless parameters in the final regularized form of the equations given in Eqs. (6.14)–(6.16) where all $O(1)$ and this requirement suggest

$$R(\epsilon) = [A(\epsilon) - 1]^2 + [B(\epsilon) - 1]^2 + [K_1(\epsilon) - 1]^2 + [K_2(\epsilon) - 1]^2 \tag{6.42}$$

where, for example, from Table 6.5, $A(\epsilon) = A'\epsilon$.

The cost function in Eq. (6.42) strongly depends on the choice of tensile modulus E_0 because this parameter is a major determinant of the theoretical wave speed a_0 [Eq. (6.3)]. The cost function in Figure 6.4 is presented for three cases that cover the range of tensile moduli: low, $E_0 = 0.6$ GPa; medium, $E_0 = 1$ GPa; and high, $E_0 = 1.4$ GPa. In all cases, the Kelvin-Voight parameters scales are robust to parameter change with the minimum of $R(\epsilon)$ of Figure 6.4 indicating a weak strain-rate feedback model as being appropriate given $\epsilon \approx 0.1$. Furthermore, the Kelvin-Voight parameter E is an order of magnitude larger than the choice of E_0 over the full range of E_0 and associated theoretical wave speed a_0.

The usage of these estimated scales to compute the pressure wave attenuation is in Figure 6.5. Three cases, Figures 6.5(a–c), respectively, correspond to weak strain-rate feedback strengths (Figure 6.4) $\epsilon = (0.11, 0.09, 0.087)$, Kelvin-Voight parameters $E = (5.4, 10, 15)$ GPa with respective $E_0 = (0.6, 1.0, 1.4)$ GPa, and relaxation times $T_w = (0.14, 0.11, 0.09)$ s. The waves peed a m/s is set to 25% greater than the theoretical wavespeed (Covas et al. ([24] 2004). Given the theoretical wavespeed a_0 and tensile modulus E_0, the Kelvin-Voight Young's modulus may be found through Eq. (6.41) while $T_w = L/a_0$. The experimental and model head at the upper and lower limits of E_0 show phase errors mainly because of discrepancies between the theoretical a_0 and empirical wave speed a. In all cases, the pressure wave attenuation approximates the empirical attenuation with an improving approximation for larger Young's modulus E_0. The model prediction pressure wave attenuation most closely

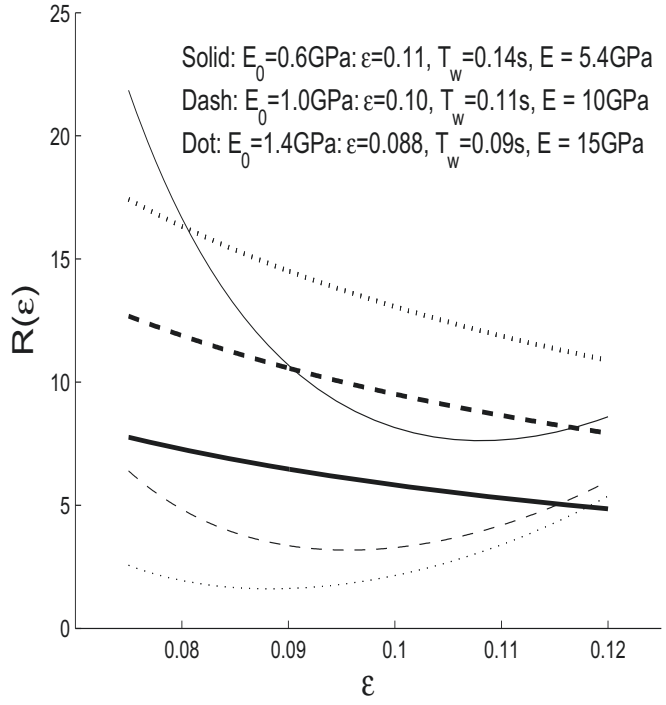

Figure 6.4: Cost function $R(\epsilon)$ in Eq. (6.42) is considered for the full range of tensile modulus $E_0 = 0.6 - 1.4$ GPa; the value of ϵ that minimizes the cost function shown as the finer line for each of three cases is presented at the top, along with the associated relaxation time and Kelvin-Voight modulus E; the heavier line associated with each cost function case is the Kelvin-Voight Young's modulus E

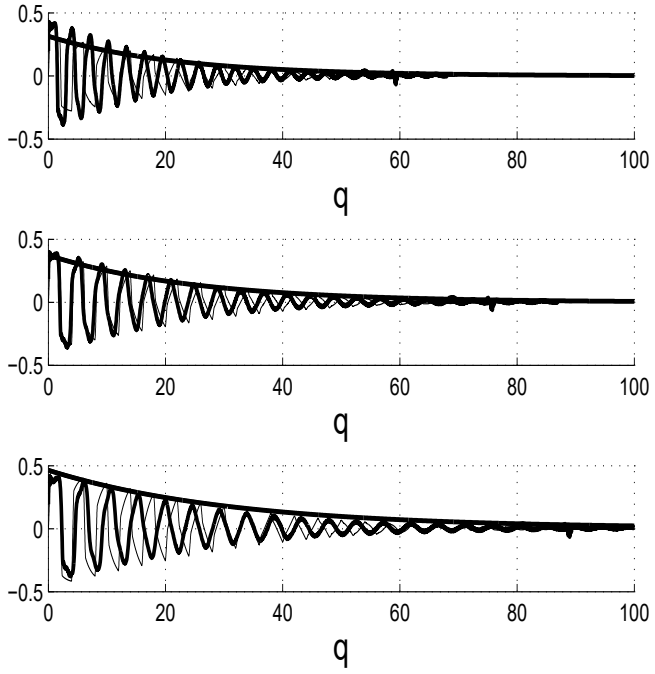

Figure 6.5: Oscillatory experimental head (heavy line), numerical solution head (fine line), and pressure wave attenuation (heavy monotonic line) show the optimal fit using parameters ϵ, E, and T_w, optimally determined in Figure 6.4 without experimental data

represents the experimental results for mid- to upper-range E_0 $(1 - 1.4$ GPa). The pressure wave attenuation errors are proportional to underestimation of the empirical wavespeed, and there is relatively little sensitivity to the Kelvin-Voight relaxation times T_w, which range from double to approximately triple the optimal value of $T_w = 0.0541$ (Weinerowska-Bords [91] 2006).

Although it is possible to estimate the scale of the Kelvin-Voight parameters for the range of tensile moduli E_0 and theoretical wave speeds, the pressure wave attenuation is sensitive to the choice of theoretical wave speed. At lower tensile moduli $E_0 \approx 0.6$ GPa, the theoretical wave speed after augmentation (Covas et al. [24] 2004) still has a 25% error of approximately 100 m/s. This wave speed error leads to roughly the same error in the pressure wave attenuation seen in Figure 6.5(a). The error in Figure 6.5(b) drops to $\approx 2\%$, and again this approximates the percent error between the theoretical and empirical wave speeds. The sensitivity of the pressure

wave attenuation to the underestimation of the empirical wave speed is apparent from Figure 6.5(c), in which the theoretical wave speed error exceeds the empirical wave speed by 15%, but the overestimation primarily increases the phase error with little change in the pressure wave attenuation error.

6.8 Conclusion

An approximation to pressure wave attenuation of water hammer in polymer pipe was described analytically. For the experimental data considered, a Kelvin-Voight model was found to describe the viscous component of the pressure wave attenuation as being attributed to a weak feedback of the strain rate. As such, the pressure wave evolution includes not only the wave transit and frictional time scales seen in descriptions of water hammer, for example, in steel pipe, but also an intermediate timescale determined by the weakness of the strain-rate feedback attributed to the plastic nature of the pipe. In the case considered, there is a weak strain-rate feedback where viscoelasticity is dominant in pressure wave attenuation, as frequently occurs in liquid-filled polyethylene pipes. However, in situations involving PVC pipes, neglecting unsteady friction, as was done here for polyethylene pipes, may be invalid, and unsteady friction would have to be included as a generalization of this work.

The results of this work may be briefly summarized into three main findings:

- The rate of attenuation of the first-mode pressure wave was determined to a first approximation entirely by the coupling parameter between the head and strain rate in the Kelvin-Voight model;

- The plastic pipe instantaneous tensile modulus magnitudes commonly seen in the water hammer literature lead to a Kelvin-Voight Young's modulus that is an order of magnitude larger than the pipe tensile modulus. It was found that this class of water hammer experimental designs fall into a "weak strain" category described here. A weak-strain classification provides a direct link between the conceptual nature of the Kelvin-Voight Young's modulus parameter scale and pipe tensile modulus magnitude; and

- A reverse viewpoint of the previous finding is that if a water hammer experimental design falls within the weak-strain category described here, then the

scale of the Kelvin-Voight modulus may be predicted without running the experiment. Assessing a "scale" is useful to narrow design parameter ranges, but more precise values of model parameters are needed for most predictions.

Identifying experimental design categories has been shown here to allow one to assess the scale of parameters in conceptual models without access to experimental data. As such, design categories provide a physical basis for the scale of parameters found in conceptual models such as the Kelvin-Voight. It is hoped that this work may present a way forward to investigate such category classification in other applications.

Chapter 7

Conclusions

In this thesis, the water hammer phenomenon in a pressurized conduit, caused by sudden valve closure at its downstream end, was studied with respect to the three models: the classical water hammer model with extended quasi-steady friction in steel pipes (Chapter 4); the classical water hammer model with extended quasi-steady friction and Brunone's unsteady friction in steel pipes (Chapter 5); and the classical water hammer model with Darcy-Weisbach steady friction in viscoelastic pipes (Chapter 6). The mathematical tools used are the method of multiple scales and two numerical methods: (1) the method of characteristics and (2) the Preissmann scheme.

In Chapter 4, an approximation form was derived for water hammer pressure wave attenuation for a generalized form of the classical water hammer equations. Unlike cases wherein water hammer is induced by rapid valve opening [42], this model added the effects of flow reversals that occur in the case of sudden valve closure that zeroes the velocity of an initial net flow. These results included the application of variable valve-closure times and it was found that the multiple-scales approximation formed a reasonable representation of the numerical solution until the valve-closure times exceeded twice the wave transit time.

The Brunone's unsteady friction was studied in Chapter 5, wherein the analytical result showed that the increased attenuation caused by unsteady friction over the standard steady friction model may be reduced to a single time-dependent exponential factor; therefore depended on the product of the Brunone's unsteady friction parameters. The obtained wave attenuation form also captured a degree of nonuniqueness nature of the unsteady friction. In particular, an extended parabolic steady-friction model could account for the increased pressure wave attenuation seen in the unsteady friction model as long as the attenuation has a weak spatial dependence. Hence, it is not yet clear whether unsteady friction terms or a simple extension of the steady friction model (to include higher order terms) is most appropriate.

In Chapter 6, an approximation form for the pressure wave attenuation in polymer pressurized conduit was obtained. For the generalized Kelvin-Voight model, it was found that there exists an intermediate timescale caused by weak feedback of the strain rate. In this sense, the pressure wave evolution is extended from two timescales, as seen in ordinary elastic (i.e., steel) pipe to three timescales when viscoelastic pipe is considered. That is, not only there are *slow steady friction* timescale and *fast wave transit* timescale but also an *intermediate weak strain* timescale identified as the effect of weak strain-rate feedback in viscoelastic (MDPE) pipes. The rate of attenuation of the first mode of the pressure wave was also found to be determined entirely by the coupling between the head and strain rate under the Kelvin-Voight model. The scaling analysis developed here showed that for weak strain-rate feedback, the lumped-parameter Kelvin-Voight parameter scales may be optimally determined without access to the experimental data. This key discovery, explains why water hammer in weak strain-rate feedback situations leads to lumped-parameters that *must* exceed those derived from a creep test for wall materials or through the data collected for flow runs by an order of magnitude. It is hoped that the idea of classifying lumped-parameter models results may lead in other instances where these parameters estimated *a priori* and thus used to assist in an experimental design.

It is suggested that, in future, the work presented herein may be extended in the following directions.

The pressure wave attenuation form was derived for the extended model with the Brunone's unsteady friction term being included in the momentum equation (Chapter 5). However, the effect of unsteady friction was not included in the study of the generalized Kelvin-Voight model (Chapter 6). If the effect of weak strain-rate feedback, from a viscoelastic pipe, is included in the continuity equation of the extended model with the Brunone unsteady friction (suggested in Weinerowska-Bords [91]), questions surrounding the relative importance of viscoelasticity and unsteady friction to wave attenuation could be answered.

Progress has been made by others on the water hammer phenomenon in the presence of cavitation (including column separation), cf. Bergant [11] and [12], and Wylie [97]. These one-dimensional models are also suitable for study after an extension of

the approach described herein. It would be useful to understand exactly how cavitation, as represented in these models, influences the pressure wave attenuation.

The success of one-dimensional models to represent water hammer phenomena continues to be explored. Weinerowska-Bords [92] presents a novel water hammer model that includes "flow memory" in the continuity equation Eq.(1.68). Once again, an explicit formulation for the dependence of pressure wave attenuation on this flow memory concept would help uncover how these model variants affect the water hammer phenomenon.

The work considered in this thesis was undertaken with the idea of developing approximations to pressure wave attenuation of water hammer as described by coupled, nonlinear partial differential equations. It required dedicated numerical methods for their approximate computational solutions. The introduction of methods such as those presented herein has shown that it is possible to find analytical representations of features of their solutions such as pressure wave attenuation. These global features were linked in a functional way directly to model parameters. An unexpected result, with wide implications, was the demonstration of a way to predict the magnitude of certain lumped-parameters without access to experimental data. These lumped-parameters can therefore be useful in trying to ensure that a given experimental setup will generate data of the kind hoped for by its designers.

Appendix A

Copyright Permissions

June 22, 2017

Quarterly of Applied Mathematics
Brown University
Providence, Rhode Island 02912, USA
Phone: 401-863-1000

I am preparing my Ph.D. thesis for submission to the Faculty of Graduate Studies at Dalhousie University, Halifax, Nova Scotia, Canada. I am seeking your permission to include a manuscript version of the following paper(s) as a chapter in the thesis:

E Yao, G Kember, and D Hansen. Analysis of Water Hammer Attenuation in the Brunone Model of Unsteady Friction. Quarterly of Applied Mathematics, 72(2):281–290, 2014.

Canadian graduate theses are reproduced by the Library and Archives of Canada (formerly National Library of Canada) through a non-exclusive, world-wide license to reproduce, loan, distribute, or sell theses. I am also seeking your permission for the material described above to be reproduced and distributed by the LAC(NLC). Further details about the LAC(NLC) thesis program are available on the LAC(NLC) website (www.nlc-bnc.ca).

Full publication details and a copy of this permission letter will be included in the thesis.

Yours sincerely,

Yue (Edward) Yao

Permission is granted for:

a) the inclusion of the material described above in your thesis.

b) for the material described above to be included in the copy of your thesis that is sent to the Library and Archives of Canada (formerly National Library of Canada) for reproduction and distribution.

Name: GOVIND MENON Title: ASSOCIATE MANAGING EDITOR QAM

Signature: _____ Date: June 27, 2017

on behalf of
Brown University

June 22, 2017

Journal of Engineering Mechanics
University of Houston
Houston, Texas 77204
(713) 743-2255

I am preparing my Ph.D. thesis for submission to the Faculty of Graduate Studies at Dalhousie University, Halifax, Nova Scotia, Canada. I am seeking your permission to include a manuscript version of the following paper(s) as a chapter in the thesis:

E Yao, G Kember, and D Hansen. Analysis of Water Hammer Attenuation in Applications with Varying Valve Closure Times. Journal of Engineering Mechanics, 141(1):04014107, 2015.

Canadian graduate theses are reproduced by the Library and Archives of Canada (formerly National Library of Canada) through a non-exclusive, world-wide license to reproduce, loan, distribute, or sell theses. I am also seeking your permission for the material described above to be reproduced and distributed by the LAC(NLC). Further details about the LAC(NLC) thesis program are available on the LAC(NLC) website (www.nlc-bnc.ca).

Full publication details and a copy of this permission letter will be included in the thesis.

Yours sincerely,

Yue (Edward) Yao

Permission is granted for:

a) the inclusion of the material described above in your thesis. (provided accounts for 25% or less of new work).

b) for the material described above to be included in the copy of your thesis that is sent to the Library and Archives of Canada (formerly National Library of Canada) for reproduction and distribution.

Name: Leslie Connelly Title: Marketing Coordinator

Signature: _____ Date: 6/29/17

Leslie Connelly, ASCE
Marketing Coordinator
703-295-6169
PERMISSIONS@asce.org
http://ascelibrary.org/page/rightsrequests

June 22, 2017

Journal of Engineering Mechanics
University of Houston
Houston, Texas 77204
(713) 743-2255

I am preparing my Ph.D. thesis for submission to the Faculty of Graduate Studies at Dalhousie University, Halifax, Nova Scotia, Canada. I am seeking your permission to include a manuscript version of the following paper(s) as a chapter in the thesis:

E Yao, G Kember, and D Hansen. Water Hammer Analysis and Parameter Estimation in Polymer Pipes with Weak Strain-Rate Feedback. Journal of Engineering Mechanics, 142(8):04016052, 2016.

Canadian graduate theses are reproduced by the Library and Archives of Canada (formerly National Library of Canada) through a non-exclusive, world-wide license to reproduce, loan, distribute, or sell theses. I am also seeking your permission for the material described above to be reproduced and distributed by the LAC(NLC). Further details about the LAC(NLC) thesis program are available on the LAC(NLC) website (www.nlc-bnc.ca).

Full publication details and a copy of this permission letter will be included in the thesis.

Yours sincerely,

Yue (Edward) Yao

Permission is granted for:

a) the inclusion of the material described above in your thesis. (provided accounts for 25% or less of new work).

b) for the material described above to be included in the copy of your thesis that is sent to the Library and Archives of Canada (formerly National Library of Canada) for reproduction and distribution.

Name: Leslie Connelly Title: Marketing Coordinator

Signature: _____ Date: 6/28/17

Leslie Connelly, ASCE
Marketing Coordinator
703-295-6169
PERMISSIONS@asce.org
http://ascelibrary.org/page/rightsrequests

Bibliography

[1] J. M. Abreu and A. B. Almeida. *Pressure Transient Dissipative Effects: A Contribution for Their Computational Prediction*. Proceedings of the 8th International Conference on Pressure Surges, BHR Group Ltd., The Netherlands, 2000.

[2] J. J. Aklonis, W. J. MacKnight, and M. Shen. *Introduction to Polymer Viscoelasticity*. Wiley-Interscience, New York, 1972.

[3] L. Allievi. Teoria generale del moto perturbato dell'acqu ani tubi in pressione. *Ann. Soc. Ing. Arch. Ithaliana (French trans- lation by Allievi (1904, Revue de me'canique)*, 1903.

[4] L. Allievi. Teoria del colpo d'ariete. *Atti Collegio Ing. Arch. (English translation by Halmos EE, 1929)*, 1913. "The Theory of Waterhammer," Trans. ASME.

[5] R. W. Angus. Simple Graphical Solution for Pressure Rise in Pipes and Pump Discharge Lines. *J. Eng. Inst. Canada*, pages 72–81, 1935.

[6] C. M. Bender and S. A. Orzsag. *Advanced Mathematical Methods for Scientists and Engineers*. McGraw-Hill, New York, 1978.

[7] A. Bergant, Q. Hou, A. Keramat, and A. S. Tijsseling. Waterhammer Tests in a Long PVC Pipeline with Short Steel End Sections. *Scientific Professional Quarterly - Hydraulic Structures*, 1 (1):23–34, 2013.

[8] A. Bergant, A. R. Simpson, and J. P. Vitkovsky. Review of Unsteady Friction Models In Transient Pipe Flow. In *The Work Group On The Behaviour Of Hydraulic Machinery Under Steady Oscillatory Conditions*, page 12pp., Brno, Czech Republic, 1999.

[9] A. Bergant and A. S. Tijsseling. Parameters Affecting Water-hammer Wave Attenuation, Shape and Timing. In *Proceedings of the 10th International Meeting of the IAHR Work Group on the Behaviour of Hydraulic Machinery under Steady Oscillatory Conditions*, pages Paper C2, 12pp., Trondheim, Norway, 2001.

[10] A. Bergant, A. S. Tijsseling, and J. P. Vitkovsky. Further Investigation on Parameters Affecting Water Hammer Wave Attenuation, Shape and Timing. Part 1: Mathematical Tools. In *International Meeting of the Working Group on the Behaviour of Hydraulic Machinery Under Steady Oscillatory Conditions, IAHR, Stuttgard*. Int M Work Group BEH, 2003.

[11] A. Bergant, A. S. Tijsseling, J. P. Vitkovsky, D. I. C. Covas, A. R. Simpson, and M. F. Lambert. Parameters Affecting Water-hammer Wave Attenuation, Shape, and Timing Part I: Mathematical Tools. *IAHR J. of Hydraulic Research*, 46(3):373–381, 2008.

[12] A. Bergant, A. S. Tijsseling, J. P. Vitkovsky, D. I. C. Covas, A. R. Simpson, and M. F. Lambert. Parameters Affecting Water-hammer Wave Attenuation, Shape, and Timing Part II: Case Studies. *IAHR J. of Hydraulic Research*, 46(3):382–391, 2008.

[13] A. Bergant, J. P. Vitkovsky, A. R. Simpson, and M. F. Lambert. Performance of Instantaneous Acceleration Models of Unsteady Skin Friction In Practical Applications. In *The 3rd Unsteady Friction Group Meeting, University of Dundee*, page 14pp., Dundee, UK, 2002.

[14] O. Bratland. Frequency-Dependent Friction and Radial Kinetic Energy Variation in Transient Pipe Flow. In *The 5th Int. Conf. on Pressure Surges, BHRA, Hannover, Germany*, pages 95–101, 1986.

[15] B. Brunone and A. Berni. Wall Shear Stress in Transient Turbulent Pipe Flow by Local Velocity Measurement. *Journal of Hydraulic Engineering*, 136(10):716–726, 2010.

[16] B. Brunone and U. M. Golia. Improvements in Modelling of Water Hammer and Cavitating Flow - Experimental Verification. In *Proc. of the XXII Italian Conference on Hydraulics and Hydraulic Constructions*, pages 147–160, Cosenza, Italy, 1990.

[17] B. Brunone and U. M. Golia. Some Considerations on Velocity Profiles in Unsteady Pipe Flows. In *Proc. of the Int. Conf. on Entropy and Energy Dissipation in Water Resources*, pages 481–487, Maratea, Italy, 1991.

[18] B. Brunone, U. M. Golia, and M. Greco. Modelling of Fast Transients by Numerical Methods. *Proc. Int. Conf. on Hydr. Transients With Water Column Separation, IAHR, Valencia, Spain*, pages 273–280, 1991.

[19] B. Brunone, U. M. Golia, and M. Greco. Some Remarks on the Momentum Equation for Fast Transients. *Proc. Int. Conf. on Hydr. Transients With Water Column Separation, IAHR, Valencia, Spain*, pages 201–209, 1991.

[20] B. Brunone, U. M. Golia, and M. Greco. Effects of Two-Dimensionality on Pipe Transients Modeling. *Journal of Hydraulic Engineering, ASCE*, 121(12):906–912, 1995.

[21] B. Brunone, B. W. Karney, M. Micarelli, and M. Ferrante. Velocity Profiles and Unsteady Pipe Friction in Transient Flow. *J. Water Resour. Plng. and Mgmt.*, 126(4):236–244, 2000.

[22] R. C. Carpenter. Experiments on Waterhammer. *Trans. ASME*, 15, 1893.

[23] M. H. Chaudhry. *Applied Hydraulic Transients*. Van Nostrand Reinhold, 1987.

[24] D. Covas, I. Stoianov, J. F. Mano, H. Ramos, N. Graham, and C. Maksimovic. The Dynamic Effect of Pipe-wall Viscoelasticity in Hydraulic Transients, Part I - Experimental Analysis and Creep Characterization. *J. of Hydraul. Res.*, 42, No. 5:516–530, 2004.

[25] D. Covas, I. Stoianov, J. F. Mano, H. Ramos, N. Graham, and C. Maksimovic. The Dynamic Effect of Pipe-wall Viscoelasticity in Hydraulic Transients. Part II - Model Development, Calibration and Verification. *Journal of Hydraulic Research*, 43(1):56–70, 2005.

[26] J. W. Daily, W. L. Hankey, R. W. Olive, and J. M. Jordaan. Resistance Coefficients for Accelerated and Decelerated Flows Through Smooth Tubes and Orifices. *Trans. ASME*, 78:1071–1077, July 1956.

[27] D. Das and J. H. Arakeri. Transition of Unsteady Velocity Profiles with Reverse Flow. *J. Fluid Mech.*, 374:251–283, 1998.

[28] R. Daugherty and J. Franzini. *Fluid Mechanics with Engineering Applications*. McGraw-Hill, Inc. 7th Edition, 1977.

[29] R. L. Daugherty, J. B. Franzini, and E. J. Finnemore. *Fluid Mechanics with Engineering Applications*. McGraw-Hill, Inc. 8th Edition, 1985.

[30] H. F. Duan, M. Ghidaoui, P. J. Lee, and Y. K. Tung. Unsteady Friction and Visco-Elasticity in Pipe Fluid Transients. *Journal of Hydraulic Research*, 48(3):354–362, 2010.

[31] S. Evangelista, A. Leopardi, R. Pignatelli, and G. de Marinis. Hydraulic Transients in Viscoelastic Branched Pipelines. *J. Hydraul. Eng.*, 2015.

[32] J. P. Frizell. Pressures Resulting from Changes of Velocity of Water in Pipes. *Trans. Am. Soc. Civ. Eng.*, 39:1–18, 1898.

[33] M. Gally, M. Guney, and E. Rieutord. An Investigation of Pressure Transients in Viscoelastic Pipes. *Journal of Fluids Engineering*, 101(4):495–499, 1979.

[34] M. S. Ghidaoui and A. A. Kolyshkin. Stability Analysis of Velocity Profiles in Water Hammer Flows. *ASCE J. of Hydraulic Engineering*, 127(6):499–511, 2001.

[35] M. S. Ghidaoui, M. Zhao, D. A. McInnis, and D. H. Axworthy. A Review of Water Hammer Theory and Practice. *Applied Mechanics Reviews*, 58(1):49–76, 2005.

[36] M. S. Ghidaoui, M. Zhao, D. A. McInnis, and D. H. Axworthy. A Review of Water Hammer Theory and Practice. *Appl. Mech. Rev.*, 58:49–76, 2005.

[37] P. Ghilardi and A. Paoletti. Additional Viscoelastic Pipes as Pressure Surges Suppressors. In *Proceedings of the 5th International Convference on Pressure Surges*, pages 113–121. Hannover, Germany, 22-24 September 1986.

[38] A. H. Gibson. *Water Hammer in Hydraulic Pipelines*. Archibald Constable and Co., Ltd., Lonton, 1908. FIG. 4.

[39] U. M. Golia. On the Evaluation of the Friction Term in Water Hammer. page Rep. 639, Napoli, Italy, 1990. Dept. of Hydraulics, Univ. of Napoli 'Frederico II'.

[40] C. A. M. Gray. The Analysis of the Dissipation of Energy in Waterhammer. *Proc. ASCE, Paper 247*, 119:1176–1194, 1953.

[41] M. Greco. Recent Findings on Column Separation during Water Hammer. pages 261–272, Padova, Italy, 1990. G.N.I. Edizioni Libreria Progetto.

[42] S. Y. Han, D. Hansen, and G. C. Kember. Multiple Scales Analysis of Water Hammer Attenuation. *Q. of Appl. Math.*, 69(4):677–690, 2011.

[43] D. Hansen, V. K. Garga, and D. R. Townsend. Selection and Application of a 1-D Non-Darcy Flow Equation for 2-D Flow Through Rockfill Embankments. *Can. Geotechnical J.*, 32(2):223–232, 1995.

[44] M. Hino, M. Sawamoto, and S. Takasu. Experiments on Transition to Turbulence in an Oscillatory Pipe Flow. *Jour. of Fluids Mechanichs*, 57(2):193–207, 1976.

[45] C. Jaeger. *Theorie Generale du Coup de Belier*. Dunod, Paris, 1933.

[46] N. E. Joukowski. Memoirs of the Imperial Academy Society of St. Petersburg. In *9(5) (Russian translated by O Simin 1904)*, pages 341–424. Proc. Amer. Water Works Assoc. 24, 1898.

[47] A. Keramat, A. G. Kolahi, and A. Ahmadi. Waterhammer Modelling of Viscoelastic Pipes with a Time-Dependent Poisson's Ratio. *Journal of Fluids and Structures*, 43:164–178, 2013.

[48] A. Keramat, A. S. Tijsseling, Q. Hou, and A. Ahmadi. Fluid-structure Interaction with Pipe-wall Viscoelasticity during Waterhammer. *Journal of Fluids and Structures*, 28:434–455, 2012.

[49] D. J. Korteweg. Uber die fortpflanzungsgeschwindigkeit des schalles in elastischen rohren. *Ann. Phys. Chemie*, 5(12):525–542, 1878.

[50] K. F. Lam and H. J. Leutheusser. Flow Establishment in Elastic Pipes. *J. Engrg. Mech.*, 128(11):1169–1173, 2002.

[51] A. S. Leon, M. S. Ghidaoui, A. R. Schmidt, and M. H. Garcia. Efficient Second-Order-Accurate Shock-Capturing Scheme for Modelling One and Two-Phase Water Hammer Flows. *ASCE J. of Hydraulic Engineering*, 134(7):970–983, 2008.

[52] D. J. Leslie and A. S. Tijsseling. Travelling Discontinuities in Waterhammer Theory: Attenuation due to Friction. In *BHR Group, Proc. of the 8th Int. Conf. on Pressure Surges (Editor A. Anderson)*, pages 323–335, The Hague, The Netherlands, 2000.

[53] Q. S. Li, K. Yang, and L. Zhang. Analytical Solution for Fluid-structure Interaction in Liquid-filled Pipes Subjected to Impact-induced Water Hammer. *ASCE J. of Engineering Mechanics*, 129(2):1408–1417, 2003.

[54] M. Lister. The Numerical Solution of Hyperbolic Partial Differential Equations by the Method of Characteristics, A Ralston and HS Wilf (eds), Numerical Methods for Digital Computers. *Wiley New York*, pages 165–179, 1960.

[55] L. F. Menabrea. Comptes rendus hebdomadaires des seances de lacademie des sciences, 47 221. Paris, France, 1858.

[56] S. Meniconi, B. Brunone, and M. Ferrante. Water-hammer Pressure Waves Interaction at Cross-section Changes in Series in Viscoelastic Pipes. *Journal of fluids and structures*, 33:44–58, 2012.

[57] S. Meniconi, B. Brunone, M. Ferrante, and C. Massari. Numerical and Experimental Investigation of Leaks in Viscoelastic Pressurized Pipe Flow. *Drink. Water Eng. Sci.*, 6(1), 2013.

[58] J. Michaud. Coups de belier dans les conduites. etude des moyens employes pour en atteneur les effects. *Bull. Soc. Vaudoise Ing. Arch.*, 4(3):65–77, 1878. (4), pp. 56 - 64.

[59] M. Mitosek and M. Chorzelski. Influence of Visco-elasticity on Pressure Wave Velocity in Polyethylene MDPE Pipe. *Archives of Hydro-Engineering and Environmental Mechanics*, 50(2):127–140, 2003.

[60] A. H. Nayfeh. *Perturbation Methods*. John Wylie and Sons, Inc., 1973.

[61] A. H. Nayfeh. *Perturbation Methods*. Wylie, New York., 2000.

[62] J. Parmakian. *Water-Hammer Analysis*. Prentice-Hall Englewood, 1955.

[63] G. Pezzinga. Quasi-2D Model for Unsteady Flow in Pipe Networks. *Journal of Hydraulic Engineering-Asce*, 125(7):676–685, 1999.

[64] G. Pezzinga, B. Brunone, D. Cannizzaro, M. Ferrante, S. Meniconi, and A. Berni. Two-Dimensional Features of Viscoelastic Models of Pipe Transients. *Journal of Hydraulic Engineering*, 140(8):04014036, 2014.

[65] G. Pezzinga and P. Scandura. Unsteady Flow in Installations with Polymeric Additional Pipe. *J. Hydraul. Eng.*, 121(11):802–811, 1995.

[66] A. Preissmann. Progration des Intumescences dans les canaux et Rivieres. In *1st Congr. des l'Assoc. Francaise de Caucul, Association Francaise de Calcul*, pages 433–442, Grenoble, France, 1961.

[67] H. Ramos, D. Covas, and A. Borga. Surge Damping Analysis in Pipe Systems: Modelling and Experiments. *J. Hydraulic Res.*, 42(4):413–425, 2004.

[68] W. J. M. Rankine. *Philos. Trans. R. Soc. London*, 160:277, 1870.

[69] G. Rich. *Hydraulic Transients*. McGraw-Hill, 1st Edition, New York, 1951 (Dover Reprint).

[70] G. Rich. Waterhammer Analysis by the Laplace-Mellin Transformations. *Trans. ASME,*, pages 1944–45, 1944.

[71] A. M. A. Sattar, A. R. Dickerson, and M. H. Chaudhry. Wavelet-Galerkin Solution to the Water Hammer Equations. *ASCE J. of Hydraulic Engineering*, 134(4):283–295, 2009.

[72] H. Schlichting. *Boundary Layer Theory*. McGraw-Hill, New York, 1960.

[73] O. Schnyder. *Druckstosse In Pumpen Steigieitungen*. Schweiz. Bauz., 1929.

[74] O. Schnyder. *Uber Druckstosse In Rohrleitungen*. Wasserkraft und Wasserwirtschaft, 1932.

[75] M. T. Shamaa and H. M. Karkuri. Implicit Numerical Scheme for Regulating Unteady Flow in Open Channel. In *The Fifteenth International Water Technology Conference, IWTC15 2011, Alexandria, Egypt*, 2011.

[76] W. F. Silva-Araya and M. H. Chaudhry. Computation of Energy Dissipation in Transient Flow. *J. Hydraul. Eng.*, 123(2):108–115, 1997.

[77] V. L. Streeter. Waterhammer Analysis with Nonlinear Frictional Resistance. In *Proc. of the 1st Australansian Conference on Hydraulics and Fluid Mechanics*, Pergamon Press, 1963.

[78] V. L. Streeter and C. H. Lai. Waterhammer Analysis Including Fluid Friction. *J. Hydraulics Div. ASCE*, 88:79–112, 1962. HY3.

[79] V. L. Streeter and E. B. Wylie. *Hydraulic Transients*. McGraw-Hill, New York, 1967.

[80] A. S. Tijsseling and A. E. Vardy. Time Scales and FSI in Unsteady Liquid-filled Pipe Flow. In *BHR Group, Proc. of the 9th Int. Conf. on Pressure Surges (Editor S.J. Murray)*, pages 135–150, Chester, United Kingdom, 2004.

[81] A. S. Tijsseling and A. E. Vardy. Time Scales and FSI in Oscillatory Liquid-filled Pipe Flow. In *BHR Group, Proc. of the 10th Int. Conf. on Pressure Surges (Editor S. Hunt)*, pages 553–568, Edinburgh, United Kingdom, 2008.

[82] A. E. Vardy and J. M. B. Brown. On Turbulent, Unsteady, Smooth-Pipe Friction, Pressure Surges and Fluid Transient. *BHR Group, London,*, pages 289–311, 1996.

[83] A. E. Vardy and J. M. B. Brown. Transient, Turbulent, Smooth Pipe Flow. In *Proc. Int. Conf. on Pressure Surges and Fluid Transients, BHR Group*, pages 289–311, Harrogate, England, 1996.

[84] A. E. Vardy and K. L. Hwang. A Characteristic Model of Transient Friction in Pipes. *Journal of Hydraulic Research*, 29(5):669–684, 1991.

[85] B. Vennatr. Unsteady Frictions in Pipelines. In *Proc. XVIII IAHR Symposium on Hydraulic Mathinery and Cavitation*, volume 2, pages 819–826, Valencia, Sapin, 1996.

[86] J. P. Vitkovsky, M. F. Lambert, A. R. Simpson, and A. Bergant. Advances in Unsteady Friction Modelling in Transient Pipe Flow. In *The 8th Int. Conf. on Pressure Surges, The Hague, The Netherlands*, 2000.

[87] J. P. Vitkovsky and A. R. Simpson. A Critique of the Brunone et al. Unsteady State Friction Method. Technical report, Hydraulics Technical Memorandum No. 90/1, Dept. of Civil and Envir. Engrg., University of Adelaide, 1998.

[88] E. M. Wabha. Turbulence Modeling for Two-dimensional Water Hammer Simulations in the Low Reynolds Number Range. *Computers and Fluids*, 38:1763–1770, 2009.

[89] G. Z. Watters. *Analysis and Control of Unsteady Flow in Pipelines*. Butterworth, Stoneham, MA, 1984.

[90] K. Weinerowska-Bords. *Materials of Seminary "Hydraulics of Transit Systems of Sanitary Engineering"*. Gdansk Univ. of Technology, AGNI, Pruszcz Gdanski (in Polish), 2006.

[91] K. Weinerowska-Bords. Viscoelastic Model of Waterhammer in Single Pipeline-Problems and Questions. *Archives of Hydro-Engineering and Environmental Mechanics*, 53(4):331–351, 2006.

[92] K. Weinerowska-Bords. Alternative Approach to Convolution Term of Viscoelasticity in Equations of Unsteady Pipe Flow. *Journal of Fluids Engineering*, 137(5):054501, 2015.

[93] E. B. Weston. Description of Some Experiments Made on the Providence, RI Water Works to Ascertain the Force of Water Ram in Pipes. *Trans. Am. Soc. Civ. Eng.*, 14, 1885. p. 238.

[94] D. J. Wood and J. E. Funk. A Boundary-Layer Theory for Transient Viscous Losses in Turbulent Flow. *ASME J. Basic Eng.*, 102:865–873, 1970.

[95] F. M. Wood. The Application of Heavisides Operational Calculus to the Solution of Problems in Waterhammer. *Trans. ASME*, 59:707–713, 1937.

[96] E. B. Wylie and V. L. Streeter. *Fluid Transients*. FEB Press, Ann Arbor, 1984.

[97] E. B. Wylie and V. L. Streeter. *Fluid Transients in Systems*. Prentice-Hall, Englewood Cliffs NJ, 1993.

[98] E. Yao, G. Kember, and D. Hansen. Analysis of Water Hammer Attenuation in the Brunone Model of Unsteady Friction. *Quarterly of Applied Mathematics*, 72(2):281–290, 2014.

[99] E. Yao, G. Kember, and D. Hansen. Analysis of Water Hammer Attenuation in Applications with Varying Valve Closure Times. *Journal of Engineering Mechanics*, 141(1):04014107, 2015.

[100] E. Yao, G. Kember, and D. Hansen. Water Hammer Analysis and Parameter Estimation in Polymer Pipes with Weak Strain-Rate Feedback. *Journal of Engineering Mechanics*, 142(8):04016052, 2016.

[101] W. Zielke. Frequency-Dependent Friction in Transient Pipe Flow. *ASME J. Basic Eng.*, 90(1):109–115, 1968.